Power allocation in overlaid DVB-LTE systems

Hiba Bawab

Thèse

THESE INSA Rennes
sous le sceau de l'Université européenne de Bretagne
pour obtenir le titre de
DOCTEUR DE L'INSA DE RENNES
Spécialité : Electronique et Télécommunications

présentée par
Hiba Bawab

ECOLE DOCTORALE : MATISSE
LABORATOIRE : IETR

Power allocation in overlaid DVB-LTE systems

Soutenue prévue le 16.12.2015
devant le jury composé de :

Pascal Chevalier
Professeur au CNAM de Paris / rapporteur
Laurent Clavier
Professeur à Télécom Lille / rapporteur
Catherine Douillard
Professeur à Télécom Bretagne / *examinateur*
Haidar El Mokdad
Maître de Conférences à la Faculté de Génie de l'Univ. Libanaise de Beyrouth / *examinateur*
Youssef Nasser
Enseignant-Chercheur à l'Université Américaine de Beyrouth / *co-encadrant*
Oussama Bazzi
Professeur à la Faculté des Sciences de l'Univ. Libanaise de Beyrouth / co-directeur de thès
Philippe Mary
Maître de Conférences à l'INSA de Rennes / co-encadrant
Jean-François Hélard
Professeur à l'INSA de Rennes / co-directeur de thèse

Power allocation
in overlaid LTE-DVB systems

Hiba Bawab

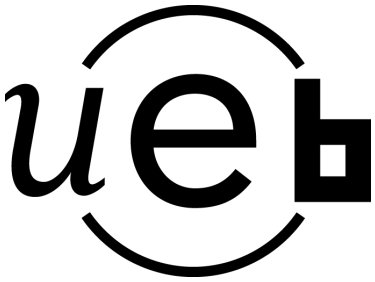

En partenariat avec

Résumé étendu en français

Introduction

Depuis le lancement des premiers réseaux de télécommunications mobiles numériques dans les années 90, la quantité de données transmises par ces réseaux n'a cessé d'augmenter passant de quelques Kbps pour le GSM (Global System for Mobile communications) à la centaine de Mbps pour le LTE (Long Term Evolution). En effet, l'avènement de terminaux très avancés comme les tablettes ou les smartphones, a permis d'accéder à divers services très exigeants en bande passante et en particulier la vidéo.

D'autre part, la ressource spectrale disponible pour faire face à cet appétit insatiable de données numériques ne croit pas de manière exponentielle si bien qu'aujourd'hui bon nombre de systèmes se partagent une ressource spectrale de plus en plus contrainte. En effet, les acteurs de la téléphonie mobile se doivent de proposer des services incluant la TV ou radio mobile, le téléchargement de fichiers volumineux ou encore les jeux en lignes. Pour ce faire, le 3GPP (3rd Generation Partnership Project) a récemment standardisé le mode de diffusion mobile. D'autre part, la communauté "diffusion" s'est adaptée aux nouveaux usages de télévision mobile avec la norme DVB-NGH (Digital Video Broadcasting – Next Generation Handled). Ces déploiements se font sur une ressource spectrale de plus en plus contrainte ce qui a amené notamment le projet ANR M^3 (Mobile MultiMedia) à étudier la possibilité de recouvrement spectral entre les technologies LTE et DVB. Les deux technologies utilisent une forme d'onde OFDM (Orthogonal Frequency Division Multiplexing) (en liaison descendante pour le LTE) et possèdent donc quelques similarités tout en étant assez différentes par leurs caractéristiques.

Dans ce contexte, l'objectif de cette thèse est d'étudier la convergence spectrale entre les réseaux DVB et LTE, en déployant une petite cellule LTE dans une large

cellule DVB, et par suite étudier les performances de ces deux réseaux dans cet environnement. Deux stratégies sont alors possibles, (i) un des deux réseaux (généralement le secondaire) accède d'une manière opportuniste au spectre réservé à l'autre (le système primaire) ou (ii) les deux réseaux partagent le même spectre. Seul le premier cas est traité dans la littérature. Dans ce travail, nous nous intéressons au recouvrement partiel ou total des spectres DVB et LTE et cherchons l'allocation de puissance optimale pour garantir la qualité de service (QoS) de ces deux réseaux.

Cette thèse a été réalisée à l'Institut d'Électronique et de Télécommunications de Rennes (IETR) et l'Université Libanaise (UL) sous une collaboration en co-tutelle entre Université Libanaise-École Doctorale de Sciences et de Technologies(UL-EDST) et l'Institut National des Sciences Appliquées de Rennes (INSA de Rennes) dans le cadre du réseau Universités de Technologies-INSA "réseau UT-INSA".

Chapitre 1
État de l'art et contexte

Ce chapitre présente les outils théoriques et techniques utilisés dans cette thèse ainsi qu'un état de l'art des études sur l'allocation de ressources en recouvrement spectral. Les caractéristiques des deux réseaux DVB et LTE sont aussi présentées avec une vision globale sur le problème de convergence entre eux.

Outils de base

Un schéma de transmission est composé d'une fonction codage de canal, d'un associateur bit vers symbole, d'un canal de propagation, d'un récepteur, un associateur symbole vers bit et d'un décodeur canal. Le signal transmis, durant son passage par le canal de communication, subit un affaiblissement de propagation exprimé en fonction de la distance d entre le transmetteur et le récepteur et l'exposant d'affaiblissement μ :

$$l_p = 1/d^{\mu} \tag{1}$$

Le signal subit aussi des réflexions et diffractions si bien qu'à la réception, différentes copies du signal sont reçues avec différentes amplitudes et phases. Le canal à multi-trajets se modélise comme suit :

$$h(t) = \sum_l a_l \delta(t - \tau_l) \tag{2}$$

$$H(f) = \sum_l a_l e^{-j2\pi f \tau_l} \tag{3}$$

où a_l et τ_l sont respectivement l'atténuation et le délai du $l-$ième chemin de propagation. Cet étalement du canal conduit à de l'interférence entre symboles (ISI) en

réception et une sélectivité en fréquence du canal de transmission, dans le domaine de Fourier, ce qui cause des distorsions à la réception. L'étape d'égalisation dans ce cas est généralement coûteuse ou de performance médiocre.

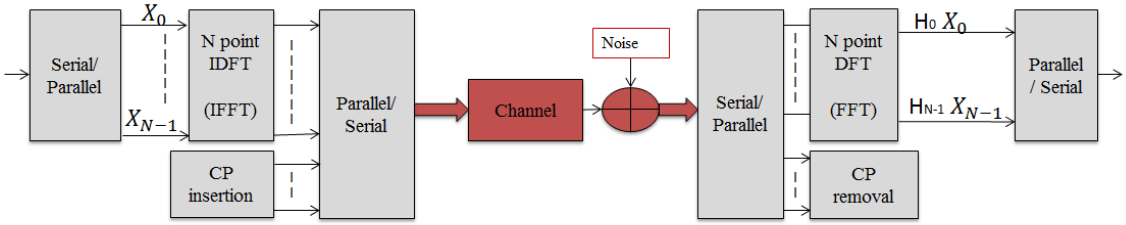

FIGURE 1 – Diagramme du bloc OFDM

La modulation OFDM (Orthogonal Frequency Division Multiplexing), est conçue pour simplifier l'étape d'égalisation en divisant le flux de symboles QAM (Quadrature Amplitude Modulation) mono-porteuse en N flux parallèles dont la durée des symboles est plus grande. En effet, la durée T_q du signal mono-flux QAM est multipliée par un facteur N, i.e. $T_s = NT_q$ où T_s est la durée d'un symbole OFDM. L'implémentation à base de IFFT/FFT (Inverse Fast Fourier Transform/FFT), illustrée sur la figure 1, est classiquement utilisée pour générer et démoduler le signal. L'implémentation à base de FFT et de filtre de mise en forme rectangulaire permet de garantir une occupation spectrale minimale tout en gardant les sous-porteuses orthogonales au sens du produit scalaire. Les symboles avant l'opération IFFT représentent le signal dans le domaine fréquentiel. La séquence dans le domaine temporel pour chaque symbole OFDM s'écrit

$$\text{IFFT}[X_k] = x_n = \frac{1}{\sqrt{N}} \sum_{k=0}^{N-1} X_n e^{j2\pi k \frac{n}{N}} \tag{4}$$

A la réception, les échantillons temporels sont démodulés par FFT pour chaque symbole OFDM tels que :

$$\text{FFT}[x_n] = X_k = \frac{1}{\sqrt{N}} \sum_{n=0}^{N-1} x_n e^{-j2\pi k \frac{n}{N}} \tag{5}$$

sous certaines conditions, le canal équivalent *IFFT-canal-FFT* est un simple produit scalaire entre la fonction de transfert du canal sur chaque sous-porteuse et les symboles QAM d'avant la IFFT. Ce canal équivalent n'est cependant possible que si un intervalle de garde constitué des N_{CP} échantillons du bloc OFDM en sortie de la IFFT est placé au début du symbole avant sa transmission dans le canal. Lorsque l'étalement du canal est inférieure à la durée du préfixe cyclique (CP), la convolution temporelle se transforme en un simple produit en fréquence comme décrit ci-dessus.

Éléments d'optimisation convexe

La forme générale d'un problème d'optimisation est [1] :

$$\begin{array}{ll} \min & f_0(x) \\ \text{s.c.} & f_j(x) \leq 0, j = 1, ..., K_i \\ & h_j(x) = 0, j = 1, ..., K_e \end{array} \tag{6}$$

où $f_0(x)$ est la fonction objectif à minimiser sous les contraintes d'inégalité $f_i(x) \leq 0, i = 1, ..., K_i$ et les contraintes d'égalité $h_i(x) = 0, i = 1, ..., K_e$. La validation des contraintes de Karush Kuhn Tucker (KKT) garantit de trouver une solution optimale au problème. Pour le problème en (6), celles-ci s'écrivent :

$$\begin{aligned} f_i(x^*) &\leq 0, i = 1, ..., m \\ h_i(x^*) &= 0, i = 1, ..., p \\ \lambda_i^* &\geq 0, i = 1, ..., m \\ \lambda_i^* f_i(x^*) &= 0, i = 1, ..., m \\ \nabla f_0(x^*) + \sum_{i=1}^{m} \lambda_i^* \nabla f_i(x^*) + \sum_{i=1}^{p} \nu_i^* \nabla h_i(x^*) &= 0, \end{aligned} \tag{7}$$

où x^* est la valeur optimale de x. Un problème est dit convexe si la fonction objective ainsi que les contraintes d'inégalités sont convexes (respectivement concaves) dans le cas d'une minimisation (respectivement maximisation) et que les contraintes d'égalité sont affines.

Toute fonctionnelle dans $\mathbb{R}^n$ avec un Hessien borné, peut se décomposer comme la somme d'une fonction convexe et d'une fonction concave [2]. On peut alors montrer que l'optimisation dans le cadre d'une procédure convexe-concave (CCCP) converge de manière monotone vers un optimum global. La procédure itérative du CCCP est donnée par :

$$\vec{\nabla} f_{vex}(\vec{x}^{t+1}) = -\vec{\nabla} f_{cave}(\vec{x}^{t}), \tag{8}$$

où $f_{vex}(x)$ et $f_{cave}(x)$ sont respectivement les parties convexe et concave de la fonction objectif. Cet algorithme garantit la convergence vers un point minimum d'énergie.

Comparatif des systèmes DVB-T2 et LTE

Nous terminons ce premier chapitre en donnant les principales caractéristiques de la couche physique des systèmes DVB et LTE. Ce dernier utilise un partage des utilisateurs basé sur l'OFDMA (Orthogonal Frequency Division Multiple Access) dans le lien descendant. Sur le lien montant, le SC-FDMA (Single-Carrier Frequency Division Multiple Access) a été choisi. Cependant, dans ces travaux nous

nous intéresserons uniquement au lien descendant. Les utilisateurs se voient allouer des blocs de ressources, constitués d'au minimum 12 sous-porteuses sur au moins 1 ms.

Le DVB-T2 est le système de télévision terrestre numérique (DTT) le plus avancé qui offre le plus de robustesse aux imperfections du canal. Les standards DVB-T et DVB-T2 utilisent également la modulation OFDM. Cependant, les caractéristiques techniques de la liaison descendante peuvent être très différentes du LTE selon le mode utilisé notamment à cause de la différence de taille entre une cellule DVB et LTE.

Le déploiement de service LTE dans la bande DVB permettrait d'optimiser la réutilisation du spectre mais causerait immanquablement de l'interférence mutuelle entre les deux systèmes. Dans le premier chapitre de contribution, nous proposons d'étudier les débits atteignables lorsque le réseau de diffusion est considéré comme le primaire et le réseau mobile comme le secondaire.

Chapitre 2
Capacité ergodique en canal croisé sous contraintes de puissances

Dans ce chapitre, on analyse la coexistence spectrale entre le réseau de diffusion considéré comme primaire et le réseau mobile considéré comme secondaire. Nous cherchons à dériver et maximiser la capacité ergodique du secondaire sous contraintes de puissance lorsque les deux systèmes interfèrent l'un avec l'autre dans ce que l'on nomme par la suite le canal croisé.

Allocation de ressources avec accès opportuniste au spectre (OSA).

Nous commençons ce chapitre par un état de l'art sur l'allocation de ressources pour la radio cognitive lorsqu'un utilisateur secondaire souhaite utiliser le canal d'un utilisateur primaire de manière opportuniste, c-à-d. idéalement, lorsque celui-ci ne l'utilise pas. Ce problème est illustré sur la figure 2 où les systèmes de diffusion et mobile sont constitués d'un émetteur et d'un récepteur notés BT (Broadcast Transmitter), BR (Broadcast Receiver) et BS (Base Station), MR (Mobile Receiver) respectivement. On remarque que le transmetteur secondaire est équipé d'un détecteur d'énergie afin de détecter si un utilisateur primaire utilise le canal ou pas. Le lien d'interférence provenant de BT vers MR n'est pas pris en compte ou est supposé inclus dans le bruit blanc Gaussien dans la Figure 2. Dans le contexte OSA,

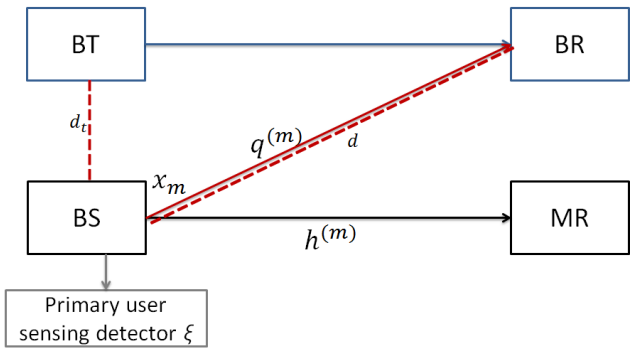

FIGURE 2 – Modèle de coexistence simplifié de radio cognitive OSA [3]

la maximisation de l'efficacité spectrale ergodique en bits/s/Hz s'exprime comme suit [3] :

$$\frac{C_m}{B} = \underbrace{\max_{P_m(|h^{(m)}|^2,\xi)}}_{} \{\mathbb{E}_{|h^{(m)}|^2,\xi}[\log_2(1+\frac{P_m(|h^{(m)}|^2,\xi)|h^{(m)}|^2}{N_0 B})]\} \tag{9}$$

$$\text{s.c.} \left\{ \begin{array}{c} \mathbb{E}_{|h^{(m)}|^2,\xi}[P_m(|h^{(m)}|^2,\xi)|\text{BT is ON}] \leq Q'_{inter} \\ P_m(|h^{(m)}|^2,\xi) \leq Q_{peak} \end{array} \right\} \tag{10}$$

où $P_m(|h^{(m)}|^2,\xi)$ est la puissance de transmission de la BS, ξ est la métrique de détection de l'activité du primaire qui suit une loi du χ^2 [4, 5] et $|h^{(m)}|^2$ est le gain du canal BS-MR supposé suivre une loi exponentielle. N_0 et B sont respectivement la densité spectrale de puissance et la bande passante du signal. L'espérance statistique de la capacité et de la puissance de transmission dans (9) et (10) est calculée en intégrant sur les réalisations du canal $h^{(m)}$ ainsi que sur la statistique de puissance reçue par l'utilisateur primaire. Dans (10), on a $Q'_{inter} = Q_{inter} d^2$ qui est la puissance d'interférence limite moyenne ramenée au BT où d est la distance entre BS et BR et Q_{inter} la valeur moyenne d'interférence au récepteur BR. De plus, Q_{peak} est la puissance de transmission maximale de la BS.

Les auteurs montrent que l'allocation optimale de puissance sous contraintes de puissance moyenne d'interférence au primaire et de puissance de transmission maximale au secondaire est donnée par [3] :

$$P_m(|h^{(m)}|^2,\xi) = \left\{ \begin{array}{cc} Q_{peak} & \frac{1}{|h^{(m)}|^2} \prec \frac{V(\xi)}{N_0 B} \\ \frac{U(\xi)}{\lambda} - \frac{N_0 B}{|h^{(m)}|^2} & \frac{V(\xi)}{N_0 B} \leq \frac{1}{|h^{(m)}|^2} \leq \frac{U(\xi)}{\lambda_s N_0 B} \\ 0 & \frac{1}{|h^{(m)}|^2} \geq \frac{U(\xi)}{\lambda_s N_0 B} \end{array} \right. \tag{11}$$

où λ_s est le multiplicateur de Lagrange correspondant à la contrainte d'interférence.

Une partie de notre travail dans ce chapitre a consisté à retrouver les résultats de [3], en modifiant les hypothèses de travail des auteurs, c-à-d. uniquement l'allocation de puissance sans l'allocation temporelle, que nous présentons sur les figures 3 et 4. Les distances ne jouant qu'un rôle relatif entre elles, nous choisissons $d_t = 1$ et $d = 3$. De plus les canaux $|h^{(m)}|$ et $|q^{(m)}|$ suivent une loi de Rayleigh normalisée en variance. On suppose que le BT est actif 50% du temps. Les figures 3 et 4 montrent respectivement l'évolution de λ_s et de la capacité ergodique du secondaire en fonction de Q_{inter} pour différentes valeurs de ρ ($\rho = \frac{Q_{peak}}{Q_{inter}}$). Comme montré dans les figures 3 et 4, l'augmentation de Q_{inter}, aboutit à une diminution de λ_s et par suite à une augmentation de capacité. De la même manière, la figure 3 nous dit que l'augmentation de ρ, qui signifie une augmentation de Q_{peak}, conduit à une augmentation des valeurs de la capacité.

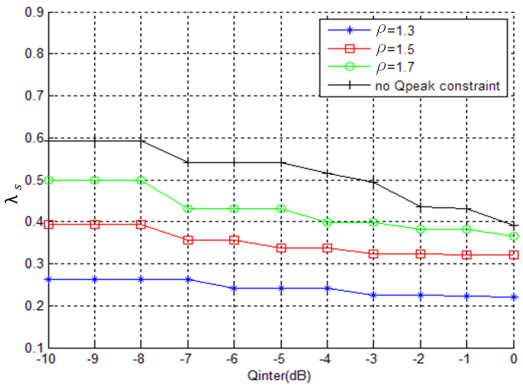

FIGURE 3 – variation de λ_s en fonction de Q_{inter}.

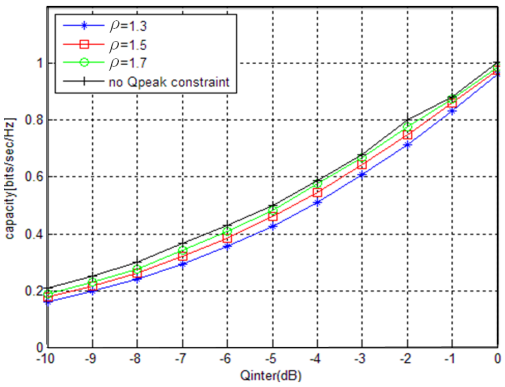

FIGURE 4 – Capacité ergodique en fonction de Q_{inter}.

Allocation de ressources avec partage du spectre (SS)

Nous analysons dans cette partie l'allocation de puissance de transmission pour la radio cognitive dans un modèle de partage du spectre (SS) illustré dans la figure 5. Dans ce modèle, on considère que les deux systèmes utilisent le même spectre et que, contrairement au modèle OSA, le lien interférant sur le secondaire, i.e. BT-MR, est considéré où $|q^{(b)}|^2$ est le gain du lien BT-MR. Le réseau primaire est considéré toujours actif. Tous les canaux dans ce modèle sont supposés plats, indépendants, distribués selon la loi de Rayleigh. On considère un bruit AWGN sur le MR de moyenne zéro et de variance N_0B. Par la suite, le débit de données reçues par MR est donné par :

$$C(P_m) = B\log_2\left(1+\frac{|h^{(m)}|^2P_m}{|q^{(b)}|^2P_b+N_0B}\right). \tag{12}$$

où P_b est la puissance de transmission de BR.

Maximisation de la capacité ergodique

Nous cherchons l'allocation de puissance de transmission de la BS, qui maximise la capacité ergodique sous contrainte de préservation de la QoS du primaire, i.e. niveau d'interférence. Le problème s'écrit :

$$\frac{C_m}{B} = \underbrace{\max_{P_m(|q^{(b)}|^2,|h^{(m)}|^2)}}\ \mathbb{E}\left[\log_2\left(1+\frac{P_m(|q^{(b)}|^2,|h^{(m)}|^2)|h^{(m)}|^2}{P_b|q^{(b)}|^2+N_0B}\right)\right] \tag{13}$$

$$\text{s.c.} \quad \begin{array}{l}\mathbb{E}\left[P_m(|q^{(b)}|^2,|h^{(m)}|^2)\right]\le Q'_{inter}\\ P_m(|q^{(b)}|^2,|h^{(m)}|^2)\le Q_{peak}\end{array} \tag{14}$$

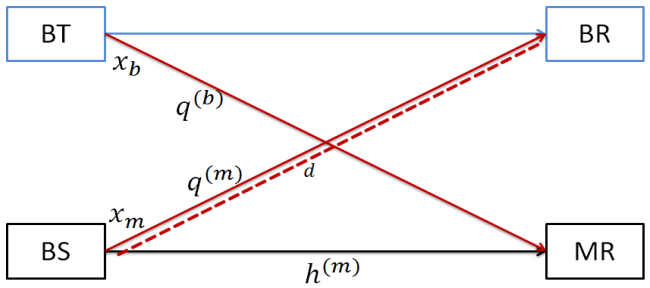

FIGURE 5 – Modèle de coexistence de radio cognitif SS.

La solution optimale du problème $P_m(|q^{(b)}|^2, |h^{(m)}|^2)$ est exprimée par :

$$P_m(|q^{(b)}|^2, |h^{(m)}|^2) = \begin{cases} Q_{peak} & P_b \frac{|q^{(b)}|^2}{|h^{(m)}|^2} \prec \frac{1}{\lambda_p} - Q_{peak} \\ \frac{1}{\lambda_p} - \frac{|q^{(b)}|^2}{|h^{(m)}|^2} P_b) & \frac{1}{\lambda_p} - Q_{peak} \leq P_b) \frac{|q^{(b)}|^2}{|h^{(m)}|^2} \leq \frac{1}{\lambda_p} \\ 0 & P_b) \frac{|q^{(b)}|^2}{|h^{(m)}|^2} \geq \frac{1}{\lambda_p} \end{cases} \tag{15}$$

où λ_p est déterminé par la contrainte d'interférence à l'égalité :

$$\mathbb{E}[P_m(|q^{(b)}|^2, |h^{(m)}|^2)] = Q'_{inter} \tag{16}$$

La solution est constituée de deux cas :

cas 1 : $\frac{1}{\lambda_p} - Q_{peak} \succ 0$

$$\frac{C_m}{B} = \log_2(1+\lambda_p) - \frac{1}{1-Q_{peak}} \left[\log_2(\lambda_p + 1 - \lambda_p Q_{peak}) + Q_{peak} \log_2(Q_{peak})\right] \tag{17}$$

cas 2 : $\frac{1}{\lambda_p} - Q_{peak} \prec 0$

$$\frac{C_m}{B} = \log_2\left(\frac{\lambda_p + 1}{\lambda_p}\right) \tag{18}$$

L'expression exacte de la capacité ergodique du lien BS-MR est exprimée par :

$$\frac{C_m}{B} = \mathbb{E}_{\frac{|q^{(b)}|^2}{|h^{(m)}|^2}} \log_2\left(1 + P_m \frac{|h^{(m)}|^2}{|q^{(b)}|^2}\right) \tag{19}$$

Les figures 6 et 7 présentent la variation de $\frac{C_m}{B}$ fonction de Q_{inter} (Q_{peak}) pour différentes valeurs de Q_{peak}(Q_{inter}) respectivement. On observe que moins les contraintes

sur les puissances crête et d'interférence sont fortes, plus la capacité du lien secondaire augmente, jusqu'à une valeur de saturation où la capacité est limitée soit par le niveau d'interférence à ne pas dépasser au primaire soit par la valeur de la puissance crête au transmetteur.

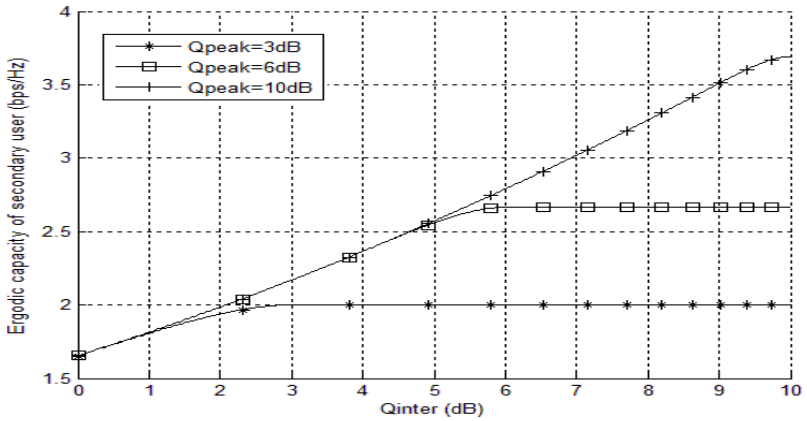

FIGURE 6 – Capacité ergodique en fonction de Q_{inter}.

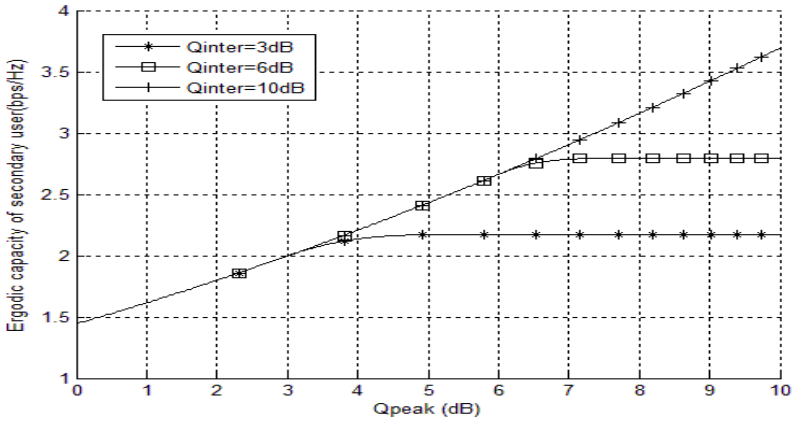

FIGURE 7 – Capacité ergodique en fonction de Q_{peak}.

Accès opportuniste et partage

Les deux stratégies OSA et SS aboutissent à une capacité qui varie de la même manière avec les contraintes données. La différence réside dans le fait que chaque méthode a des objectifs différents et la capacité maximale est obtenue selon ces objectifs.

Chapitre 3
Expression de la capacité ergodique globale des systèmes co-existants DVB et LTE

Dans ce chapitre, on analyse le problème de recouvrement spectral entre les réseaux mobile et diffusion en déployant une petite cellule LTE dans une large cellule DVB, comme illustré figure 8. Dans ce modèle, les deux réseaux partagent la même bande spectrale. Dans ce chapitre, un modèle considérant une interférence totale est étudié avec l'hypothèse que tous les canaux suivent une loi de Rayleigh. On rappelle que le premier système de diffusion est composé d'un émetteur (BT) et d'un récepteur (BR). Alors que le deuxième système mobile est constitué d'une station de base (BS) et d'un récepteur mobile (MR). Dans ce chapitre, on a dérivé la capacité ergodique globale et on a évalué son comportement en fonction des paramètres réels des deux systèmes.

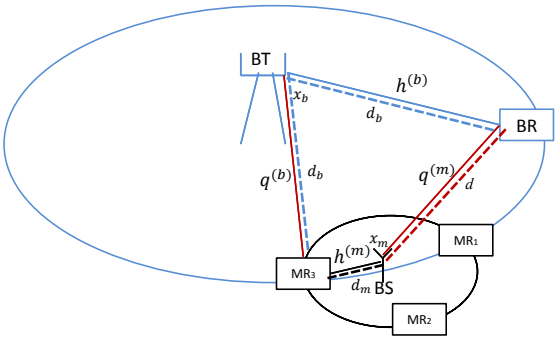

Figure 8 – Cellule LTE au sein d'une grande cellule DVB avec interférence totale.

Les signaux reçus par les récepteurs MR et BR sont respectivement donnés par :

$$y_m = \sqrt{p_m l_m} h^{(m)} x_m + \sum_{b=1}^{R_b} \sqrt{p_b l_{bm}} q^{(b)} x_b + w_m \tag{20}$$

$$y_b = \sqrt{p_b l_b} h^{(b)} x_b + R_m \sqrt{p_m l_{mb}} q^{(m)} x_k + w_b \tag{21}$$

où p_m et p_b sont respectivement les puissances de transmission de BS et BT sur chaque sous-porteuse. De plus, l_m, l_{bm}, l_b et l_{mb} représentent respectivement les affaiblissements des propagations pour les liens BS-MR, BT-MR, BT-BR et BS-BR.

Par suite, $h^{(m)}$, $q^{(b)}$, $h^{(b)}$ et $q^{(m)}$ sont les coefficients complexes gaussiens des canaux des liens BS-MR, BT-MR, BT-BR et BS-BR sachant que $h^{(m)} \sim \mathcal{CN}(0,1)\,\forall k$, $q^{(b)} \sim \mathcal{CN}(0,1)$, $h^{(b)} \sim \mathcal{CN}(0,1)$ et $q^{(m)} \sim \mathcal{CN}(0,1)$. w_m et w_b représentent le bruit blanc additif Gaussien (AWGN). Les sous-porteuses des systèmes DVB et LTE ont des espacements différents. Le système DVB a un espacement entre sous-porteuses plus grand que celui du système LTE. Par suite, R_b sous porteuses du DVB interfèrent sur une seule sous-porteuse LTE tandis qu'une fraction R_m d'une sous porteuse LTE interfère sur une sous porteuse DVB. R_b peut avoir la valeur 13 si le DVB est en mode 8K et ainsi $R_m = 1/R_b$.

Expression analytique de la capacité ergodique globale

Pour obtenir la capacité ergodique globale, on a négligé le bruit devant la valeur de l'interférence. Le rapport signal sur interférence (SIR) des signaux reçus par MR et BR sont exprimés respectivement par :

$$\tilde{\gamma}_m = \frac{p_m l_m \left|h^{(m)}\right|^2}{R_b p_b l_{bm} \left|q^{(b)}\right|^2} \tag{22}$$

$$\tilde{\gamma}_b = \frac{p_b l_b \left|h^{(b)}\right|^2}{R_m^2 p_m l_{mb} \left|q^{(m)}\right|^2} \tag{23}$$

où on a supposé que le canal est invariant dans le temps, et on a la même puissance de transmission pour toutes les sous-porteuses ce qui induit que l'interférence du DVB sur MR est égale à l'interférence provenant d'une seule sous porteuse DVB multipliée par R_b. les densités de probabilité (PDF) des SIR $\tilde{\gamma}_m$ et $\tilde{\gamma}_b$, en tenant compte que $\left|h^{(m)}\right|^2$, $\left|q^{(b)}\right|^2$, $\left|h^{(b)}\right|^2$ et $\left|q^{(m)}\right|^2$ suivent une distribution exponentielle, sont calculées en se basant sur la méthode de la loi conjointe. Elles sont définies respectivement par :

$$p_{\tilde{\gamma}_m}(u) = \frac{p_m p_b l_m l_{bm} R_b}{\left(p_b l_{bm} R_b u + p_m l_m\right)^2} \tag{24}$$

$$p_{\tilde{\gamma}_b}(u) = \frac{p_m p_b l_m l_{mb} R_m^2}{\left(r^2 p_m l_{mb} u + p_b l_b\right)^2} \tag{25}$$

Suite à cela, les capacités ergodiques du réseau mobile et du réseau de diffusion sont exprimées respectivement par :

$$C_{\mathrm{m}} = \frac{p_m l_m}{R_b p_b l_{bm} - p_m l_m} \log_2 \frac{R_b p_b l_{bm}}{p_m l_m} \tag{26}$$

$$C_{\mathrm{b}} = \frac{p_b l_b}{R_m^2 p_m l_{mb} - p_b l_b} \log_2 \frac{R_m^2 p_m l_{mb}}{p_b l_b} \tag{27}$$

La capacité ergodique globale qui est la somme des capacités des deux systèmes est donnée par :

$$C_{\text{global}}(bits/s) = B_{min}\left(\frac{P_m l_p^{(m)}}{R_b P_b l_p^{(b)} - P_m l_p^{(m)}} \log_2 \frac{R_b P_b l_p^{(b)}}{P_m l_p^{(m)}} + \frac{P_b l_p^{(b)}}{R_m^2 P_m l_p^{mb} - P_b l_p^{(b)}} \log_2 \frac{R_m^2 P_m l_p^{mb}}{P_b l_p^{(b)}}\right) \quad (28)$$

où B_{min} est la bande passante minimale parmi celles du DVB et du LTE.

Performances

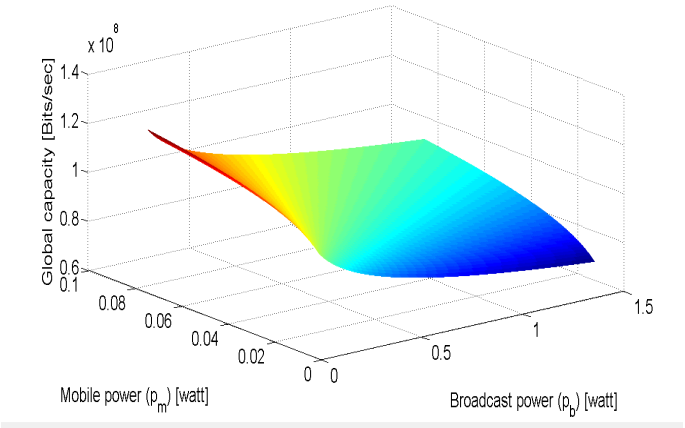

FIGURE 9 – Capacité globale (bits/sec) en fonction de p_b et p_m, mode 8K du DVB, bande recouverte = 7.61 MHz, d=100m.

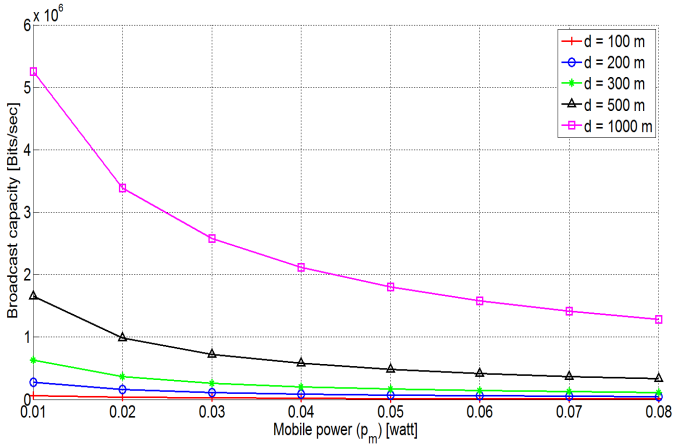

FIGURE 10 – Capacité du DVB en fonction de p_m avec $d = 100, 200, 300, 500, 1000$ m ($p_b = 1.47$ W).

La figure 9 présente la variation de la capacité du système de coexistence global en fonction des puissances de transmission des deux systèmes p_m et p_b. Cette figure montre que la capacité globale n'est ni concave ni convexe en fonction de p_m et p_b et qu'elle prend sa valeur maximale dans le cas de non transmission du DVB dans l'intervalle donné de puissance. La figure 10 présente la variation de C_b en fonction de la distance d'interférence d entre la BS et le BR. Cette figure montre que C_b diminue lorsque la puissance du LTE augmente et que d diminue.

Chapitre 4
Optimisation de la capacité ergodique globale des systèmes co-existants DVB et LTE

Dans ce chapitre, on traite le problème d'optimisation de l'efficacité spectrale du modèle de coexistence entre le DVB et le LTE utilisé dans le chapitre précédent. Cette optimisation est réalisée en respectant des contraintes données qui garantissent la QoS des deux réseaux coexistants dans la figure 11.

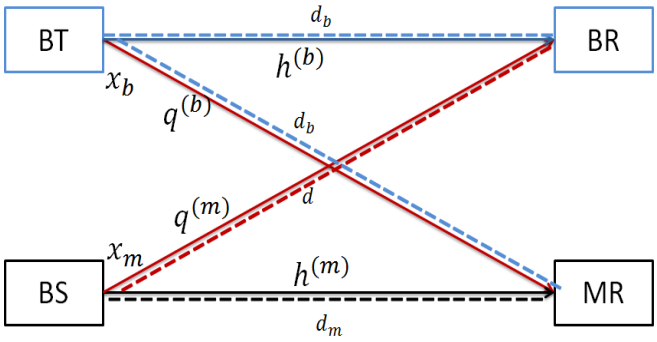

Figure 11 – Modèle de coexistence DVB-LTE avec interférence totale.

Optimisation de la capacité du modèle de coexistence

L'expression de la capacité globale obtenue dans le chapitre précédent est utilisée dans ce chapitre avec un changement de variable dans le but de diminuer sa complexité et par la suite de la maximiser. La capacité ergodique globale du modèle de coexistence DVB-LTE est exprimée par :

$$C_g(\beta) = \frac{1}{\beta - 1} \log_2 \beta + \frac{1}{\frac{A}{\beta} - 1} \log_2 \frac{A}{\beta} \tag{29}$$

où $\beta = \frac{R_b p_b l_{bm}}{p_m l_m}$ et $A = \frac{l_{mb} l_{bm}}{R_b l_b l_m}$. La capacité globale dans (29) est composée des deux termes $C_m(\beta) = \frac{1}{\beta - 1} \log_2 \beta$ et $C_b(\beta) = \frac{1}{\frac{A}{\beta} - 1} \log_2 \frac{A}{\beta}$.

Ainsi, le problème de maximisation de la capacité globale sous des contraintes

de QoS est exprimée par :

$$\max_{\beta} \quad C_g(\beta) \tag{30}$$
$$\text{s.t.} \quad \begin{cases} C_m(\beta) \geq C_{mth} \\ C_b(\beta) \geq C_{bth} \end{cases}$$

où C_{mth} et C_{bth} sont respectivement les seuils minimaux à respecter pour la capacité du mobile et celle du DVB. Les capacités sont représentées 12. Comme c'est illustré, C_m et C_b varient d'une manière contradictoire. Quand l'une augmente, l'autre diminue et vice versa. Par ailleurs, la capacité globale a une valeur minimale qui représente un point d'équilibre entre C_m et C_b, et une valeur maximale. Suite à cela, on a résolu le problème d'optimisation suivant deux méthodes différentes, l'algorithme CCCP (Concave Concex Procedure) et le MP (Maximization Procedure), qui aboutissent respectivement à C_{gmin} et C_{gmax}.

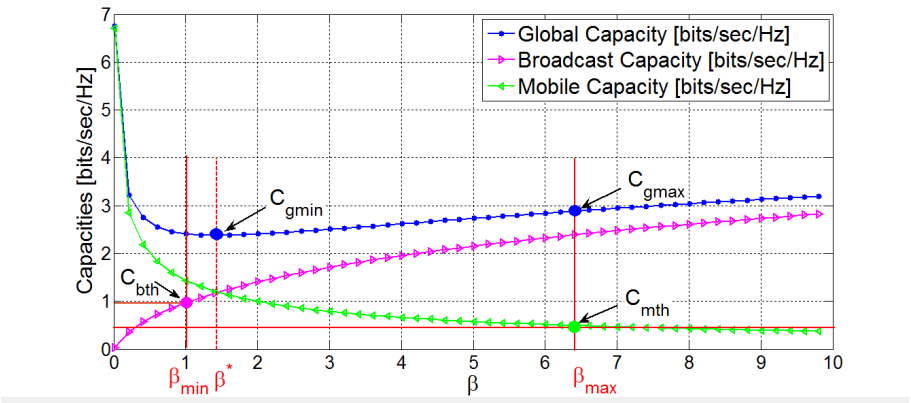

FIGURE 12 – C_g, C_m et C_b en fonction de β, $d = 100$ m, $C_{mth} = 0.5$ bit/s/Hz and $C_{bth} = 1$ bit/s/Hz.

Procédure CCCP

Comme la fonction objective dans (4.10) est une somme de fonction convexe et fonction concave, on a utilisé l'algorithme CCCP. La fonction de Lagrange du problème d'optimisation est donnée par :

$$L(\beta, \lambda, \nu) = (1 + \lambda)C_m(\beta) + (1 + \nu)C_b(\beta) - \lambda C_{mth} - \nu C_{bth} \tag{31}$$

où $\lambda \geq 0$ et $\nu \geq 0$ sont les multiplicateurs de Lagrange qui correspondent respectivement aux contraintes du C_m et du C_b. Par suite, l'algorithme itératif obtenu selon l'algorithme est représenté par [2] :

$$\nabla_\beta L_{\text{vex}}(\beta^{t+1}) = -\nabla_\beta L_{\text{cave}}(\beta^t) \tag{32}$$

où ∇_β représente la dérivée en fonction de β. $L_{\text{vex}}(\beta)$ et $L_{\text{cave}}(\beta)$ sont respectivement les parties convexe et concave de la fonction de Lagrange. β^t et β^{t+1} représentent respectivement la valeur courante et la valeur suivante de β.

Procédure MP

Comme C_m varie d'une manière contradictoire avec C_b, la capacité maximale de C_g se trouve sur l'une de ses deux extrémités comme illustré figure 12. Pour respecter les contraintes de QoS, ces extrémités sont définies par l'intersection des capacités des deux systèmes par leurs contraintes, c.-à-d. c_{mth} et c_{bth}. Par la suite, l'algorithme MP trouve la valeur maximale de C_g parmi ces deux valeurs selon les paramètres des systèmes.

Choix optimal

Comme on a déjà vu, l'algorithme CCCP conduit à un point d'équilibre entre les capacités des deux systèmes. Alors que l'algorithme MP conduit au point maximal strict de la capacité globale tout en maximisant simultanément l'une des deux capacités et minimisant l'autre. La figure 4.7 représente les capacités obtenues avec les deux méthodes en fonction de la distance d'interférence entre BS et BR.

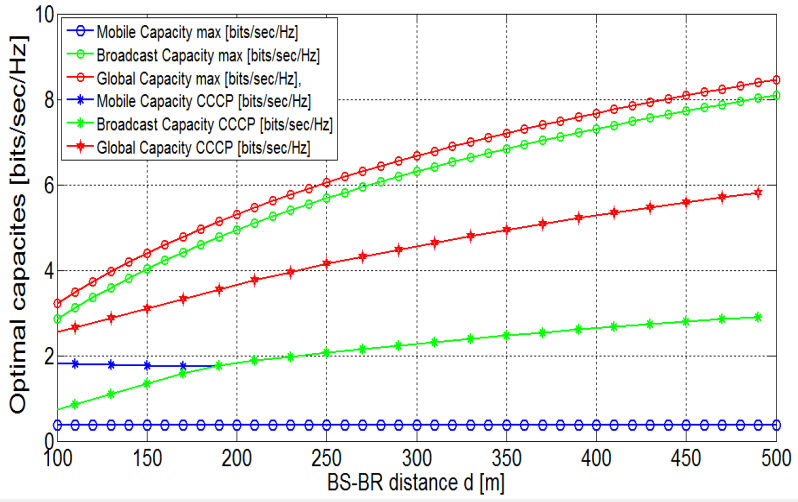

FIGURE 13 – C_g, C_m et C_b obtenues avec Algorithme 1 et Algorithme 2 et selon d, $C_{mth} = C_{bth} = 0.36673$ bits/sec/Hz.

Bien que l'algorithme CCCP converge vers la valeur minimale de la capacité globale, il reste toujours intéressant car il maximise les capacités des deux systèmes LTE et DVB, d'une manière équitable. D'autre part, l'algorithme MP maximise la

capacité globale du système mais en favorisant une des deux capacités sur l'autre. Ces deux algorithmes sont intéressants car ils sont complémentaires. Par conséquent, le choix optimal entre les résultats des deux algorithmes est effectué selon le besoin et la condition requise des opérateurs.

Chapitre 5
Efficacité spectrale dans les réseaux DVB et LTE en fonction de leur chevauchement spectral

Dans les chapitres précédents, l'interférence entre DVB et LTE a été étudiée en considérant que les deux systèmes se recouvraient totalement. De plus, il a été considéré qu'une sous-porteuse d'un système interférait seulement avec un nombre fini de sous-porteuses et non pas l'ensemble du spectre. Dans ce chapitre, nous étudions le cas de recouvrement spectral partiel dans le but d'évaluer l'effet de variation du taux de recouvrement entre les bandes passantes des deux systèmes sur l'efficacité spectrale. Un modèle de signal par banc de filtre est proposé afin de prendre en compte l'asynchronisme temporel des deux technologies ainsi que des fréquences d'échantillonnage différentes.

Modèle de signaux et notations

La figure 14 présente le chevauchement spectral entre les deux bandes LTE et DVB ainsi que les notations utilisées. Dans cette figure, Δf_0 représente la plage fréquentielle recouverte entre les deux bandes B et B' de fréquences centrales respectives f_c et f'_c. On définit le taux de recouvrement par

$$\alpha = \frac{\Delta f_0}{B_{\min}} = \frac{1+\chi}{2\chi} - \frac{\Delta f}{B_{\min}} \tag{33}$$

avec $\chi = \frac{B_{\min}}{B_{\max}}$ et $B_{\min} = \min\{B, B'\}$ et $B_{\max} = \max\{B, B'\}$.

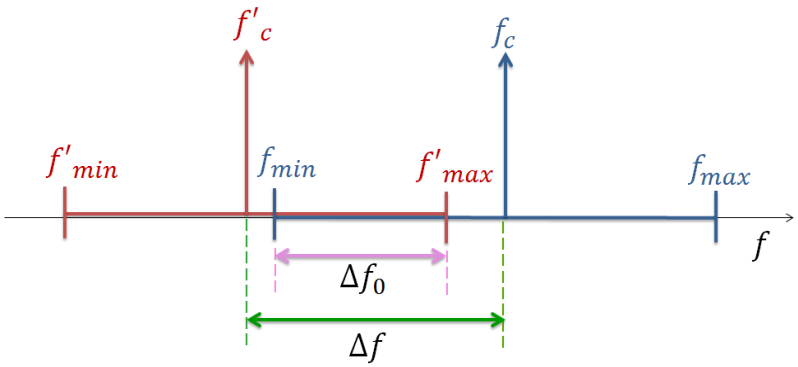

Figure 14 – Présentation du recouvrement spectral

Les systèmes DVB et LTE n'ont pas les mêmes paramètres de modulation OFDM, e.g. durée symbole, fréquence d'échantillonnage. L'objectif du chapitre est de déter-

miner la variance de l'interférence créée par un système sur l'autre lorsqu'un recouvrement partiel existe entre les deux systèmes. La présence d'un signal interférent détruit l'orthogonalité entre sous-porteuses du signal d'intérêt et génère de l'interférence entre symboles qu'il est non trivial de modéliser finement lorsque les deux systèmes n'ont pas les mêmes caractéristiques sur la modulation OFDM.

Modèle du signal

La forme d'onde OFDM avec une mise en forme rectangulaire classique et ajout du CP peut s'écrire

$$s^{(L)}(t) = \frac{1}{\sqrt{T_s^{(L)}}} \sum_{l\in\mathbb{Z}} \sum_{k=0}^{N^{(L)}-1} X_k^{(L)}[l] e^{j2\pi \frac{k}{T_s^{(L)}} t} \Pi\left(\frac{t - lT^{(L)} + T_g^{(L)}}{T^{(L)}}\right) \tag{34}$$

où $X_k^{(L)}[l]$ est le symbole du $l-$ème bloc OFDM transmis sur la $k-$ème sous porteuse. De plus $N^{(L)}$, $T_s^{(L)}$, $T_g^{(L)}$ représentent le nombre de sous porteuses, la durée du symbole OFDM et la durée de l'intervalle de garde du LTE respectivement. De plus, $T^{(L)} = T_s^{(L)} + T_g^{(L)}$. La forme d'onde $\Pi(t)$ est la fonction porte définie par :

$$\Pi(t) = \text{rect}(t) = \begin{cases} 1 & \text{si } 0 \leq t \leq 1 \\ 0 & \text{sinon} \end{cases} \tag{35}$$

Après passage dans le canal multi-trajets, le signal reçu s'exprime :

$$r^{(L)}(t) = \frac{1}{\sqrt{T_s^{(L)}}} \sum_{l\in\mathbb{Z}} \sum_{k=0}^{N^{(L)}-1} \sum_{n=1}^{L} X_k^{(L)}[l] h_n^{(L)} e^{j2\pi \frac{k}{T_s^{(L)}} \left(t-\tau_n^{(L)}\right)} \Pi\left(\frac{t - \tau_n^{(L)} - lT^{(L)} + T_g^{(L)}}{T^{(L)}}\right) \tag{36}$$

où $h_n^{(L)}$ est le coefficient complexe du $n-$ème trajet supposé normalement distribué. Le signal reçu au récepteur LTE est projeté sur les fonctions de base de durée $T_s^{(L)}$ en enlevant le CP avant. Le symbole sur la sous-porteuse p du $m-$ème bloc OFDM s'écrit :

$$\tilde{X}_p^{(L)}[m] = \int_{\mathbb{R}} r^{(L)}(t) \phi_{p,m}^{(L)}(t) dt \tag{37}$$

où $\phi_{p,m}^{(L)}(t)$ est le filtre de réception défini par :

$$\phi_{p,m}^{(L)}(t) = \frac{1}{\sqrt{T_s^{(L)}}} e^{-j2\pi \frac{p}{T_s^{(L)}} t} \Pi\left(\frac{t - mT^{(L)}}{T_s^{(L)}}\right) \tag{38}$$

ce qui donne lorsque l'émetteur et le récepteur sont parfaitement synchronisés :

$$\tilde{X}_p^{(L)}[m] = X_p^{(L)}[m] H_p^{(L)} \tag{39}$$

avec $H_p^{(L)} = \sum_{n=1}^{L} h_n^{(L)} e^{-j2\pi \frac{p}{T_s^{(L)}} \tau_n}$ la réponse fréquentielle du canal LTE sur la $p-$ème sous-porteuse.

De la même manière, le signal transmis par la station DVB s'écrit :

$$s^{(D)}(t) = \frac{1}{\sqrt{T_s^{(D)}}} \sum_{l' \in \mathbb{Z}} \sum_{k'=0}^{N^{(D)}-1} X_{k'}^{(D)}[l'] e^{j2\pi \frac{k'}{T_s^{(D)}} t} \Pi \left(\frac{t - l' T^{(D)} + T_g^{(D)}}{T^{(D)}} \right) \tag{40}$$

où $X_{k'}^{(D)}[l']$ est le symbole du $l'-$ème bloc OFDM transmis sur la $k'-$ème sous porteuse. De plus $N^{(D)}$, $T_s^{(D)}$, $T_g^{(D)}$ sont le nombre de sous porteuses, la durée du symbole OFDM et la durée de l'intervalle de garde du DVB respectivement et $T^{(D)} = T_s^{(D)} + T_g^{(D)}$. De plus, par rapport au LTE le signal DVB est décalé de $\Delta f^{(D)}$ et n'est pas synchronisé sur celui du LTE. Le signal DVB reçu sur l'antenne d'un récepteur LTE s'écrit :

$$\begin{aligned} r^{(D)}(t) &= \frac{e^{j2\pi \Delta f^{(D)} t}}{\sqrt{T_s^{(D)}}} \sum_{l' \in \mathbb{Z}} \sum_{k'=0}^{N^{(D)}-1} \sum_{n'=1}^{L'} X_{k'}^{(D)}[i'] e^{-j2\pi \frac{k'}{T_s^{(D)}} \theta^{(D)} t} q_{n'}^{(D)} e^{j2\pi \frac{k'}{T_s^{(D)}} (t - \tau_{n'}^{(D)})} \\ &\qquad \Pi \left(\frac{t - \tau_{n'}^{(D)} - l' T^{(D)} + T_g^{(D)} - \theta^{(D)}}{T^{(D)}} \right) \end{aligned} \tag{41}$$

où $\theta^{(D)}$ est l'asynchronisme entre le signal DVB et LTE, $q_{n'}^{(D)}$ est le coefficient du $n'-$ème trajet supposé normalement distribué.

$$Q_{k'}^{(D)} = \sum_{n'=1}^{L'} q_{n'}^{(D)} e^{-j2\pi \frac{k'}{T_s^{(D)}} \tau_{n'}} \tag{42}$$

Variance de l'interférence DVB

Le récepteur LTE subit ce signal et le projette sur ses fonctions de base et l'échantillonne au temps $T_s^{(L)}$. Le terme interférent sur la $p-$ème sous porteuse du $n-$ème bloc OFDM est obtenue en calculant :

$$I_p^{(D)}[m] = \int_{\mathbb{R}} r^{(D)}(t) \phi_{p,m}^{(L)}(t) dt \tag{43}$$

Après un calcul fastidieux et en moyennant sur les symboles, le canal et l'asynchronisme entre les deux systèmes, on obtient :

$$V^{(D)} = Pr_\theta \mathbb{E}^{(1)}_{x_{k'}, q_{n'}} [|I_p^{(D)}[m]|^2] + \mathbb{E}^{(2)}_{x_{k'}, \theta, q_{n'}} [|I_p^{(D)}[m]|^2] \tag{44}$$

où

$$\mathbb{E}^{(1)}_{X_{k'}, q_{n'}} \left[|I_p^{(D)}[m]|^2 \right] = \frac{1}{\xi} \sum_{k'=0}^{N_b - 1} \left| \text{sinc} \left(\pi \left(\frac{\Delta f^{(D)} T_s^{(D)}}{\xi} + \frac{k'}{\xi} - p \right) \right) \right|^2 \sum_{n'=1}^{L'} \Omega_{n'}^{(D)} \tag{45}$$

et

$$\begin{aligned}\mathbb{E}^{(2)}_{x_{k'},\theta,q_{n'}}[|I_p^{(D)}[m]|^2] &= \frac{\xi}{\left(T_s^{(D)}\right)^2 T_s^{(L)}} \sum_{k'=0}^{N^{(D)}-1} \frac{1}{\pi^2 A(k')^2} \sum_{n'}^{L'} \frac{\Omega_{n'}}{2} \left\{ 2\frac{T_s^{(D)}}{\xi} \right. \\ &+ \frac{\sin\left(2\pi A(k')\left(\frac{mT^{(D)}}{\xi} + \frac{T_s^{(D)}}{\xi} - B(n', \frac{Ts^{(D)}}{\xi})\right)\right)}{2\pi A(k')} \\ &- \frac{\sin\left(2\pi A(k')\left(\frac{mT^{(D)}}{\xi} + \frac{T_s^{(D)}}{\xi} - B(n', 0)\right)\right)}{2\pi A(k')} \\ &\frac{\sin\left(2\pi A(k')\left(\frac{mT^{(D)}}{\xi} - B(n', \frac{Ts^{(D)}}{\xi})\right)\right)}{2\pi A(k')} \\ &\left. - \frac{\sin\left(2\pi A(k')\left(\frac{mT^{(D)}}{\xi} - B(n', 0)\right)\right)}{2\pi A(k')} \right\} \end{aligned} \quad (46)$$

où $A(k') = \Delta f^{(D)} + \frac{k'}{T_s^{(D)}} - \frac{p}{T_s^{(L)}}$, $B(n', \theta) = l'T^{(D)} - T_g^{(D)} + \tau_{n'}^{(D)} + \theta^{(D)}$, $\xi = \frac{T^{(D)}}{T^{(L)}} > 1$, $\Omega_n^{(D)} = \mathbb{E}\left[|q_{n'}|^2\right]$ et $Pr_\theta(\theta^{(D)}) = 1 - \frac{T_s^{(D)}}{\xi T^{(D)}}$.

Variance de l'interférence LTE

De la même manière, on s'intéresse à la variance de l'interférence produite par le LTE sur un récepteur DVB. Après de longs calculs fastidieux mais en suivant le même raisonnement que précédemment on obtient :

$$\begin{aligned} V^{(L)} &= \mathbb{E}_{X_k,h_n,\theta}\left[|I_{p'}^{(L)}[m']|^2\right] \quad (47) \\ &= \frac{1}{T_s^{(D)} T_s^{(L)} T^{(L)}} \sum_{k=0}^{N^{(L)}-1} \sum_{n=1}^{L} \Omega_n^{(L)} \left(\frac{1}{\pi^2 C(k)^2}(T1 + T2) + \lfloor \xi' \rfloor (T^{(L)})^3 \mathrm{sinc}^2\left(\pi C(k) T^{(L)}\right) \right) \end{aligned}$$

où $T1$ et $T2$ sont définis par :

$$T1 = \frac{1}{2}T^{(L)} + \frac{\sin\left(2\pi C(k)\left(m\xi T^{(L)} - G(n, T^{(L)})\right)\right) - \sin\left(2\pi C(k)\left(m\xi T^{(L)} - G(n,0)\right)\right)}{4\pi C(k)} \quad (48)$$

$$\begin{aligned} T2 &= \frac{1}{2}T^{(L)} + \frac{\sin\left(2\pi C(k)\left(\xi\left(mT^{(L)} + T_s^{(L)}\right) - \lfloor \xi' \rfloor T^{(L)} - G\left(n, T^{(L)}\right)\right)\right)}{4\pi C(k)} \\ &\quad - \frac{\sin\left(2\pi C(k)\left(\xi\left(mT^{(L)} + T_s^{(L)}\right) - \lfloor \xi' \rfloor T^{(L)} - G\left(n, 0\right)\right)\right)}{4\pi C(k)} \end{aligned} \quad (49)$$

où $C(k) = \Delta f^{(L)} + \frac{k}{T_s^{(L)}} - \frac{p'}{T_s^{(D)}}$ et $G\left(n, \theta^{(L)}\right) = lT^{(L)} - T_g^{(L)} + \tau_n^{(L)} + \theta^{(L)}$. Il convient de noter que les deux expressions des variances obtenues ne sont pas symmétriques l'une de l'autre. En effet, le signal LTE interférant sur le DVB n'a pas du tout la même forme que le signal DVB interférant sur le LTE.

Efficacité spectrale globale

L'efficacité spectrale du système global en fonction de α est donnée par :

$$S_T(\alpha) = \frac{1}{B_T(\alpha)}(D^{(L)} + D^{(D)}) \tag{50}$$

où B_T est la bande passante totale du système de coexistence définie par :

$$B_T(\alpha) = B_{max} + (1 - \alpha)B_{min} \tag{51}$$

et $D^{(L)}$ et $D^{(D)}$ sont respectivement les débits de données atteignables sur les

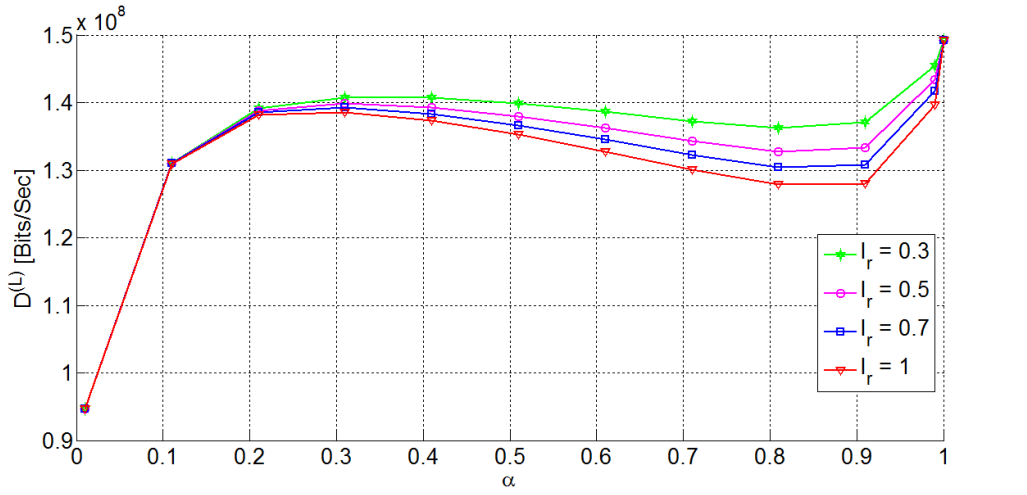

FIGURE 15 – LTE data rate w.r.t. α labeled on interference-cancellation coefficient and $d = 1000$ m.

liens BS-MR et BT-BR. Dans ce chapitre, on autorise également, les systèmes à allouer la puissance sur les sous-porteuses différemment selon qu'elles sont soumises à l'interférence du système adjacent ou pas. Les deux récepteurs, i.e. LTE et DVB, ont également la possibilité de rejeter une partie de l'interférence. Les figures 15, 16 et 17 présentent respectivement les débits des systèmes LTE et DVB et l'efficacité spectrale totale du système LTE+DVB en fonction de la fraction de recouvrement α et pour différentes valeurs du pourcentage d'interférence rejeté. Ces figures montrent

notamment que le débit DVB, $D^{(D)}$, présente un taux de recouvrement optimale pour lequel le débit est maximale fonc de sa capacité à rejeter l'interférence. On remarque également que l'efficacité spectrale globale augmente sensiblement avec α notamment grâce à la forte efficacité spectrale du LTE qui n'est jamais complétement recouvert même pour $\alpha = 1$ lorsque la bande du LTE est de 10 MHz.

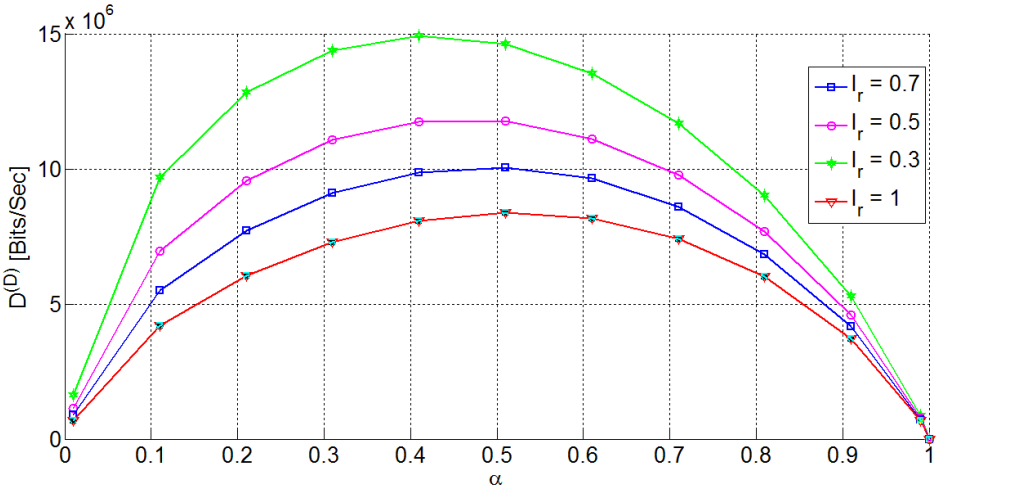

FIGURE 16 – DVB data rate w.r.t. α labeled on interference-cancellation coefficient and $d = 1000$ m.

Conclusion

Dans ce chapitre, on a étudié l'impact du chevauchement spectral entre les bandes passantes des systèmes DVB et LTE qui se recouvrent avec un taux de recouvrement α. L'étude fine de l'efficacité spectrale des deux systèmes passent par une analyse rigoureuse de l'interférence produite par le système adjacent et par l'évaluation de sa puissance. On a montré que celle-ci dépendait bien sûr du recouvrement et des périodes symboles de chaque système. Cette analyse a permis d'étudier la capacité globale atteignable lorsque α varie et que les récepteurs sont équipés d'une capacité de réjection de l'interférence. On a montré notamment qu'une allocation de puissance intelligente prenant en compte la partie recouverte des spectres permet d'augmenter sensiblement les débits atteignables.

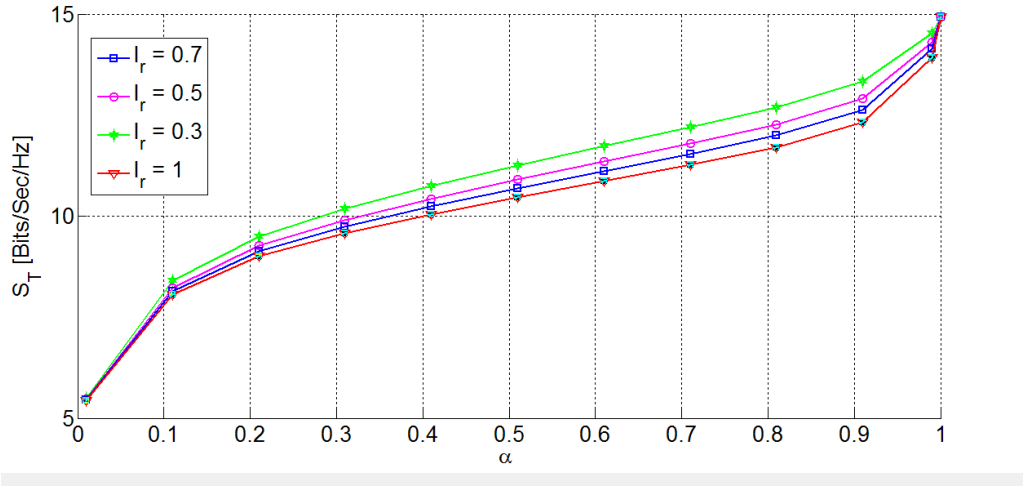

Figure 17 – Total spectral efficiency w.r.t. α labeled on interference-cancellation coefficient and $d = 1000$ m.

Conclusions et perspectives

Dans cette thèse, nous avons étudié la convergence spectrale entre les deux réseaux DVB et LTE. On a étudié la performance de ces deux réseaux avec une coexistence spectrale entre eux mais sans coopération.

Dans le premier chapitre, on a présenté les bases des systèmes DVB et LTE et la possibilité de leur coexistence spectrale au travers d'un état de l'art sur la gestion de leur interférence mutuelle. On a remarqué que les deux technologies présentent des similarités au niveau de l'utilisation de la modulation OFDM (voie descendante du LTE) tout en étant assez différentes de part leurs caractéristiques techniques et leurs paramètres.

Dans le deuxième chapitre, nous avons étudié un problème d'allocation de ressources lorsqu'un système secondaire interfère avec un système primaire dans un scénario de recouvrement spectral ce qui est analogue à une coexistence DVB-LTE. On a dérivé la capacité ergodique du système secondaire sous contraintes de puissance d'interférence moyenne sur le récepteur primaire et de puissance de transmission crête du secondaire. Le débit maximal du secondaire est étudié analytiquement et par simulation ainsi que ses limites d'opération.

Dans le troisième chapitre, la capacité ergodique des systèmes LTE et DVB sous recouvrement spectral total est étudiée. On a analysé le problème de déploiement d'une petite cellule LTE dans une large cellule DVB sous un scénario de recouvrement spectral. Les densités de probabilité des rapports signal à interférence des deux réseaux ont été calculées et la capacité ergodique globale du système DVB+LTE a été dérivée. Les résultats numériques obtenus avec les paramètres réels du DVB et

du LTE ont montré que la capacité globale n'est ni convexe ni concave en fonction des puissances de transmission des deux systèmes.

Dans le chapitre suivant, nous avons proposé de trouver l'allocation de puissance optimale maximisant la capacité ergodique dérivée dans le chapitre précédent. Il a été montré que la capacité ergodique est composée de deux parties, l'une convexe qui est la capacité du mobile et l'autre concave qui est celle du DVB. La capacité globale a ensuite été optimisée par allocation des puissances par sous-porteuse sous contraintes de qualité de service des deux réseaux coexistants. Nous avons d'abord proposé une procédure avec l'algorithme CCCP qui donne l'efficacité spectrale minimale du système global mais qui est un point d'équilibre entre les capacités des deux systèmes pris individuellement. D'autre part, nous avons proposé une procédure qui maximise strictement la somme capacité du système mais induit invariablement de favoriser un système sur l'autre.

Dans le dernier chapitre, nous avons proposé de prendre en compte de manière fine au niveau du signal, les différences de caractéristiques entre les deux technologies afin d'avoir une description la plus précise possible de l'effet d'un recouvrement spectral partiel entre les deux systèmes. Pour cela, nous proposons de revenir à la description continue avec banc de filtres d'un système OFDM. Cela a permis de décrire de manière précise la variance de l'interférence en moyennant sur l'asynchronisme, les symboles et le canal lorsque les deux systèmes interfèrent partiellement. La capacité globale est ensuite étudiée lorsque le récepteur possède une capacité de réjection de l'interférence.

Les perspectives ouvertes dans cette thèse sont nombreuses et pourraient être listées comme suit :

- Extension au cas multi-utilisateurs avec allocation des ressources blocs pour le système LTE.
- Intégration explicite de techniques de réduction de l'interférence à l'aide d'antennes multiples par exemple.
- Etude des performances lorsque les deux systèmes permettent une coopération.

Ce dernier point nous semble notamment très important. En effet, les deux communautés ont toutes deux des contenus et des services similaires à offrir aux utilisateurs, mais pour le moment la "convergence" envisagée reste théorique. Par exemple, afin d'améliorer les performances présentées dans cette thèse, qui présente finalement deux systèmes interférants, un codage de l'interférence par "dirty paper coding" entre les deux systèmes pourrait permettre d'améliorer sensiblement les débits, puisque ce schéma permet d'atteindre la capacité du canal broadcast. Il s'agirait notamment d'étudier quelles informations devraient être échangées entre les deux systèmes pour quelles performances théoriques.

Contents

List of acronyms

ACI	Adjacent Channel Interference
ANR	French National Research Foundation
AWGN	Additive White Gaussian Noise
BB	Baseband
BER	Bit error rate
BR	Broadcast Receiver
BS	Base Station
BT	Broadcast Transmitter
CCCP	Concave Convex Procedure
CDMA	Code Division Multiple Access
CFR	Channel Frequency Response
CIR	Channel Impulse Response
C/N	Carrier to Noise Ratio
CP	Cyclic Prefix
CR	Cognitive Radio
DSSS	Direct-sequence Spread Spectrum
DTT	Digital Terrestrial Television
DFT	Discrete Fourier Transform
DVB	Digital Video Broadcasting
DVB-NGH	Digital Video Broadcasting-Next Generation Handheld
DVB-T	Digital Video Broadcasting Terrestrial
DVB-T2	Second Generation for Digital Video Broadcasting-Terrestrial
EDST	Doctoral School of Sciences and Technologies
eMBMS	evolved Multimedia Broadcast Multicast Service
eNB	evolved Nodes B

EPC	Evolved Packet Core
EPS	Evolved Packet System
EU	European Union
E-UTRA	Evolved Universal Terrestrial Radio Access
E-UTRAN	Evolved Universal Terrestrial Radio Access Network
FFT	Fast Fourier Transform
FEF	Future Extension Frame
FIC	Full Interference Channel
GI	Guard Interval
GSM	Global System for Mobile Communications
HD	High Definition
IBI	Inter Block Interference
ICI	Inter-carrier Interference
IDFT	Inverse Discrete Fourier Transform
IETR	Institute of Electronics and Telecommunications of Rennes
IFFT	Inverse Fast Fourier Transform
IMT	International Mobile Telecommunications
IMB	Integrated Mobile Broadcasting
INSA	National Institute of Applied Sciences
IP	Internet Protocol
IR	Impulse response
ISI	Inter symbol interference
KKT	Karush Kuhn Tucker
L1	Layer 1
LoS	Line of Sight
LTE	Long Term Evolution
MIMO	Multiple-Input Multiple-Output
MODCOD	Modulation and Coding
MR	Mobile Receiver
MS	Mobile Station
MUD-MLSEs	Multiuser Detection Maximum Likelihood Sequence Estimators
NITA	National IT and Telecom Agency
OFDM	Orthogonal Frequency Division Multiplexing
OFDMA	Orthogonal Frequency Division Multiple Access
OOB	Out Of Bound
OSA	Opportunistic Spectrum Access
PAPR	Peak to Average Power Ratio
PDF	Probability Density Function
PF	Picture failure
PLP	Physical Layer Pipe
PSD	Power Spectral density

PU	Primary User
QAM	Quadrature Amplitude Modulation
QoS	Quality of Service
RB	Resource Block
RF	Radio Frequency
RO	Receiver Overload
SC-FDMA	Single Carrier Frequency Division Multiple Access
SD	Standard Definition
SEM	Spectral Emission Mask
SINR	Signal to Interference and Noise Ratio
SIR	Signal to Interference Ratio
SS	Spectrum Sharing
SU	Secondary User
3G	3rd generation
3GPP	3rd Generation Partnership Project
TPA	Transmit Power Allocation
UHF	Ultra High Frequency
UL	Lebanese University
UMTS	Universal Mobile Telecommunications System
UT	Technological Universities
VHF	Very High Frequency
WLAN	Wireless Local Area Networks
WSD	White Space Devices

Notations

a_l	l^{th} propagation path attenuation
a_p	Peak amplitude of the dominant non fading component
a_{ray}	Rayleigh distributed envelope amplitude of the received signal
a_{ric}	Rician distributed envelope amplitude of the received signal
B	Channel bandwidth
$\mathrm{B_b}$	Broadcast channel bandwidth
B_c	Coherence bandwidth
$\mathrm{b_k}$	k^{th} sub-band
$\mathrm{B_m}$	Mobile channel bandwidth
d	BT-MR protection distance
d_b	Broadcast cell radius
d_m	Mobile cell distance
d_t	BS-BT distance
$\delta(t)$	Dirac function
dom	function domain
d_0	Normalized reference distance
$f_0(x)$	Objective function of x
f_c	Central subcarrier frequency
f_d	Doppler frequency shift
$f_{d_{max}}$	Maximum Doppler frequency shift
$f_j(x)$	Inequality constraint functions of x
F_N	$N * N$ FFT matrix
f_0	First subcarrier frequency
γ_b	SINR of the broadcast signal
$\tilde{\gamma}_b$	SIR of the broadcast signal
γ_m	SINR of the mobile signal

$\tilde{\gamma}_m$	SIR of the mobile signal
$[]^H$	Complex conjugate Hermitian
H_{CIR}	$N * N$ circulant matrix
H_{ICI}	$P_{CP} * P_{CP}$ lower triangular Toeplitz matrix
H_{ISI}	$P_{CP} * P_{CP}$ upper triangular Toeplitz matrix
$h^{(b)}$	Channel impulse response of BT-BR link
$h^{(m)}$	Channel impulse response of BS-MR link
$h_j(x)$	Equality constraint functions of x
$\mathbf{h}_L$	$L * 1$ channel impulse response vector
$\mathbf{h}_N$	$N * 1$ channel coefficient vector
i	OFDM transmitted block index
I_N	$N * N$ Identity matrix
k	OFDM sub-carrier index of the i^{th} transmitted block at the modulation phase
K_i	Number of inequality constraints in the standard optimization problem
K_e	Number of equality constraints in the standard optimization problem
l	Propagation path index
L	Channel length
λ	Lagrangian multiplier vector corresponding to the inequality constraints
L_{data}	Number of data symbols in T2 Frame
L_F	Number of symbols in T2 Frame
l_p	Path loss
l_p^b	Path loss on the link BT-BR
l_p^{bm}	Path loss on the interference link BT-MR
l_p^m	Path loss on the interference link BS-MR
l_p^{mb}	Path loss on the link BS-BR
M	Number of observation samples
μ_A	Non centrality parameter of state 'ON'.
n	Temporal index
N	FFT length
N_{CP}	Cyclic prefix duration
N_{FEF}	Number of FEF parts in a DVB-T2 super frame
N_{P2}	Number of P2 symbols
N_{T2}	Number of T2 frames
N_0	White noise spectral density
ν	Lagrangian multiplier vector corresponding to the equality constraints
P	Average received total power

P_b	Total broadcast power
p_b	Broadcast subcarrier power
P_{CP}	$N_{CP} + N$
p_k	k^{th} subcarrier power
P_m	Total mobile power
p_m	Mobile subcarrier power
p	OFDM sub-carrier index at the demodulation phase
$q^{(b)}$	Channel impulse response of BT-MR interfering link
Q_{inter}	Interference limit value
$q^{(m)}$	Channel impulse response of BS-BR interfering link
Q_{peak}	Peak power value
R_b	Number of DVB subcarriers interfering on one LTE subcarrier
$\mathbf{R}_{CP}$	Cyclic prefix removal matrix
R_m	Ratio of LTE interfering subcarrier to one DVB subcarrier
σ^2	variance
$s(t)$	transmitted OFDM signal in time domain
$[]^T$	Complex conjugate Transpose
t	Time presentation
τ_b	Broadcast sampling period
τ_l	l^{th} propagation path delay
τ_m	Mobile sampling period
τ_{max}	Maximum length of the channel spreading
τ_s	Sampling period
T	OFDM Symbol period
T^b	DVB OFDM symbol period
T^m	LTE OFDM symbol period
T_c	Coherence time
$\mathbf{T}_{CP}$	Cyclic prefix insertion matrix
T_F	Total T2 frame duration
T_{FEF}	FEF part duration
T_g	Guard interval duration
T_g^b	DVB Guard interval duration
T_g^m	LTE Guard interval duration
T_{P1}	P1 symbol duration
T_s	Useful OFDM symbol period
T_s^b	Useful DVB OFDM symbol period
T_s^m	Useful LTE OFDM symbol period
T_{SF}	Super frame duration
η	Path loss exponent
$w^[i]$	AWGN term
$\mathbf{W}[i]$	AWGN vector after CP removal

$\mathbf{W}^{CP}[i]$	AWGN vector before CP removal
$w^{k,n}$	FFT matrix element
$\mathbf{y}[i]$	i-th received OFDM signal block
$\mathbf{x}[i]$	i-th transmitted OFDM signal block
$\mathbf{X}[i]$	i-th FFT input data block
x_b	BT transmitted signal
x_m	BS transmitted signal
ξ_s	Sensing metric
$y(t)$	Received OFDM signal in time domain
z_q	q^{th} sub-carrier output after demodulation
0_{N*N}	all-zeros $N * N$ matrix

List of Figures

List of Tables

Introduction

SINCE the launch of the first numerical mobile telecommunication networks in the nineties, the quantity of the transmitted data over these networks are increasing year by year. Indeed, the offered data rate increased from a few Kbps with Global System for Mobile Communications (GSM) standard in the nineties to hundreds of Mbps today with LTE standard. Currently, most operators are experiencing huge growth in data rate demand which will soon lead to network congestions. This is also due to the increasing popularity of mobile terminals such as smart-phones and tablets. These terminals allow to access several services hungry in bandwidth especially video services which represent two-thirds of the mobile data traffic. The users today are intensive consumers of internet, including web radio listening, file downloading and sharing, discussions on social networks (Facebook, Twitter, etc), web TV but also video on demand, games online,etc. Moreover, users still keep a high level of expectation whatever the location, time and situation.

The non stop evolution of integrated cellular phones providing high speed data transmission and the implementation of new services requiring high data rate transmission have forced mobile operators to cope with this increasing demand on available spectrum. To address this rising problem, the 3rd Generation Partnership Project (3GPP) has launched Long-Term Evolution (LTE) standard to ensure higher performance, backward compatibility and wide applications. Throughout consecutive releases, LTE project aimed at overcoming setbacks and conflicts with existing systems to ensure stability and higher capabilities.

At the same time, the universal TV broadcasting systems have moved from analog to digital to satisfy the increasing demand on higher quality TV experience. Switching from analog to digital, a valuable part of the overcrowded frequency spectrum previously reserved for analog TV is released. This band, designated as digital dividend, is currently under consideration by mobile operators. For instance,

in France, according to the European commission recommendation, a part of the released spectrum (790-862 MHz) is already deployed by LTE networks [6].

Technically wise, different similarities exist between Digital Video Broadcasting (DVB) and LTE networks. This includes, but not limited to, waveform design through OFDM, MIMO techniques, coding schemes, frames duration, application mode, etc. Due to these similarities, a study item was initiated in 2011 to launch a possible collaboration between the two standardization groups so that a common technical framework could be initiated and evolved. Since 2011, studies on cooperation and/or coexistence between cellular and broadcasting technologies have slowly evolved due to different reasons, not always on a technical basis. The Mobile and Multimedia (M^3) project, funded by the French National Research Foundation (ANR), studied the possibility to merge broadcast and cellular technologies specified for digital TV. This includes the next generation broadcasting 3GPP (Evolved Multimedia Broadcast Multicast Service (E-MBMS) and/or its advanced version) and DVB standards as DVB - Next Generation Handled (DVB-NGH). This is due to the fact that similar demand from users in terms mobile TV and multimedia can be addressed by both technologies, in particular the Integrated Mobile Broadcasting (IMB) standardized by the 3GPP group can offer mobile broadcasting services to cellular subscribers.

On the other hand, as the spectrum congestion becomes a major issue to develop new wireless services, the spectral overlap of some wireless technologies is more and more envisaged. A part of M^3 project was dedicated to this point and this work takes place in that part. This thesis aims at studying the spectral convergence between Second Generation for Digital Video Broadcasting-Terrestrial (DVB-T2) and LTE networks, by deploying a small LTE cell in a large DVB cell, and therefore studying the performance of these two overlapping networks. The convergence can be envisaged from two points of view : (i) one of both networks could access opportunistically as a cognitive radio on the spectrum of the other considered as primary, (ii) both networks could share the same spectrum or a part of it. In the first case, since secondary user, e.g. LTE user, accesses opportunistically to the primary user's spectrum, quality of service (QoS) may be not guaranteed. In the second case, the mutual interference created may be higher than in the first case but an access is guaranteed and the situation might not be worse than a full frequency reuse deployment in LTE systems. The goal of our thesis is to see how QoS, i.e. spectral efficiencies, of both networks can be guaranteed in a spectral convergence scenario in both cases mentioned above.

Thesis overview and contributions

This thesis was carried out at the Institute of Electronics and Telecommunications of Rennes (IETR) in Rennes, France and at Lebanese University (UL) in Hadath, Lebanon under co-advise collaboration agreement between the Doctoral School of Sciences and Technologies (EDST) of UL and National Institute of Applied Sciences (INSA) of Rennes. This thesis was among the first theses organized under the co-supervision program between the Lebanese University and the network "Technological Universities/INSA (UT/INSA)". The manuscript is organized as follows :

In **Chapter 1**, we firstly present the background materials that is used throughout the thesis. General basic prerequisites on wireless transmission, including OFDM modulation and demodulation blocks and channel models adopted in this work, are presented. We then go through some convex optimization background and we present the Concave Convex Procedure (CCCP) and their applicability conditions are also provided. Next, we introduce the general context of our research by presenting the PHY layer characteristics of LTE and DVB. A review of solutions on the coexistence between DVB and LTE existing in literature is provided.

Chapter 2 deals with our first contribution on the convergence between DVB and LTE. In this chapter, we propose a coexistence model between the broadcast network considered as primary and the mobile network considered as secondary. This coexistence model is similar to the one discussed in [3] but in our model the secondary network shares the primary network spectrum without having any idea about its activity, contrary to [3] where the secondary network detects the primary spectrum occupation thanks to an energy detector in order to limit as much as possible the cross-interference. Our extension consists in the maximization of the secondary spectral efficiency under constraints of limiting interference power at the primary receiver and by considering the interfering link from the primary transmitter to the secondary receiver. This work has led to the publication [C1].

In **Chapter 3**, primary and secondary systems are explicitly defined as DVB and LTE systems. Hence, the problem of global ergodic capacity expression, i.e. defined as the summation of both ergodic capacities, LTE and DVB, is analysed with the assumption that both systems coexist on the same bandwidth but with different characteristics, i.e. different sub-carriers spacing, different transmission power and different cell radius. We start by a simple interference model between sub-carriers and we derive analytically the global ergodic capacity in closed-form with Rayleigh fading channel on each link. The capacity of each system is also expressed as a function of power ratio between DVB and LTE and some basic system characteristics. The influence of real system parameters on the global, DVB and LTE data rates is investigated. The work presented in this chapter has led to the publication [C2].

In **Chapter 4**, we focus on resource allocation maximizing the global ergodic ca-

pacity, derived in the previous chapter. Maximization is done by taking into account constraints on DVB-T2 and LTE capacities, to guarantee the QoS of both networks. Both systems being largely unbalanced in term of cell-size, maximizing the global capacity generally leads to favor one system to another. To avoid this drawback, we propose a CCCP which is not max-capacity achieving but leads to a fair sharing of spectral efficiency between both systems. This work has led to the publication [C3].

The interference model used so far is highly idealized, where timing asynchronization and non equal sampling rate between both systems have not been taken into account. In **Chapter 5**, an accurate interference signal model is detailed where differences between systems are finely written. One of the main difficulty comes from the fact that both system sampling rates are not multiple from each other and the reception of the mixed signal from one receiver implies a linear, variant in time filtering. The received discrete time OFDM signal cannot be expressed as simply as usual. The interference is expressed as a function of the frequency overlap between LTE and DVB-T2 bandwidths. We hence evaluate the global spectral efficiency as a function of overlap ratio and assuming that the receiver is able to reject a part of interference.

Finally, this work is summarized by providing some **conclusions and perspectives**.

List of Publications

International Conferences

[C1] - Ghanem, M. ; Bawab, H. ; Bazzi, O. ; Nasser, Y. ; Mary, P. ; Hélard, J.F., "Closed-form expression of the ergodic capacity in a cognitive radio link under power constraints," Ultra Modern Telecommunications and Control Systems and Workshops (ICUMT), 2014 6th International Congress on , vol., no., pp.468,472, 6-8 Oct. 2014.

[C2] - Bawab, H. ; Mary, P. ; Hélard, J.-F. ; Nasser, Y. ; Bazzi, O., "Global Ergodic Capacity Closed-Form Expression of Coexisting DVB-LTE-Like Systems," Vehicular Technology Conference (VTC Spring), 2014 IEEE 79th , vol., no., pp.1,5, 18-21 May 2014.

[C3] - Bawab, H. ; Mary, P. ; Hélard, J.F. ; Nasser, Y. ; Bazzi, O., "Ergodic capacity optimization in coexisting DVB-LTE-like systems," Ultra Modern Telecommunications and Control Systems and Workshops (ICUMT), 2014 6th International Congress on, vol., no., pp.54,59, 6-8 Oct. 2014 [Best Paper AWARD].

1 State of Art and Background

THIS chapter consists in defining basic background that will be used throughout the thesis. In the first part, some basic materials about the transmission scheme in a typical orthogonal frequency division multiplexing (OFDM) technology including the propagation channel models and OFDM modulation and demodulation are presented. The channel capacity in OFDM systems is also presented. In a second part, different optimization methods are described with their conditions and their constraints of operation. The third and final part gives the definition of LTE and DVB networks with their parameters.

1.1 Transmission scheme

Each communication system has a common general structure as illustrated in Fig. 1.1. This block diagram is limited to the baseband (BB) equivalent chain and is composed of six major elements : channel encoder, mapper, channel, equalizer, demapper and channel decoder. Channel encoder provides redundancy to make the information signal robust to channel fading and noise. The mapper maps the coded bit stream into complex symbols, chosen in a finite constellation pattern and produce a temporal waveform according to a pulse shaping filter. The signal is then sent through the BB equivalent channel impulse response and noise and interferences are eventually added. Before being processed, the signal is match-filtered and symbol-time sampled. Then the multipath channel is compensated thanks to an equalizer. The demapper converts complex symbols to output bit stream which is then processed by the channel decoder to recover the information bits.

Several physical properties of wireless propagation produce attenuation and distortion on the received signal like multiple reflections and diffractions on the surrounding objects between transmitter and receiver. Section 1.1.1 presents different fading channel models used in the following chapters.

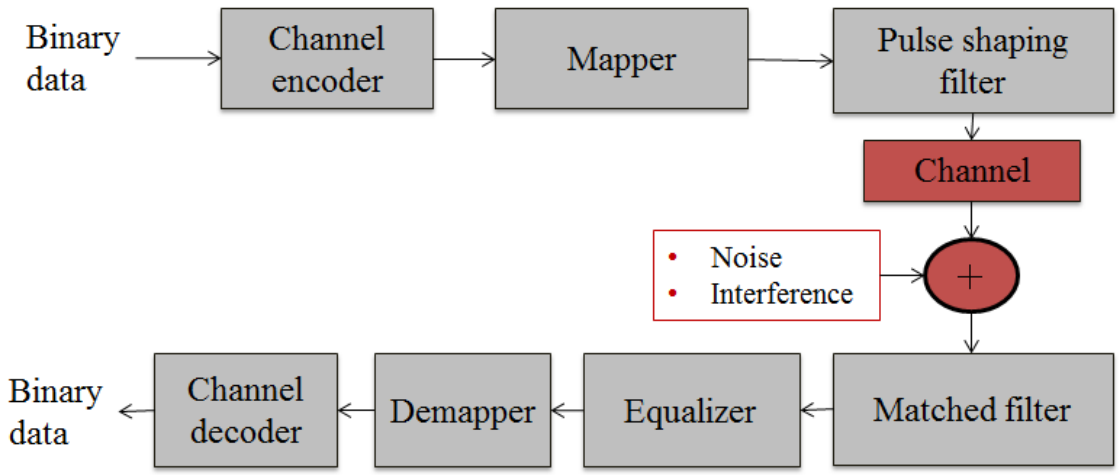

Figure 1.1 – General communication channel block diagram

1.1.1 Channel propagation models

In wireless communications, the transmitted signal is exposed to several variations during its passage through the communication channel. Due to the distance between transmitter and receiver, the signal power undergoes an attenuation that is called path loss attenuation which can be expressed as :

$$l_p = 1/d^{\eta} \tag{1.1}$$

with η is the path loss exponent, d is the distance between transmitter and receiver and considering a normalized reference distance d_0.

1.1.1.1 Additive White Gaussian Noise (AWGN) Channel

The AWGN channel is the most fundamental channel model. In this model, in addition to eventually path loss effect described above, a white Gaussian noise is simply added to the signal sent by the transmitter. It allows to derive performance bounds for system evaluation. The AWGN model is the most ideal and simple channel model that does not account for fading, frequency selectivity, interference, nonlinearity or dispersion. Although being simple, this model is close to real situations with low data rate and mobility and when transmitter and receiver are in a line of sight (LOS) like in spatial communications. The source of AWGN is the thermal noise at the receiver. It is often used as a channel model in which the only deterioration to communication is a linear addition of white noise with a constant spectral density and a Gaussian distribution of amplitude. It is characterized by a one-sided Power Spectral Density (PSD) N_0 Watts/Hz.

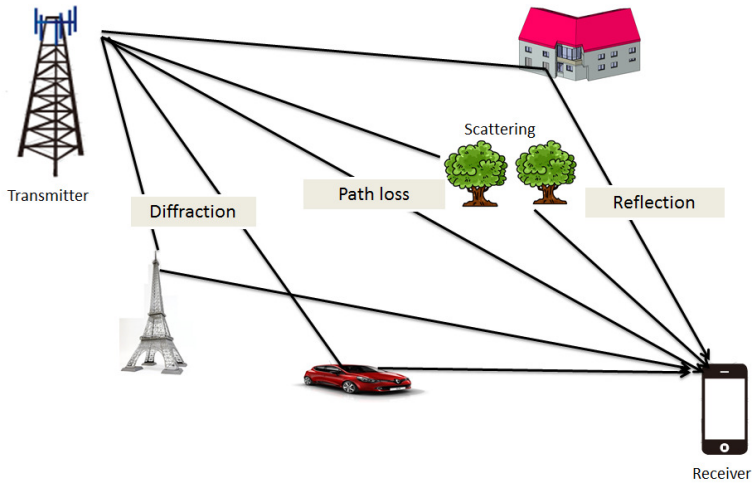

Figure 1.2 – Multipath channel

1.1.1.2 Multipath Channel

The existence of different surrounding objects with reflecting surfaces in the physical channel, causes scattering, reflection and diffraction of the transmitted signal. These phenomena create several copies of the transmitted signal with different amplitudes, phases, and time delays. The physical phenomena experienced by the transmitted signal are illustrated in Fig.1.2. Due to the multiple reflections, the channel is called multipath channel. Therefore, the channel impulse response (CIR) can be expressed as :

$$h(t) = \sum_{l} a_l \delta(t - \tau_l) \tag{1.2}$$

where a_l and τ_l are respectively the attenuation and delay of the l^{th} propagation path. $\delta(t)$ is the Dirac function at time t. This delay spread leads to Inter symbol Interference (ISI) and frequency selectivity, in Fourier domain, which causes severe distortion at the reception. The characteristic of the multipath channel can be viewed in the frequency domain by the Channel Frequency Response (CFR) expressed as :

$$H(f) = \sum_{l} a_l e^{-j2\pi f \tau_l} \tag{1.3}$$

Moreover, the relative motion between transmitter and receiver causes a shift in the carrier frequency which is called the Doppler frequency shift f_d. $f_{d_{max}} = \frac{f_0 v}{c}$ is defined as the maximum Doppler frequency shift while f_0 the carrier frequency, v the relative velocity of the receiver and c the velocity of waves. The frequency shift caused by the Doppler effect affects the signal demodulation at the receiver.

Rayleigh and Rician fading

The relative motion of transmitter and receiver implies a time variation of CIR described above. The magnitude of each equivalent discrete tap is then described by a statistical law depending on the environment. If no Line of Sight (NLOS) occurs between transmitter and receiver, CIR taps are modeled under some conditions by Rayleigh distribution [7]. Therefore, the envelope (magnitude) of the received signal is distributed with the Rayleigh probability density function (PDF) expressed by :

$$P_{ray}(a_{ray}) = \frac{a_{ray}}{\sigma^2_{ray}} \exp^{-a^2_{ray}/(2\sigma^2)} \tag{1.4}$$

with a_{ray} is the Rayleigh distributed envelope amplitude of the received signal and $2\sigma^2$ is the mean power of the multipath signal.

When a strong LOS propagation exists, which means that there is a dominant signal component, the channel is often considered as Rician fading channel. In this case, the received signal envelope follows the Rician distribution. At the receiver, the signal appears as a continuous component added with a random multi-path component [7]. The amplitude PDF of the Rician distributed variable is given by :

$$P_{ric}(a_{ric}|a_p, \sigma) = \frac{a_{ric}}{\sigma^2} \exp(\frac{-(a^2_{ric} + a^2_p)}{2\sigma^2}) I_0(\frac{a_{ric}a_p}{\sigma^2}) \tag{1.5}$$

with a_{ric} being the Rician distributed envelope amplitude of the received signal, a_p is the peak amplitude of the specular component and I_0 is the modified zero order Bessel function of the first kind.

1.1.2 Coherence time and frequency

In communication systems, it is necessary to know the range of the time and frequency in which the transmitted signal is non-varying.

1.1.2.1 Coherence bandwidth and coherence Time

Coherence bandwidth B_c is a statistical measurement of the range of frequencies over which the channel response holds approximately the same gain and linear phase for all spectral components. In other term, B_c is the approximate maximum bandwidth or frequency interval such as within its borders the frequency attenuations have strong potential similarities and the signal experiences the same fading. Hence, coherence bandwidth gives information on how strong will be the frequency selectivity on the designed system. The coherence bandwidth estimation is the reciprocal of the maximum delay spread estimation and is classically defined as :

$$B_c \approx \frac{1}{\tau_{max}} \tag{1.6}$$

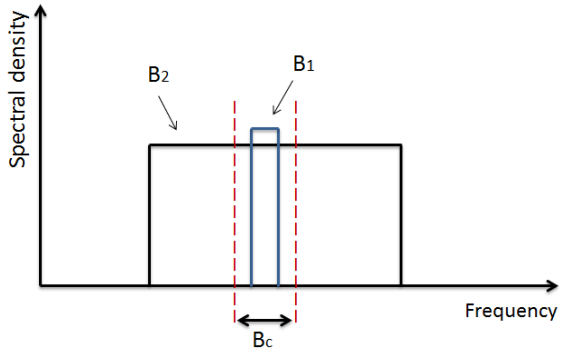

Figure 1.3 – Frequency selective and flat fading

where τ_{max} is the maximum channel spreading length.

In time domain, the coherence time $\mathrm{T_c}$ is the time duration within which the channel response is basically unchanged, i.e. channel characteristics can be considered as time-invariant. This quantity depends on the rate of the variation of the channel conditions, more specifically on the maximum Doppler frequency shift. Hence, the coherence time is often approximated as :

$$T_c \approx \frac{1}{f_{d_{max}}} \tag{1.7}$$

1.1.2.2 Flat and selective frequency channel

In the frequency domain, if the signal bandwidth B is smaller than the coherence bandwidth, i.e. $B < \mathrm{B_c}$, the channel affects all signal frequency components in the same manner. This is the case of flat fading illustrated in Fig.1.3, where $\mathrm{B_1}$ is the signal bandwidth for which flat fading occurs.

On the contrary, if the signal bandwidth is larger than the coherence bandwidth, i.e. $B > \approx B_c$, all signal frequency components are not affected equally by the channel and the latter is said frequency selective. Some frequency components suffer destructive recombinations while others experience constructive multipath summations. The signal bandwidth $\mathrm{B_2}$ in Fig.1.3 is the bandwidth for which a frequency selective channel occurs.

1.1.2.3 Fast and slow fading

In time domain, if the signal symbol duration T is shorter than the coherence time, i.e. $T < \mathrm{T_c}$, the channel changes at a rate slower than the signal symbol rate and slow fading occurs [7].

If the signal symbol duration is longer or equal than the coherence time, i.e. $T >\approx \mathrm{T_c}$, the channel varies significantly within a symbol duration and this type of fading is called fast fading.

Summary

Combining the selectivity/non-selectivity fading in frequency and the fast/slow fading in time, the channel can be classified into four cases :

1. Flat fading with slow fading : $B < \mathrm{B_c}$ and $T < \mathrm{T_c}$.
2. Flat fading with Fast fading : $B < \mathrm{B_c}$ and $T >\approx \mathrm{T_c}$.
3. Frequency-selective fading with slow fading : $B > \mathrm{B_c}$ and $T < \mathrm{T_c}$.
4. Frequency-selective fading with fast fading : $B > \mathrm{B_c}$ and $T >\approx \mathrm{T_c}$.

1.1.3 OFDM modulation

When consecutive signal symbols are spread and overlapped, an interference phenomenon is appearing that is the ISI. It is caused by the channel memory effects such as the dispersion of signal arrival time with the multipath channel which weakens the receiver performance. In order to avoid ISI, the symbol duration should be designed significantly longer than the maximum time delay spread of CIR. Multi-carrier transmission comes as a possible solution to solve this problem.

To lengthen the symbol duration, multi-carrier modulation divides the bandwidth in several sub-bands. Hence, the high speed data rate stream is transmitted in multiple low speed data rate streams which can tolerate or correct the ISI effect. In this context, multi-carrier modulation technology OFDM uses several sub-bands as subcarriers to transmit data symbols in parallel instead of sending them over one carrier. Consequently, It consists in splitting the symbols over N subcarriers with small rate. Therefore, a data symbol stream each of duration t_s in single carrier modulation is divided into N parallel streams in OFDM modulation where each of them is transmitted over the duration $T_s = N \cdot t_s$ which represents the useful OFDM symbol duration and where t_s is the original symbol period. N is the number of subcarriers used in OFDM modulator.

1.1.3.1 OFDM basics

Sub-carriers should be spaced and separated in frequency domain in order to forbid the mutual interference between them. Mathematically, sub-carriers should be "orthogonal" in the scalar product sense. With a rectangular pulse shaping filter on each sub-stream, the sub-carriers spacing can be reduced to $1/T_s$ while maintaining the orthogonality conditions between them. Such an OFDM spectrum is illustrated

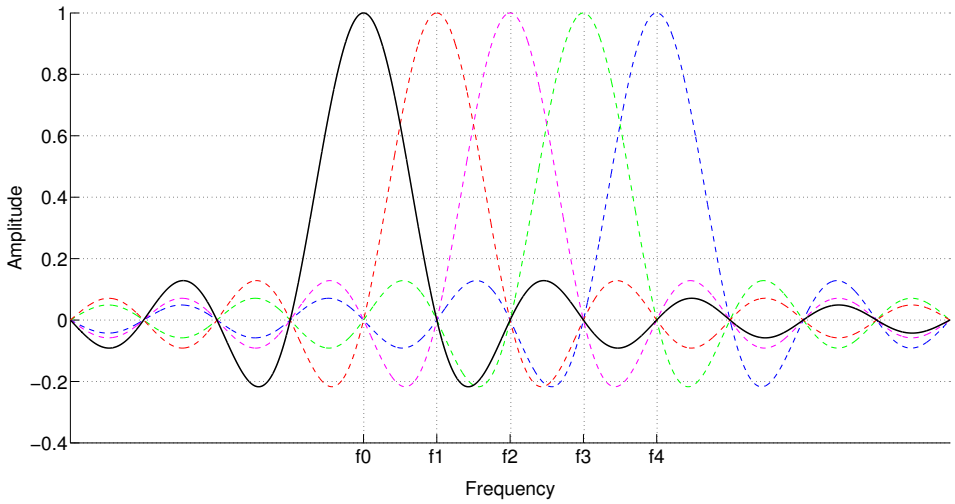

Figure 1.4 – OFDM signal waveform in frequency domain

on Fig.1.4 where the classical sinus cardinal spectrum can be observed. The frequency overlap of each sub-carrier is interference-free provided that the sampling is done precisely at the sub-carrier center frequency where the peak of each sub-carrier is located at the null values of the other subcarriers waveforms.

1.1.3.2 OFDM modulation

As shown in Fig.1.5, serial data stream is converted to N parallel low-speed streams then modulated by the Inverse Discrete Fourier Transform (IDFT). The parallel data symbols are transmitted block-wise. Each data block contains N data symbols. The i-th transmitted block is an $N \times 1$ column vector defined as :

$$\mathbf{x}[i] = [X_0[i], X_1[i], ..., X_{N-1}[i]]^T \tag{1.8}$$

where $X_k[i] = X_{k+iN}, 0 \leq k \leq N-1$. The transmitted Radio Frequency (RF) multi-carrier signal, which is the sum of the individual signals, can be expressed by :

$$s(t) = \frac{1}{\sqrt{T_s}} \sum_{i=-\infty}^{i=+\infty} \sum_{k=0}^{N-1} X_k[i] g_k(t - iT_s) e^{j2\pi f_k t} \tag{1.9}$$

where $g_k(t)$ is defined as :

$$g_k(t) = \Pi\left(\frac{t}{T_s}\right) \tag{1.10}$$

where $\Pi(t)$ is the rectangular function defined as :

$$\Pi(t) = \text{rect}(t) = \begin{cases} 1 & 0 \leq t \leq 1 \\ 0 & otherwise \end{cases} \tag{1.11}$$

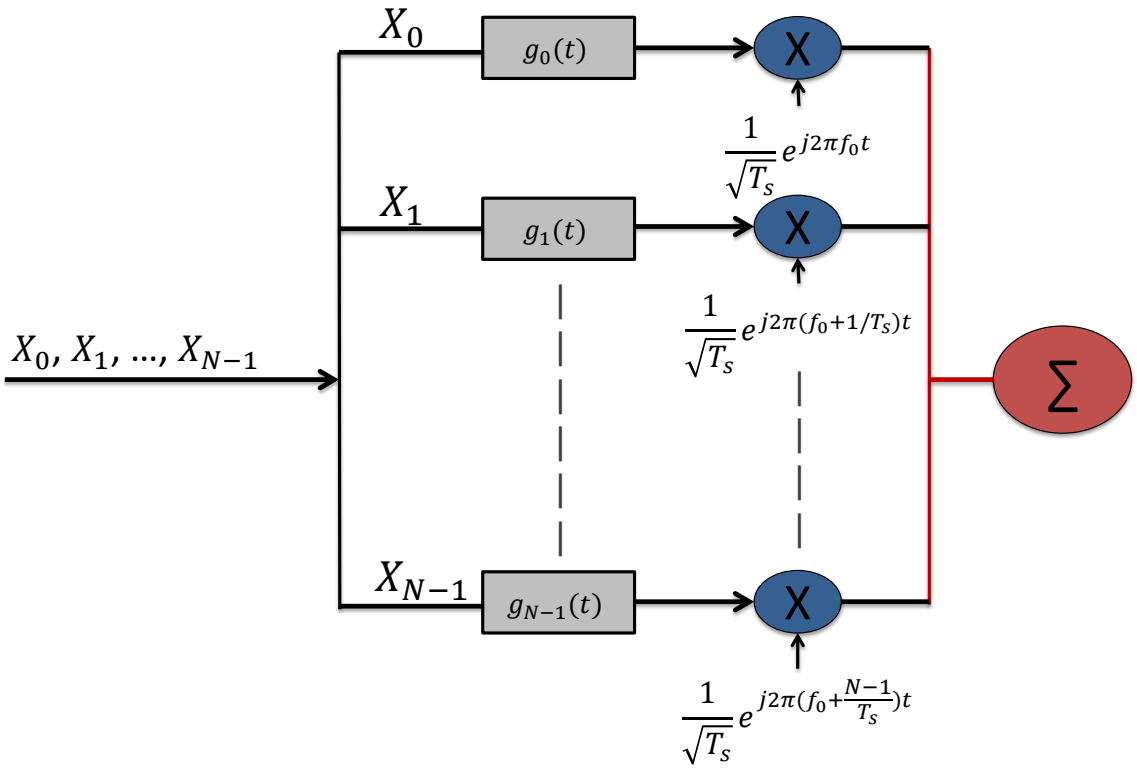

Figure 1.5 – Block diagram of IDFT OFDM modulator

and f_k is the k-th sub-carrier frequency such as $f_k = f_0 + \frac{k}{T_s}$ where f_0 is the first sub-carrier frequency defined as :

$$f_0 = f_c - \frac{N}{2T_s} \tag{1.12}$$

where f_c is the central sub-carrier frequency as shown in Fig.1.6.

By omitting time index i, the transmitted signal with a rectangular time-limited window for each OFDM symbol is given by :

$$s(t) = \frac{1}{\sqrt{T_s}} \sum_{k=0}^{N-1} X_k e^{j2\pi f_k t}. \tag{1.13}$$

It can be re-written as :

$$s(t) = \frac{1}{\sqrt{T_s}} \sum_{k=0}^{N-1} X_k e^{j2\pi(f_c - \frac{N}{2T_s} + \frac{k}{T_s})t} \tag{1.14}$$

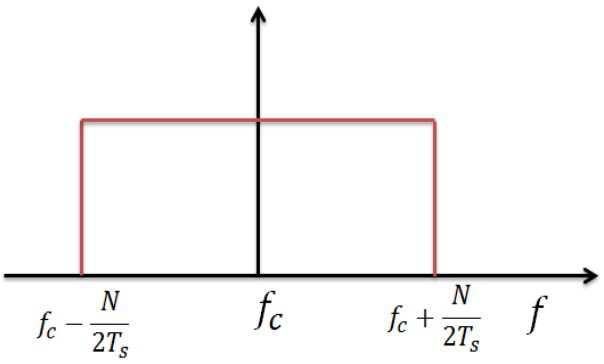

Figure 1.6 – Central subcarrier frequency

1.1.3.3 Guard time and Cyclic prefix

The orthogonality reached with the scheme above holds when no ISI is present. In case of multipath channel, each OFDM symbol overlaps with the previous one creating inter-block interference (IBI) and destroying the orthogonality between subcarriers creating inter-carrier interference (ICI). To completely avoid IBI, a guard interval (GI) is inserted between adjacent OFDM symbols which is obtained by extending its duration to $T = T_s + T_g$, where T_g is the GI duration. If $T_g \geq \tau_{\max}$, the useful period of the signal remains free of ISI. With zero-padding OFDM systems, no signal is transmitted during T_g. Hence, there is no power loss. But the problem of ICI remains, because subcarriers are no longer orthogonal. This is due to the non-integer number of cycles difference between subcarriers within the DFT integration time.

Standard OFDM with cyclic prefix

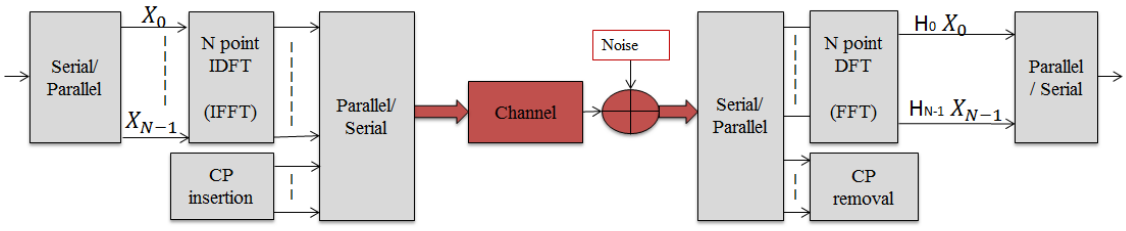

Figure 1.7 – OFDM block diagram

Today, classical implementation of OFDM is performed via Fast Fourier Transform (FFT) / Inverse FFT blocks and is illustrated in Fig.1.7. With cyclic prefix

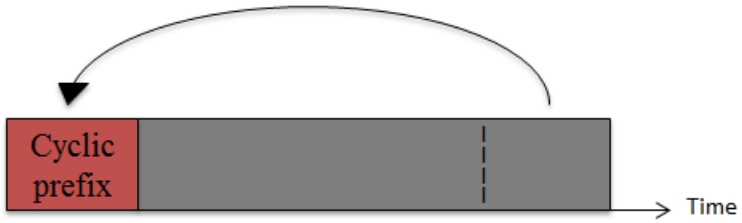

Figure 1.8 – The cyclic prefix is a copy of the last part of the OFDM symbol

(CP) OFDM which is the selected solution for most of the multicarrier standardized systems, OFDM symbol is cyclically extended in the guard time with the so-called CP which is composed of the last N_{CP} samples of an OFDM block as illustrated in Fig.1.8. The CP is selected longer than the length of the channel dispersion. It is inserted before each data block to prevent ISI between successive data blocks. In that case, the delayed replicas of OFDM symbol always have an integer number of cycles within the FFT integration time, as long as the delay is smaller than the guard time. The OFDM with CP suffers from a power efficiency loss, because the signal is transmitted during GI. CP introduces ripples in the useful bandwidth of the transmitted signal spectral power density. Discarding CP at the receiver not only eliminates ISI, but also converts the linear channel convolution into a circular one, which allows the diagonalization of the channel matrix.

1.1.3.4 OFDM demodulation

Assuming during the transmission :

— frequency non selective fading per subcarrier
— time invariance during each OFDM signal
— absence of ISI and ICI in the useful part of each OFDM symbol by the use of a guard interval larger than the delays spread of the impulse response of the channel,

the received signal can be written as :

$$y(t) = \frac{1}{\sqrt{T_s}} \sum_{k=0}^{N-1} X_k H_k e^{j2\pi(f_c - \frac{N}{2T_s} + \frac{k}{T_s})t}. \tag{1.15}$$

where H_k is the CFR of the k^{th} frequency sub-carrier assumed non invariant over the symbol period T_s. At the reception side, the received signal y_t is demodulated by N point Discrete Fourier Transform (DFT) process as illustrated in Fig.1.9. The

signal received on the p^{th} sub-carrier after DFT is :

$$\begin{aligned} Z_p &= \frac{1}{\sqrt{T_s}} \int_0^{T_s} y(t) e^{-j2\pi f_p t} dt \\ &= \frac{1}{T_s} \sum_{k=0}^{N-1} \int_0^{T_s} X_k H_k e^{j2\pi(k-p)\frac{t}{T_s}} dt \\ &= \frac{1}{T_s} \left[\int_0^{T_s} X_p H_p e^0 dt + \sum_{k\neq p, k=0}^{N-1} \int_0^{T_s} X_k H_k e^{j2\pi(k-p)\frac{t}{T_s}} dt \right] \\ &= X_p H_p \end{aligned} \tag{1.16}$$

because $\frac{1}{T_s} \int_0^{T_s} e^{j2\pi(k-p)\frac{t}{T_s}} dt = 0$ if $k \neq p$, and 1 if $k = p$.

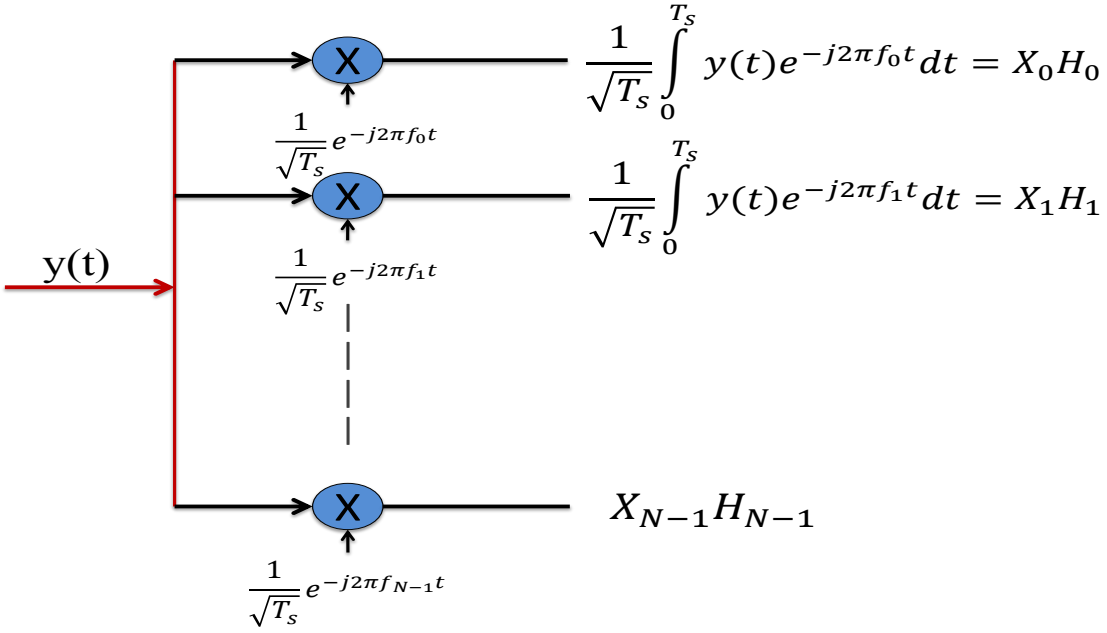

Figure 1.9 – Block diagram of DFT OFDM demodulator

Matrices representation

At transmitter, N QAM symbols modulate N sub-carriers thanks to N point IFFT. IFFT and FFT operation can be represented by a linear transformation such as :

$$\mathbf{s}[i] = \mathbf{F}^H \mathbf{x}[i] \tag{1.17}$$

where i stands for the i-th OFDM symbol and $\mathbf{F}^H$ is the complex conjugate Hermitian of the unitary $N \times N$ FFT matrix $\mathbf{F}$ defined as :

$$\mathbf{F} = \frac{1}{\sqrt{N}} \begin{bmatrix} (w^0)^0 & \cdots & (w^0)^{N-1} \\ \vdots & \ddots & \vdots \\ \left(w^{N-1}\right)^0 & \cdots & \left(w^{N-1}\right)^{N-1} \end{bmatrix} \tag{1.18}$$

where

$$\left(w^k\right)^n = e^{-j2\pi kn/N} \tag{1.19}$$

A time sample at the IFFT output is expressed as :

$$\text{IFFT}[X_k] = s_n = \frac{1}{\sqrt{N}} \sum_{k=0}^{N-1} X_k e^{j2\pi k \frac{n}{N}} \tag{1.20}$$

Let $\mathbf{T}_{CP}$ being the $P \times N$ matrix that inserts CP on the data vector block where $P = N + N_{CP}$. $\mathbf{T}_{CP}$ is defined as :

$$\mathbf{T}_{CP} = [\mathbf{I}_{CP}^T \mathbf{I}_N^T]^T \tag{1.21}$$

where $\mathbf{I}_{CP}$ is the $N_{CP} \times N$ identity matrix and $\mathbf{I}_N$ is the $N \times N$ identity matrix. The transmitted OFDM block after CP insertion is :

$$\mathbf{s}^{CP}[i] = \mathbf{T}_{CP}\mathbf{s}[i] \tag{1.22}$$

The discrete equivalent CIR is written as $\mathbf{h} = [h_0, h_1, ..., h_{L-1}]^T$ where L is the channel length. Assuming that the system is perfectly synchronized in time and frequency, the received signal is affected by the multipath channel and AWGN :

$$y_n^{CP}[i] = \sum_{l=0}^{L-1} h_l s_{n-l}^{CP}[i] + w_n[i] \tag{1.23}$$

where $w_n[i]$ is the AWGN term. The P received samples of the $i-$th OFDM block are grouped into the vector $\mathbf{y}^{CP}[i]$:

$$\mathbf{y}^{CP}[i] = \mathbf{H}_{ICI}\mathbf{s}^{CP}[i] + \mathbf{H}_{IBI}\mathbf{s}^{CP}[i-1] + \mathbf{w}^{CP}[i] \tag{1.24}$$

where $\mathbf{w}^{CP}[i]$ is the AWGN vector, while $\mathbf{H}_{ICI}$ and $\mathbf{H}_{IBI}$ are respectively the $P \times P$ lower and upper triangular Toeplitz matrix :

$$\mathbf{H}_{ICI} = \begin{bmatrix} h_0 & 0 & \cdots & \cdots & \cdots & 0 \\ \vdots & \ddots & \ddots & \ddots & \ddots & \vdots \\ h_{L-1} & \ddots & \ddots & \ddots & \ddots & \vdots \\ 0 & \ddots & \ddots & \ddots & \ddots & \vdots \\ \vdots & \ddots & \ddots & \ddots & \ddots & 0 \\ 0 & \cdots & 0 & h_{L-1} & \cdots & h_0 \end{bmatrix} \tag{1.25}$$

$$\mathbf{H}_{IBI} = \begin{bmatrix} 0 & \cdots & 0 & h_{L-1} & \cdots & h_1 \\ \vdots & \ddots & \ddots & \ddots & \ddots & \vdots \\ \vdots & \ddots & \ddots & \ddots & \ddots & h_{L-1} \\ \vdots & \ddots & \ddots & \ddots & \ddots & 0 \\ \vdots & \ddots & \ddots & \ddots & \ddots & \vdots \\ 0 & \cdots & \cdots & \cdots & \cdots & 0 \end{bmatrix} \tag{1.26}$$

which represent respectively the interference between the samples within the i-th OFDM block and the interference between two successive OFDM blocks. CP is removed from the received signal by applying the $N \times P$ CP removal matrix $\mathbf{R}_{CP} = [\mathbf{0}_{N \times N_{CP}} \mathbf{I}_N]$ where $\mathbf{0}_{N \times N_{CP}}$ is the $N \times N_{CP}$ all-zeros matrix. When $L < N_{CP}$, IBI term is completely removed :

$$\begin{aligned} \mathbf{y}[i] &= \mathbf{R}_{CP}\mathbf{H}_{ICI}\mathbf{s}[i] + \mathbf{R}_{CP}\mathbf{H}_{IBI}\mathbf{s}[i] + \mathbf{w}[i] \\ &= \mathbf{R}_{CP}\mathbf{H}_{ICI}\mathbf{T}_{CP}\mathbf{F}^{\mathbf{H}}\mathbf{x}[i] + \mathbf{R}_{CP}\mathbf{H}_{IBI}\mathbf{T}_{CP}\mathbf{F}^{H}\mathbf{x}[i-1] + \mathbf{w}[i] \\ &= \mathbf{H}_{CIR}\mathbf{F}^{H}\mathbf{x}[i] + \mathbf{w}[i] \end{aligned} \tag{1.27}$$

where $\mathbf{w}[i]$ is the AWGN vector after CP removal and $\mathbf{H}_{CIR}$ is the $N \times N$ circulant matrix defined as :

$$\mathbf{H}_{CIR} = \mathbf{R}_{CP}\mathbf{H}_{ICI}\mathbf{T}_{CP} = \begin{bmatrix} h_0 & 0 & \cdots & 0 & h_L & \cdots & h_1 \\ h_1 & \ddots & \ddots & \ddots & \ddots & \ddots & \vdots \\ \vdots & \ddots & \ddots & \ddots & \ddots & \ddots & h_L \\ h_L & \ddots & h_1 & h_0 & 0 & \ddots & 0 \\ 0 & \ddots & \ddots & \ddots & \ddots & \ddots & \vdots \\ \vdots & \ddots & \ddots & \ddots & \ddots & \ddots & 0 \\ 0 & \cdots & 0 & h_L & \cdots & h_1 & h_0 \end{bmatrix} \tag{1.28}$$

and

$$\mathbf{R}_{CP}\mathbf{H}_{ICI}\mathbf{T}_{CP} = \mathbf{0}_{N \times N} \tag{1.29}$$

Then FFT demodulator is applied leading to :

$$\begin{aligned} \mathbf{z}[i] &= \mathbf{F}\mathbf{H}_{CIR}\mathbf{F}^{H}\mathbf{x}[i] + \mathbf{F}^{H}\mathbf{w}[i] \\ &= \mathbf{D}_H\mathbf{x}[i] + \tilde{\mathbf{w}}[i] \end{aligned} \tag{1.30}$$

where $\mathbf{D}_H$ is the $N \times N$ diagonal matrix of the frequency coefficients of the $N \times 1$ channel vector $\mathbf{H}_N = [H_0, H_1, ..., H_{N-1}]^T$ whose the k^{th} element is defined as $H_k = \sum_{l=0}^{L-1} h_l e^{-j2\pi l \frac{k}{N}}$.

1.1.3.5 OFDM channel capacity

The channel capacity is the maximum rate at which an information can be communicated across a noisy channel with arbitrary reliability. The capacity of the AWGN channel is probably the most well-known result of information theory, but it is in fact only a special case of Shannon's general theory applied to a specific channel [8]. The achievable data rate of the continuous AWGN channel with bandwidth B, average received power P, and white noise spectral density N_0 is given by :

$$R_{AWGN} = \mathrm{B}\log_2\left(1+\frac{P}{N_0\mathrm{B}}\right)\text{bits/s} \tag{1.31}$$

The overall spectral efficiency of a multi-carrier system is the summation of the individual data rates of all sub-bands. Therefore, a separate capacity achieving code is used to communicate over each of the sub-channels [8]. If p_k is the allocated power to the k^{th} sub-channel, the spectral efficiency of reliable communication using this scheme is :

$$C_{OFDM} = \sum_{k=0}^{N-1}\log_2\left(1+\frac{p_k|h_k|^2}{N_0\mathrm{b_k}}\right)\text{bits/s/Hz} \tag{1.32}$$

where h_k is the $k-$th sub-carrier channel coefficient and $\mathrm{b_k}$ is the bandwidth of the $k-$th sub-band.

1.2 Optimization problem

An optimization problem consists in finding the best solution among all feasible solutions of a problem. Here superlative "best" should be understood in the sense that it gives the extremal value (minimal or maximal) of an objective function. The optimization problem can be a maximization or minimization of an objective function under given constraints. The standard form of an optimization problem is :

$$\begin{aligned} \underset{x}{\text{minimize}} \quad & f_0(x) \\ \text{subject to} \quad & f_j(x) \leq 0, j = 1, ..., K_i \\ & h_j(x) = 0, j = 1, ..., K_e \end{aligned} \tag{1.33}$$

where $f(x)$ is the objective function to be minimized. A maximization problem can be easily turned into standard form in (1.33) by minimizing the opposite objective function. $f_j(x)$ and $h_j(x)$ are the inequality and equality constraint functions respectively. Solving the problem in 1.33 consists in finding the optimal x^* that minimizes $f(x)$ while respecting and satisfying the denoted equality and inequality constraints.

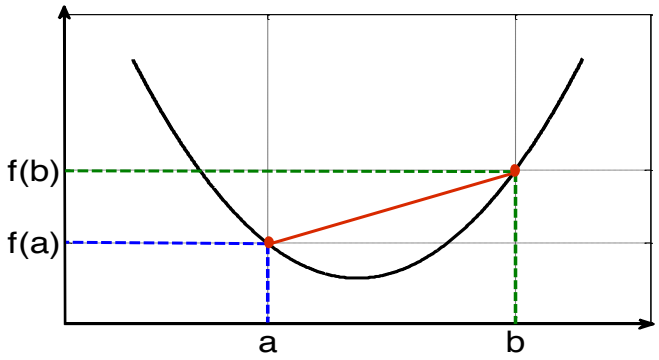

Figure 1.10 – Convex function graph : the line segment between any two points on the graph lies above the graph.

1.2.1 Concave and convex functions

A set S_{vex} is convex if the line segment between any two points in S_{vex} lies in S_{vex}, i.e., if for any $a, b \in S_{vex}$ and any θ with $0 \leq \theta \leq 1$, we have $\theta a + (1-\theta)b \in S_{vex}$. Roughly speaking, a set is convex if every point in the set can be seen by every other point, along an unobstructed straight path between them, where unobstructed means lying in the set.

A set S_{aff} is affine if the line through any two distinct points in S_{aff} lies in S_{aff}, i.e., if for any $a, b \in S_{aff}$, we have $\theta a + (1-\theta)b \in S_{aff}$. In other terms, S_{aff} contains the linear combination of any two points in S_{aff}, provided the coefficients in the linear combination sum to one.

A function $f(x) : \mathbb{R}^n \to \mathbb{R}$ is convex if $\mathbf{dom} f(x)$ is a convex set [1] and if for all $a, b \in \mathbf{dom} f(x)$, and θ with $0 \leq \theta \leq 1$, we have :

$$f(\theta a + (1-\theta)b) \leq \theta f(a) + (1-\theta) f(b) \tag{1.34}$$

where $\mathbf{dom} f(x)$ signifies the domain of function $f(x)$. Geometrically, this inequality means that the line segment between $(a, f(a))$ and $(b, f(b))$ which is the chord from a to b, lies above the graph of $f(x)$ (Fig. 1.10). A function f is strictly convex if strict inequality holds in (1.34), whenever $x \neq y$ and $0 \prec \theta \prec 1$. $f(x)$ is considered concave if $-f(x)$ is convex, and strictly concave if $-f(x)$ is strictly convex [1].
A function is convex if and only if it is convex when restricted to any line that intersects its domain. Moreover, a convex function is continuous on the relative interior of its domain and it can have discontinuities only on its relative boundary.

1.2.1.1 First order condition

Suppose $f(x)$ is differentiable (i.e., its gradient $\nabla f(x)$ exists at each point in $\mathbf{dom}f$). Then f is convex if and only if $\mathbf{dom}f(x)$ is convex and :

$$f(b) \geq f(a) + \nabla f(a)^T(b-a) \tag{1.35}$$

holds for all $a, b \in \mathbf{dom}f(x)$.

1.2.1.2 Second order condition

If $f(x)$ is twice differentiable, that is, its Hessian or second derivative $\nabla^2 f(x)$ exists at each point in $\mathbf{dom}f(x)$. Then $f(x)$ is convex if and only if $\mathbf{dom}f(x)$ is convex and its Hessian is positive semi-definite : for all $x \in \mathbf{dom}f(x)$,

$$\nabla^2 f(x) \geq 0 \tag{1.36}$$

For a function on $\mathbf{R}$, this reduces to the simple condition $f"(x) \geq 0$ (and $\mathbf{dom}f$ is convex), which means that the derivative is non-decreasing.

1.2.2 Convex optimization

There is in general no analytical formula for the solution of convex optimization problems, but there are very effective methods for solving them.

1.2.2.1 Lagrange function

The basic idea in Lagrangian is to take the constraints into account by augmenting the objective function with a weighted sum of the constraint functions. Hence, the Lagrangian function associated with the optimization problem presented in (1.33) is defined as :

$$L(x, \boldsymbol{\lambda}, \boldsymbol{\nu}) = f_0(x) + \sum_{j=1}^{K_i} \lambda_j f_j(x) + \sum_{j=1}^{K_e} \nu_j h_j(x) \tag{1.37}$$

where λ_j is the Lagrange multiplier associated with the j-th inequality constraint $f_j(x) \leq 0$; and ν_j is the Lagrange multiplier associated with the j-th equality constraint $h_j(x) = 0$. The vectors $\boldsymbol{\lambda}$ and $\boldsymbol{\nu}$ are called the dual variables or Lagrange multiplier vectors associated with the problem presented in (1.33).

1.2.2.2 Karush-Kuhn-Tucker (KKT) conditions

To solve any optimization problem (convex, concave, etc) with differentiable objective and constraint functions, Karush-Kuhn-Tucker (KKT) conditions are required and must be written and computed. KKT conditions corresponding to the optimization problem presented in (1.33) are defined as :

$$\begin{aligned} f_j(x^*) &\leq 0, j = 1, ..., K_i \\ h_j(x^*) &= 0, j = 1, ..., K_e \\ \lambda_j^* &\geq 0, j = 1, ..., K_i \\ \lambda_j^* f_j(x^*) &= 0, j = 1, ..., K_i \\ \nabla f_0(x^*) + \sum_{j=1}^{K_i} \lambda_j^* \nabla f_j(x^*) + \sum_{j=1}^{K_e} \nu_j^* \nabla h_j(x^*) &= 0, \end{aligned} \tag{1.38}$$

where λ_i^* and ν_i^* are the optimal Lagrange multipliers for the j-th constraint. The satisfaction of KKT conditions leads to the optimal solution of the problem by expressing it with an explicit or implicit form in function of the Lagrange multipliers. Therefore, this helps to apply the corresponding algorithm that searches the optimal solution while respecting the given constraints.

Problem convexity

The problem in (1.33) is said convex if and only if :
— The objective function must be convex in case of minimization problem.
— The inequality constraint functions must be convex.
— The equality constraint functions must be affine.

1.2.2.3 Concave maximization problems

We refer to :

$$\begin{aligned} \text{maximize} \quad & f_0(x) \\ \text{subject to} \quad & f_j(x) \leq 0, j = 1, ..., K_i \\ & h_j(x) = 0, j = 1, ..., K_e \end{aligned} \tag{1.39}$$

as a concave optimization problem if the objective function $f_0(x)$ is concave and the inequality constraint functions $f_1, ..., f_m$ are convex. Let us remind that any maximization problem can be turned into a minimization problem by minimizing $-f_0$ over x. Hence, all results, conclusions, and algorithms that are described for minimization problem are easily transposed to the maximization case.

1.2.3 Concave Convex Procedure (CCCP)

The Concave Convex Procedure (CCCP) is an optimization method which leads to find the minimum or the saddle point of the objective function in an optimization problem. To apply the CCCP, the objective function should be divided in two parts, i.e. two functions, where the first one is a convex function and the second one is a concave function. Consequently, an objective function, proven that is composed of concave and convex parts, can be optimized with the CCCP. The CCCP principle is based on the fact that the convex function, which has always a minimum point, is divisible into a sum of a concave and a convex functions. Therefore, an objective function composed of concave and convex functions can always converge with the CCCP towards a saddle or minimum point. Moreover, an objective function, $f_0(\vec{x})$ for example, must have a bounded Hessian $\partial^2 f_0(\vec{x})/\partial\vec{x}\partial\vec{x}$.

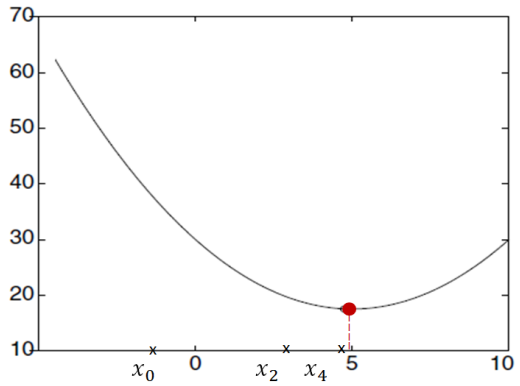

Figure 1.11 – Convex function example containing minimum value.

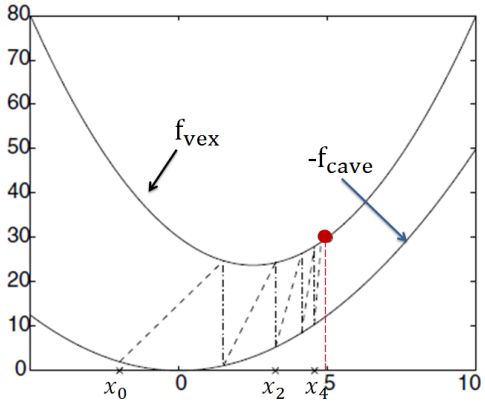

Figure 1.12 – Convex function is the sum of convex and concave functions.

The CCCP algorithm can be graphically illustrated by the reformulation shown in Fig. 1.11 and Fig. 1.12. Firstly, the objective convex function $f_0(\vec{x})$, presented in Fig. 1.11, is decomposed into $f_{v1}(\vec{x}) - f_{v2}(\vec{x})$, presented in Fig. 1.12, where both $f_{v1}(\vec{x})$ and $f_{v2}(\vec{x})$ are convex. This is equivalent to decompose $f_0(\vec{x})$ into a convex term $f_{v1}(\vec{x})$ plus a concave term $(-f_{v2}(\vec{x}))$. The CCCP algorithm proceeds in Fig.1.12 by matching points on the two terms which have the same tangents. For an input $\vec{x}_0$, the gradient $\vec{\nabla} f_{v2}(x_0)$ can be calculated and the point x_1 can be found such that $\vec{\nabla} f_{v1}(\vec{x}_1) = \vec{\nabla} f_{v2}(\vec{x}_0)$. Then, the point $\vec{x}_2$ is determined such that $\vec{\nabla} f_{v1}(\vec{x}_2) = \vec{\nabla} f_{v2}(\vec{x}_1)$, and so on.

Hence, the discrete iterative CCCP algorithm $\vec{x}^t \longmapsto \vec{x}^{t+1}$ is given by :

$$\vec{\nabla} f_{vex}(\vec{x}^{t+1}) = -\vec{\nabla} f_{cave}(\vec{x}^t), \tag{1.40}$$

where $f_{vex}(\vec{x})$ and $f_{cave}(\vec{x})$ are respectively the convex and the concave part of $f_0(\vec{x})$. The CCCP constructs discrete time iterative dynamical systems which are guaranteed to monotonically decrease towards a global optimum. Therefore, it guarantees to monotonically decrease $f_0(\vec{x})$ as a function of time and hence to converge to the minimum or the saddle point of it.

To calculate $\vec{x}^{t+1}$, an inner loop is needed. Then, standard techniques such as conjugate gradient descent [9] and a lot of other existing methods can be used according to the problem case [2].

1.3 On the coexistence of LTE and DVB-T2

In this part, we present briefly the DVB and LTE basics with their characteristics. The parameters corresponding to OFDM modulation are also presented. Then we cite some relevant works dedicated to the coexistence between DVB and LTE.

1.3.1 Long Term Evolution (LTE)

In the last years, mobile data usage and new applications (mobile TV, mobile multimedia, Web, streaming) evolve rapidly. Traditionally, operators have built multiple networks to provide multiple services to customers such as fixed phone net-

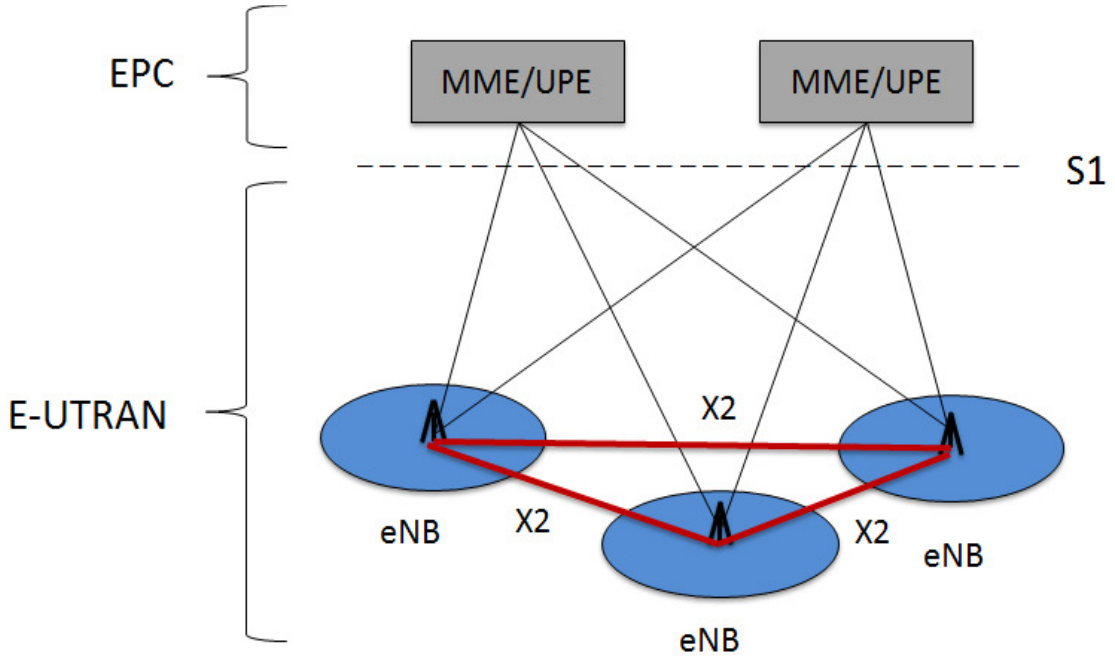

Figure 1.13 – LTE system architecture

works, cable TV networks, cellular telephone networks and data networks. 3GPP has been motivated by users' demand, which have widely evolved with the integrated cellular phones and mobile services, to provide the fourth generation of mobile network known as LTE. This latter provides a high spectral efficiency, short round trip time as well as flexibility in frequency and bandwidth. Moreover, LTE generates three to four times the throughput on the downlink provided by the 3GPP Release 6 [10].

1.3.1.1 LTE basics

To enable possible deployment around the world, supporting as many regulatory requirements as possible, LTE is developed for a number of frequency bands, the Evolved Universal Terrestrial Access (E-UTRA) operating bands, currently ranging from 700 MHz up to 2.7GHz. The available bandwidths are also flexible starting with 1.4 MHz up to 20 MHz. It is worth noting that LTE can operate on the 700 MHz band reserved for TV broadcasting. The LTE Downlink is based on Orthogonal Frequency Division Multiple Access (OFDMA) combined with high order modulation (up to 64 Quadrature Amplitude Modulation (QAM)), scalable bandwidth (up to 20 MHz), and spatial multiplexing (up to 4x4). LTE is theoretically able to achieve 75 Mbps in uplink and up to 300 Mpbs in downlink with spatial multiplexing [11].

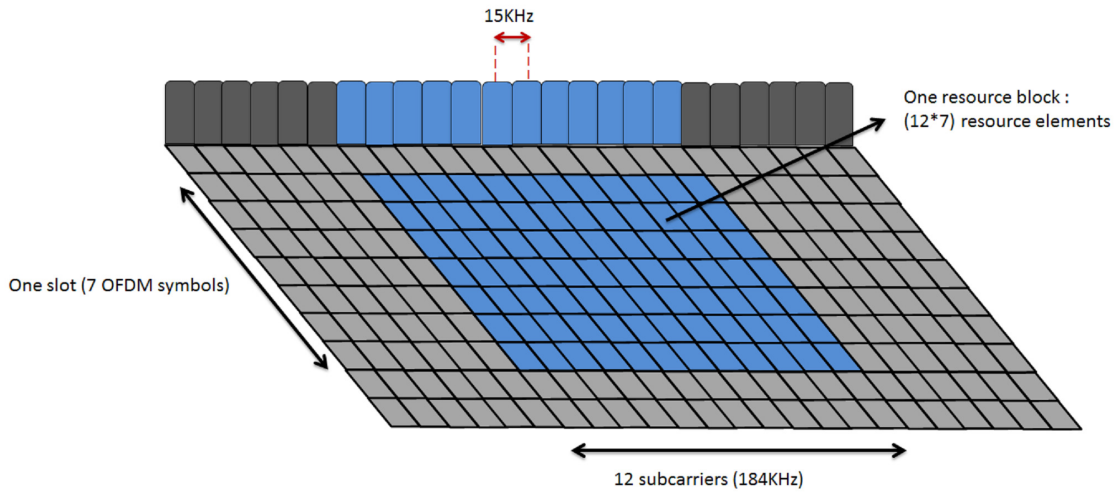

Figure 1.14 – OFDM subcarriers with LTE

LTE is subject to more development. Newer versions of this technology are emerging presenting higher data rate, higher spectral efficiency, increased number of simultaneous active users, and improved performance at cell edges [12, 13].
As shown in Fig. 1.13, the LTE network is composed of two major parts :

1. The Evolved Packet Core (EPC) or Evolved Packet System (EPS) is purely Internet Protocol (IP) based.
2. The Evolved Universal Terrestrial Access Network (E-UTRAN) made of evolved Nodes B (eNodeB) generating a flat architecture with no centralized intelligent controller. The reason for distributing the intelligence amongst the base-stations in LTE is to speed up the connection set-up and reduce the time required for handover.

1.3.1.2 LTE and OFDM

To overcome the multipath fading effect, LTE has adopted the OFDM technique in downlink ; likewise to reduce the Peak to Average Power Ratio (PAPR) in uplink, Single Carrier Frequency Division Multiple Access (SC-FDMA) has been adopted. SC-FDMA is similar to OFDMA but in this case each data symbol is firstly spread using DFT modulation before being sent over the conventional IFFT block of the OFDM transmission chain. In fact, OFDM meets the LTE requirement for spectrum flexibility and enables cost-efficient solutions for very wide carriers with high peak rates.

LTE signals are organized into radio frames with 10 *ms* duration ; each frame is composed of ten equally sized sub-frames of 1 *ms* long ; each sub-frame is further divided into two slots, each of 0.5 *ms* duration.

Table 1.1 – LTE System Downlink Parameters

Channel Bandwidth (MHz)	1.25	2.5	5	10	15	20
Sub-carrier Spacing ΔF (KHz)	15					
Useful symbol duration T_s (μs)	66.7					
Sampling Frequency (MHz)	1.92	3.84	7.68	15.36	23.04	30.72
FFT size	128	256	512	1024	1536	2048
Occupied subcarriers	76	151	301	601	901	1201
Guard Subcarriers	52	105	211	423	635	847
Number of resource blocks	6	12	25	50	75	100
Occupied Channel Bandwidth (MHz)	1.140	2.265	4.515	9.015	13.515	18.015
Downlink Bandwidth Efficiency	77.1%	90%	90%	90%	90%	90%
Frame duration (ms)	10					
Subframe Duration (ms)	1					
OFDM Symbols/Subframe	7/6(short/long CP)					
CP Length (short CP) (μ s)	5.2(first symbol)/4.69(six following symbols)					
CP Length (Long CP) (μ s)	16.67					

Slots consist of either 6 or 7 OFDM symbols, depending on whether normal or extended CP is employed. Table 1.1 summarizes the key LTE parameters presented

in [14]. OFDM subcarriers are spaced by 15 KHz. E-UTRAN combines OFDM symbols in Resource Blocks (RB). As illustrated in Fig.1.14, each RB contains 12 consecutive subcarriers during one slot therefore each RB occupies 180 KHz. The number of RBs in a system may vary from a minimum of 6 (corresponding to 72 subcarriers) up to 110 RBs (corresponding to 1320 subcarriers). It is the scheduler's task to assign RBs to physical channels belonging to different users. Pilots for synchronization, radio resource management and channel estimation are also transmitted in the first and sixth sub-frame of each frame.

1.3.2 Second Generation for Digital Video Broadcasting-Terrestrial (DVB-T2)

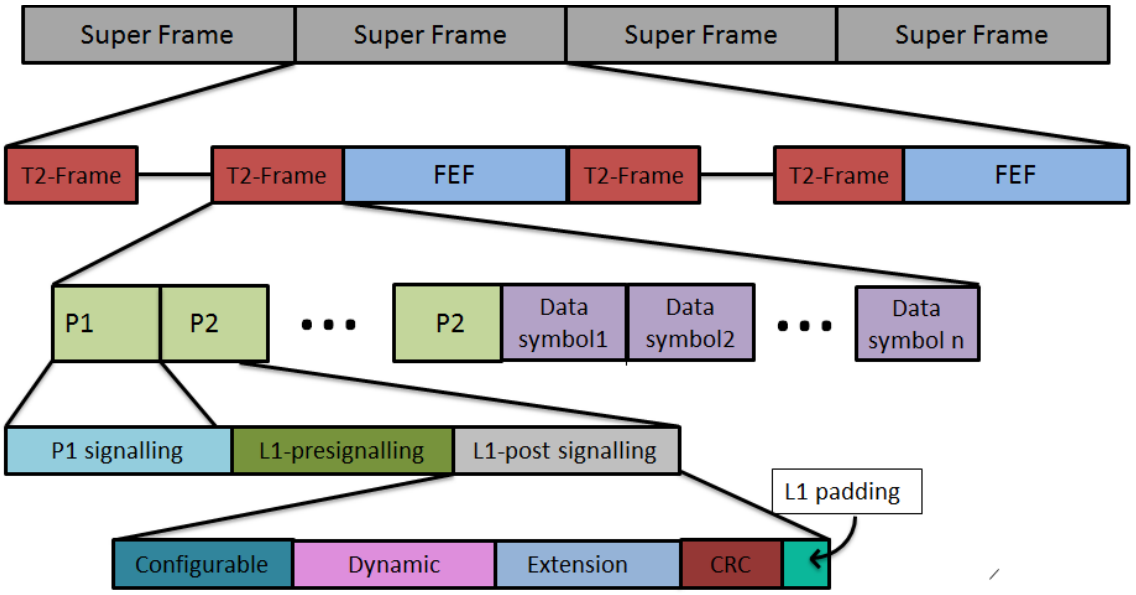

Figure 1.15 – DVB super frame structure

DVB-T is the most widely adopted and deployed digital terrestrial television (DTT) standard. Since its publication in 1997, over 70 countries have deployed Digital Video Broadcasting-Terrestrial (DVB-T) services and 69 countries have now adopted or deployed DVB-T2. This well-established standard benefits from massive economies of scale and very low receiver prices. DVB-T2 is the world's most advanced DTT system, offering more robustness, flexibility and 50% more efficiency than any other DTT system.

Due to the European analogue switch-off and increasing scarcity of spectrum, DVB drew up commercial requirements for a more spectrum-efficient and updated standard. DVB-T2 easily fulfills these requirements, including increased capacity,

robustness and the ability to reuse existing reception antennas.

The first DVB-T2 version was published in 2009. In addition, DVB has considered broadcasting formats for mobile receivers such as DVB-Next Generation Handheld (DVB-NGH) or DVB-T2-Lite, both targeting the same category of users. These two formats tend to use a more robust Modulation and Coding (MODCOD) scheme allowing High Definition (HD) reception at much lower Signal to Interference and Noise Ratio (SINR) than the standard DVB-T2.

1.3.2.1 DVB-T2 transmission and OFDM

The input of the T2 system consists of one or more logical data streams. The encoding of each data stream is usually done on two Physical Layer Pipe (PLP) each with a different modulation assuring the delivery of the channel in both HD and Standard Definition (SD). The main difference between those two PLPs is the MODCOD scheme. In the OFDM structure, the transmitted signal is organized in frames.

As illustrated in Fig. 1.15, data symbols obtained previously are paired with Layer 1 (L1) signaling which provides the receiver with a mean to access PLP within the T2 frame. The L1 signaling structure is split into three main sections : P1 signaling, L1 pre-signaling and L1 post-signaling that is further split into two main parts : configurable and dynamic, followed by an optional extension field. L1 pre-signaling and L1 post-signaling form the P2 symbol.

Table 1.2 – DVB-T and DVB-T2 Parameters (new/improved options in **Bold**)

Parameters	DVB-T		DVB-T2					
Mode	2K	8K	**1K**	2K	**4K**	8K	**16K**	**32K**
FFT size	2048	8192	1024	2048	4096	8192	16384	32768
Active subcarriers number	1 705	6817	853	1705	3409	6817	13633	27265
Subcarrier spacing ΔF* (Hz)	4464	1116	8929	4464	2232	1116	558	279
Useful symbol duration* $T_s(\mu s)$	224	896	112	224	448	896	1792	3584
Sampling frequency* (MHz)	9.14							
Occupied Bandwidth* (MHz)	7.61		7.61					
Typical data rate (Mbit/s)	24		40					
Max.data rate @20dB C/N*(Mbit/s)	31.7		45.5					
Required C/N ratio @24Mbit/s(dB)	16.7		10.8					
Mapping	QPSK, 16QAM, 64QAM		QPSK, 16QAM, 64QAM, **256 QAM**					
Guard interval	t_sx1/4, 1/8, 1/16, 1/32		t_sx 1/4, 1/8, **19/256**, 1/16, 1/32, **1/128**					

*Only for a 8 MHz channel bandwidth.

The P1 symbol is inserted in the T2 frame after the final OFDM modulation. The DVB-T2 frame comprises one P1 symbol followed by one or more P2 preamble. The beginning of the first preamble symbol P1 marks the beginning of the T2-frame ; the number of P2 symbols N_{P2} is determined by FFT size. The number of data symbols L_{data} in T2 frame is a configurable parameter signaled in L1 pre-signaling.

Table 1.3 – DVB-T2 vs LTE

Parameters	DVB-T2	LTE
Modulation	OFDM	OFDM
Subcarriers spacing	279 Hz to 8.9 KHZ	7.5, 15 KHz
Guard interval duration	7 to 532 μs	4.69 to 33,3 μs
Gross spectral efficiency	0.99 to 6.65 bps/Hz	0.15 to 5.55 bps/Hz

Table 1.4 – Downlink LTE operating bands

E-UTRA operating band	Operating band in MHz (Duplex mode FDD) F_{low} to F_{High}
5	869 to 894
12	728 to 746
13	746 to 756
17	734 to 746
19	875 to 890
20	791 to 821

The total number of symbols in a frame, excluding P1, is given by $L_F = N_{P2} + L_{data}$ and thus the total T2 frame duration is given by $T_F = L_F * T + T_{P1}$, where T_{P1} is the duration of the P1 symbol and we recall that T is the total OFDM symbol duration. The maximum duration of the T2 frame is 250 *ms*. DVB-T2 frames can be grouped into super frames where the number of T2 frames in a super frame is a configurable parameter that is signaled in L1-pre-signaling. The current frame is signaled by a frame index in the dynamic L1-post-signaling.

A Future Extension Frame (FEF), which may carry data in a way unknown to DVB-T2 receivers, can be inserted between T2 frames. A super frame duration is given by $T_{SF} = N_{T2} * T_F + N_{FEF} * T_{FEF}$ where N_{FEF} is the number of FEF parts in a super frame, T_{FEF} is the duration of one FEF part equal to 250 *ms* and N_{T2} is the number of T2 frames. The maximum duration of a super frame is 63.75 *s* if no FEF part is present and 127.5 *s* if the super frame contains FEF part.

Pilot Signals are then inserted in a certain pattern in L1 signaling, to allow receivers to compensate for channel distortions, frame synchronization, frequency synchronization, channel estimation, transmission mode identification and to follow the phase noise. Some of the main DVB-T and DVB-T2 parameters are presented in Table 1.2. More details about the input data modulation and rearrangement in the transmission are discussed in [15] and [16].

1.3.3 DVB vs LTE specifications

Despite LTE and DVB-T2 standards can coexist together, there are many differences between them. First of all, each of them gives raise to different applications. LTE is used to communicate from point to point, precisely from BS to mobile terminals moving in a small cell zone, while DVB-T2 is used to broadcast videos for a large number of users in a wide coverage zone. It is also worth mentioning that LTE has the possibility to offer a broadcasting service by the eMBMS (evolved Multimedia Broadcast Multicast Service).

Another difference is that LTE consists of two transmission links, i.e. uplink and downlink, while DVB-T2 transmits only in downlink. The uplink in LTE standard helps to improve its quality by adapting the signal according to the transmission link conditions known by the received information at BS from users. But in DVB-T2, the worst case must be supposed to satisfy all the users transmission conditions.

LTE and DVB-T2 are recent standards and use some advanced techniques in telecommunications. Despite they both use OFDM modulation, they have different OFDM parameters, e.g. different guard interval duration, different subcarrier spacing. This is mainly because of the difference of coverage area size implying different channel effects on signals.

Table 1.3 shows some parameter specifications of both systems. Table 1.4 shows some LTE downlink operating bands existing in or near TV bands [17] where FDD stands for frequency division duplexing. F_{low} and F_{high} are respectively the lower and higher frequencies in the operating band. The E-UTRA operating band 19 is used in Japan while the E-UTRA operating band 20 is a part of the European Union (EU) digital dividend used in Europe. Table 1.5 shows frequency range in which DVB bandwidth can exist where VHF, UHF stand for very/ultra high frequency. These two tables ensure the possibility for DVB-T2 and LTE to share the same frequency band or to operate over adjacent frequency bands.

Table 1.5 – DVB frequency range

Band	Frequency range	Signal bandwidth
VHF III	174-230 MHz	7 MHz
UHF IV	470-606 MHZ	8 MHz
UHF V	606-862 MHz	8 MHz

1.3.4 State of the art of resource allocation and interference link

The congestion of the spectrum arises as a serious problem to be solved. This problem has led to search for the maximum spectral band efficiency by increasing the spectrum reuse factor. The problem of the reuse of licensed users spectrum by

secondary users has drawn a lot of attention for industrial and academic communities. In particular, the use of the broadcasting network spectrum by a cellular network or even in opportunistic manner by unlicensed Cognitive Radio (CR) systems is an up-to-date and hot topic of interest in the wireless communication world. Nowadays, universal TV broadcasters are switching from analog to digital thus freeing valuable parts of the overcrowded frequency spectrum previously reserved. This will open doors for coexistence with LTE at these frequencies. On the other hand, the deployment of small-cells (micro, pico, femto) under the main macro cell is an envisaged mode of communication in the LTE standard. In this mode, femto or micro cells can use a separated band from the macro or reuse the same band and hence interfere with the macro [18]. Small cells can offer a better coverage in some scenarios experiencing high shadowing effect as well as an increase of the data rate for small-cell users [19]. 3GPP and DVB are becoming increasingly aware of mutual benefits they can bring in case of convergence for a common offer of services in terms of QoS, profit sharing and power consumption. Many studies reached a conclusion that a hybrid LTE-DVB system is the optimal solution.

From the economical side, another noticeable advantage of LTE-DVB cooperation is studied in [20] where the energy consumption of both systems is always less than the total consumption in a separate LTE and DVB networks. This decrease of demanded energy is reflected in a decrease of operational fees and leads to an eco-friendly service network. In [21], a conclusion is drawn, that an upgrade should take place for the existing LTE networks to serve DVB content while maintaining the QoS of the unicast services. This proposed upgrade poses a financial problem for LTE bearers and could put a hold to any plan of cooperation between both systems. But in [22], based on the cost of this upgrade, it has been proven that this convergence would bring profit to DVB and LTE bearers in both single operator or separate operators for both services.

The sharing of resources between different communication systems needs a management strategy to control it. A lot of works have studied the resources allocation problem and analyzed it based on different constraints like the QoS of systems, their needs and their operation conditions. Most of the studies take the received data rate as an important parameter to evaluate the certified resource management strategy. The received data rate in each system shows the reached QoS. Because of this, the maximization of the received data rate is always a goal to reach. Recently, the study of the ergodic capacity of a secondary link under spectrum-sharing has attracted a lot of attention. Ergodic capacity defined as the maximum achievable rate averaged over all fading states is of particular used as a long-term throughput measure in these systems.

In [23], the ergodic and outage capacities of multiple relay channels are derived in closed form expression and investigated in different fading and shadowing environments under constraints. It is assumed that Secondary User (SU) is allowed to share

the spectrum band with a Primary User (PU) provided that its transmit power remains below an interference power threshold set by the PU. Li and Goldsmith in [24] have investigated the ergodic capacity of multi-user broadcast fading channels. In particular, they found the optimal power allocation policy for the code division multiple access (CDMA) scheme. In [25], a study of the information-theoretic limits has been done on the secondary cognitive radio (CR) under spectrum sharing condition with an existing primary user. In these works, the authors have analyzed the ergodic capacity under individual power constraint and acceptable interference level at the primary receivers from the secondary transmitters. It was also derived analytically in [26], where the capacity gains offered by spectrum sharing approach in Rayleigh fading environments are investigated. In particular, the fading channel capacity of the SU subject to both average and peak received power constraints at the PU is derived without considering the interference from the primary transmitter onto the secondary receiver. In these cited works, the reliance on the capacity is shown. Moreover, the existence of different priorities, between the networks sharing the same spectrum, is clearly seen.

Naturally, when two networks are operating on adjacent or overlapped frequency bands, an interference arises between them. In Denmark, the National IT and Telecom Agency (NITA) has conducted a study preparing to auction out the 800 MHz bandwidth as detailed in [27]. Two interference modes were studied : Adjacent Channel Interference (ACI) and Receiver Overload (RO) both when transmitters are at full power and realistic transmitting power. A lot of works have analyzed this problem from different faces using different parameters to evaluate the interference effects.

For instance, in [28] and [29], the signals of LTE and DVB networks are operating in adjacent UHF spectrum bands. The authors have estimated the interference effects of LTE system on DVB receivers and they have computed the protection distance by a simulation software tool. A test scenario was proposed in Zagreb, Croatia [30], to study the interference between both systems. It consists of 10 DVB-T transmitters radiating $24 \sim 37$ dBW (Decibel-Watt) and 120 LTE Base Stations (BS)s radiating 30 dBW ; both systems working in the $790 \sim 862$ MHz band. As a result, almost 5% of the population has lost DVB-T reception showing that further network optimizations should be made in order to decrease the number of people loosing DVB-T reception. In [31] and [32], the LTE network uses the digital dividend spectrum of DVB network in the context of coexistence between LTE and DVB. The authors have analyzed the interference effects caused by the digital broadcasting system on LTE, by using Monte Carlo simulations. The protection distance is the interested parameter in their studies. Their results show that the LTE uplink is interfered more seriously than the LTE downlink and should be paid more attention and that the effect of increasing protecting distance is not significant if it is already large. They conclude that the coexistence of the two systems in adjacent channels

is possible if reasonable measures are taken in the network plan and spectrum plan.

In [33], the authors have proposed a methodology that takes into account the mutual interference in DVB-LTE services in the context of coexistence in the same and adjacent frequency bands. In the case of coexistence on same frequency bands, both services are employed in neighbouring countries or regions, while in the other case, both services are operating in the same territory. Their investigation is based on Monte Carlo simulation. Similarly in [34], the authors have developed a simulation methodology to analyze the mutual interference between the international mobile telecommunications (IMT) and digital television (DTV) systems when they operate in adjacent frequency bands. Likewise in [35], Shamsan has investigated the coexistence between IMT and digital broadcasting systems with different channel overlapping scenarios. In his study, he has used a graphical scheme for spectral emission mask (SEM) and interference power level but he did not study analytically the ergodic capacity, where SEM is a filter applied to a signal in order to diminish the Out Of Band (OOB) emissions that are the main reasons of interference with adjacent spectrum bands. In [36], the authors have explored and measured the coexistence of DVB-T2 and LTE in different scenarios. Mainly, they have studied the influence of the LTE services on DVB-T2 services and vice versa when they are operating on neighbouring frequency spectrum.

Furthermore, some works have studied the resource management problem in coexistence scenario between DVB and LTE systems. In spectrum sharing scenario works, the dominant idea is that the primary network has the highest priority to transmit properly its signals. In [37], the tradeoff of opportunistic and regulated access of multi-user cognitive networks w.r.t. a primary licensed network has been explored. The authors showed that a non-zero interference level at the primary receivers allows more aggressive transmission policy of the secondary users and a high opportunity to transmit data compared to the strict zero interference requirement at the primary receivers. A lot of other works in the literature have considered primary and secondary networks, and used the capacity in their analysis. In [38], the authors study the appropriate transmit power allocation (TPA) strategies among the cognitive in order to optimize the performance of the CR system while limiting the interference in direction of the primary receivers, without requiring any adaptation of the transmitted signal spectra at the cognitive nodes. In [39], downlink channel assignment and power control for cognitive users are investigated in order to maximize the number of cognitive users in an opportunistic cellular network under a satisfactory interference level at the primary users. In [40] and [41], the authors have estimated the optimal power allocation schemes in order to maximize the system utility and satisfy the QoS requirement of SUs and interference constrains of the PU. In all these works, the symmetric interfering link from the primary user to the secondary user was not considered.

Further studies have addressed the inter-system interference offering different

solutions in order to decrease it. A test was conducted in [42] to measure the interference intensity on a DVB receiver by an LTE service in terms of bit error rate (BER), protection ratio, and Picture Failure (PF) before and after applying a SEM to the LTE signal. It was shown that an increase in the BER leads to an increase in PF. Then a BER of $9 \cdot 10^{-4}$ was taken in order to not exceed one PF every 30 s. This concluded that a much higher protection ratio was offered at a same Carrier to Noise Ratio (C/N) when a mask was applied. This study concluded that when an appropriate mask is applied to LTE signal, the separation between LTE and DVB-T towers can be reduced from a range of $1700 \sim 2200$ m to $800 \sim 1000$ m.

In the context of interference reduction also, plans have been made in order to switch to DVB operating on adjacent bands to LTE in Korea [43]. The SEAMCAT simulation, based on Monte-Carlo method, showed that in order to keep the probability of interference on a victim's receiver below 5% and protection distance negligible, a guard band of 8 MHz should be applied in addition to emission masks on both BS and Mobile Station (MS). Moreover, in [44], the authors analyzed the performance of the more realistic case of spatially close Wireless Local Area Networks (WLAN) systems interfering asynchronously in Direct-Sequence Spread Spectrum (DSSS) mode and on adjacent channels. The authors expose the performance of optimum and sub-optimum Multiuser Detection Maximum Likelihood Sequence Estimators (MUD-MLSEs) under varying conditions, e.g. level of interference, degree of spectral overlap, etc. This facilitates a better understanding and design of future interference-limited WLAN systems. The performance results are also important to spectrum policy makers, allowing to knowledgeably estimate the degree of tolerated interference in license exempt bands. Moreover, in [45], they study the reduction of the state-space of a MLSE detector in the case of a desired WLAN receiver experiencing delayed interference from some other transmitters operating in partially overlapping spectral bands and over independent frequency-selecting block-fading channels. A sub-optimum receiver of reduced complexity is derived and its satisfactory performance in the context of strong interference based on the formulation of the optimum receiver is demonstrated.

Another approach to reduce the interference and to maximize the spectrum usage is the CR approach discussed in [46]. CR is an intelligent radio that can be programmed and configured dynamically. CR devices are called White Space Devices (WSD) because they exploit holes in the spectrum using a sophisticated sensing algorithm to find unused or under-utilized bands, paired with SEM in order to limit emission leakage to adjacent channel's. In recent years, the concept of CR network has gained a great research interest in the academic, industrial, and regulation committees [47,48]. CR enables secondary wireless devices using unlicensed spectrum to communicate without interfering with primary users. Traditionally, the performance of CR systems is evaluated using capacity as a paramount metric [49].

Many works have investigated the spectrum sensing method in cognitive radio in

order to improve the spectrum use efficiency. In [50], the authors have studied the impact of the sensing accuracy on the transmission capacity achievable by the cognitive radio and they have introduced a new performance metric for cognitive radio networks measuring the actual capacity for cognitive users under imperfect sensing methods. Moreover, in [51], the authors have proposed an optimal spectrum sensing design for mobile primary user scenarios to determine the optimal transmission time and the optimal sensing time threshold. The authors in [52] have introduced the fundamentals, the architecture and the applications of the cognitive radio network, and they have investigated the important issues in dynamic spectrum allocation and sharing. In these works, the interference link, from the primary transmitter to the secondary receivers is not taken into account.

We cite also another interesting work on CR with spectrum sensing scenario in [3] and [53]. In these works, Asghari and Aissa have analyzed an adaptive resource-sharing in CR fading broadcast channel, particularly concerning transmission time and power allocation among users, under appropriate constraints on the average interference at the primary receiver and peak transmit-power at the secondary transmitter. They have attempted to find an optimal rate, time-sharing policy and transmit power to achieve the ergodic capacity of fading cognitive radio broadcast channel. But the symmetric interfering link, which is from the primary transmitter to the secondary receiver has not been considered. The idea presented in [3] is interesting especially at the spectral convergence application level between primary and secondary networks, which can be respectively a broadcasting and a cellular network. Consequently, we have analyzed its cognitive radio idea in the next chapter to make a comparison with our contribution work that is not based on the sensing of the primary activity.

1.4 Conclusion

This chapter presents some background knowledge that is used in this thesis. The transmission channel has been first described with the different channel models. After that, basic concepts of the OFDM transmission scheme have been introduced and formulated. Then, we have recalled the optimization problem standard form and some optimization methods. We have briefly introduced LTE and DVB networks basics and characteristics. A state of the art of different works concerning the LTE-DVB coexistence is presented. Both technologies are based on the same OFDM principle and must work side by side on the overcrowded spectrum due to the fact that both operate on similar frequency bands. But the mutual interference always arises as a major problem by degrading QoS of both systems. This opens the door to this thesis work and gives a general context of the following chapters. To start, in the next chapter, we analyze spectral coexistence between broadcasting and mobile

networks by using CR in order to maximize the capacity of LTE network considered as a secondary network.

2

Ergodic Capacity in a Cognitive Radio Link under Power Constraints

CR aims at overcoming the spectrum scarcity problem by enabling secondary wireless devices to opportunistically use the licensed primary users' spectrum when the latter do not use it. In this chapter, we consider a CR link operating in a spectrum sharing mode with a primary network. In this coexistence model, the users of the broadcast network, considered as primary, and the mobile network, considered as secondary, can share the same frequency band as long as the interference caused by the secondary network on the primary network is properly regulated. Besides, the optimal ergodic capacity of the secondary link that can be achieved is being investigated under the presence of two practical limiting constraints : average interference power affecting the capacity of the primary user and peak transmit power in the secondary transmitter.

2.1 Cognitive Radio Model

There are two strategies of CR : Opportunistic Spectrum Access (OSA) strategy, where a secondary network is allowed to transmit in the band originally allocated to the primary network, in an opportunistic way [54] ; and Spectrum-Sharing (SS) strategy, where the secondary is allowed to transmit simultaneously with the primary at the same band even if it is active [48], provided that interference caused on primary receivers stays below a pre-definite threshold.

OSA and SS approaches of CR are presented respectively in the block diagrams in Figures 2.1 and 2.2. The system in both models is constituted of one pair of Broadcast Transmitter (BT) and Broadcast Receiver (BR) and one pair of Base Station (BS) as transmitter and Mobile Receiver (MR).

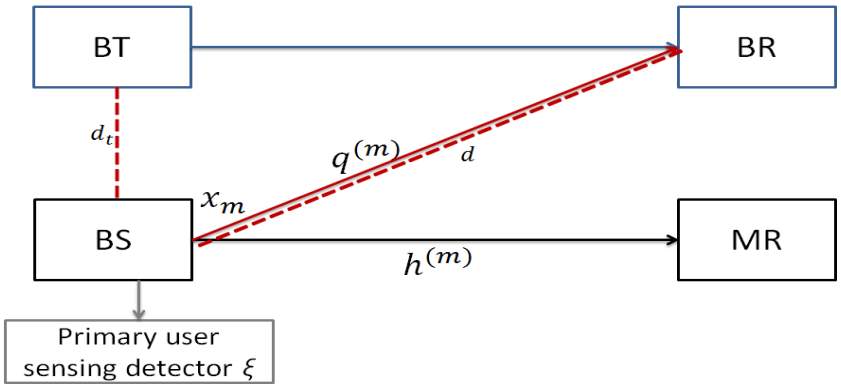

Figure 2.1 – Cognitive radio simplified model (OSA)

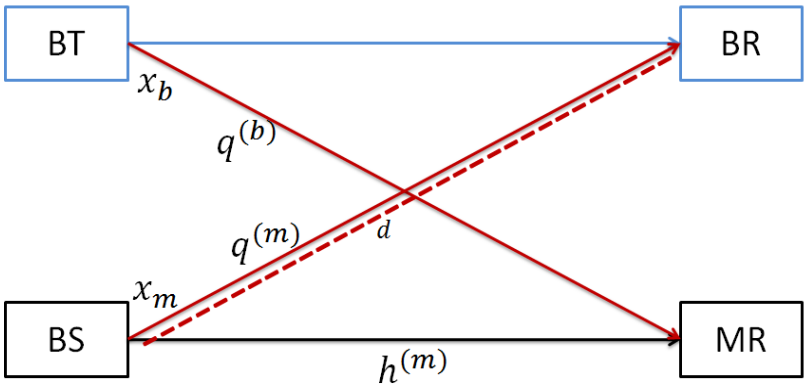

Figure 2.2 – Cognitive radio model with full interfering channels (SS)

The authors in [3], have studied the scenario illustrated in Fig. 2.1, where BS is equipped with a spectrum sensing detector whose function is to assess the frequency band of BT. The secondary transmitter calculates a single sensing metric ξ_s corresponding to the energy in the sensed band. The authors have found the optimal time and power allocation in order to maximize the secondary user ergodic capacity. However, the interference link BT-MR is not taken into account in the OSA model.

It is assumed that the interference from BT to MR can be ignored or included in the AWGN at MR. In this chapter, we focus on the scenario of Fig. 2.2 in order to study another spectrally convergence aspect without sensing the broadcast network activity while respecting its QoS conditions. In this model, the interfering link from BT to MR is considered. Moreover, the secondary transmitter is assumed not to have an energy detector for the free band sensing and fully interfere with the primary transmitter.

We first start revisiting the results in [3] in order to summarize the basic behaviour of ergodic capacity in OSA scenario.

2.2 CR with Opportunistic Spectrum Access

2.2.1 System and channel models

In this approach, the mobile system detects the activity of the broadcast system in order to make a power allocation for the BS according to this detection. In Fig.2.1, d signifies the distance between BS and BR, while d_t is the distance between BS and BT. We denote the channel gain between BS and MR by $|h^{(m)}|^2$ and the interference channel gain between BS and BR by $|q^{(m)}|^2$. $\left|h^{(m)}\right|$ is assumed to be Rayleigh distributed with unit mean, while $\left|q^{(m)}\right|$ is assumed to be Rayleigh distributed with variance that depends on the distance between BS and BR. The channel gains are assumed to be independent and they include the path loss attenuation depending on the distances between transmitter and receiver. AWGN is considered at MR with zero mean and variance N_0B, N_0 being the one-sided noise power spectral density and B the signal bandwidth. The received signal by MR is represented by :

$$y_m = \sqrt{P_m} h^{(m)} x_m + w_m \tag{2.1}$$

where x_m is the BS transmitted information symbol, P_m is the BS transmission power and w_m is AWGN noise sample. BT is considered active (ON state) with probability c or inactive (OFF state) with probability $\bar{c} = 1 - c$. Conditioned on the BT being on or off, the single sensing metric ξ_s is calculated based on the sum of i.i.d. Gaussian random variables and, consequently, is distributed according to Chi-square PDFs, each with M degrees of freedom, where M is the number of observation samples in each sensing interval [3]. Accordingly, under "PT is ON" condition, ξ_s has a non-central Chi-square distribution $f_A(\xi_s)$ with variance σ_A^2 and non centrality parameter μ_A [5], such that $f_A(\xi_s)$ is defined by :

$$f_A(\xi_s) = \frac{1}{2}\left(\frac{\xi_s}{\mu_A}\right)^{\frac{M-2}{4}} e^{-\frac{-\mu_A+\xi_s}{2}} I_{\frac{M}{2}-1}\left(\sqrt{\mu_A \xi_s}\right) \tag{2.2}$$

where σ_A^2 is defined as $\sigma_A^2 = 2\mu_A$, μ_A is obtained in terms of the ratio of BT's signal energy to noise spectral density, as detailed in [4], such that $\mu_A = M\left(\frac{P_b}{d_t^2} + 1\right)$ where P_b is the BT transmission power and d_t is the distance between BT and BS. $I_v(.)$ is the v^{th} order modified Bessel function. Similarly, under "PT is OFF" condition, ξ_s has a central Chi-square PDF $f_I(\xi_s)$ with variance σ_I^2, such that $f_I(\xi_s)$ is defined by :

$$f_I(\xi_s) = \frac{1}{2^{\frac{1}{2}}\Gamma\left(\frac{M}{2}\right)} \xi_s^{\frac{M}{2}-1} e^{-\frac{-\xi_s}{2}} \tag{2.3}$$

where σ_I^2 is defined as $\sigma_I^2 = 2M$, and $\Gamma(.)$ is the Gamma function.

2.2.2 Power adaptation and ergodic capacity

We calculate the ergodic capacity of MR in this model where $P_m(|h^{(m)}|^2, \xi_s)$ is the BS transmitted power of MR depending on $|h^{(m)}|^2$ and ξ_s. We start by investigating the power adaptation policy under the constraints : maximal average interference power present at the broadcast receiver below a threshold and the peak transmit power constraint at the secondary transmitter. Therefore, the maximal ergodic capacity of mobile transceiver, in bits/sec/Hz, represents the solution of the following problem :

$$\frac{C_m}{B} = \underbrace{\max}_{P_m(|h^{(m)}|^2,\xi_s)} \left\{ \mathbb{E}_{|h^{(m)}|^2,\xi_s} \left[\log_2 \left(1 + \frac{P_m(|h^{(m)}|^2, \xi_s)|h^{(m)}|^2}{N_0 B} \right) \right] \right\} \tag{2.4}$$

s.t.

$$\mathbb{E}_{|h^{(m)}|^2,\xi_s} \left[\left| q^{(m)} \right|^2 P_m(|h^{(m)}|^2, \xi_s) \mid \text{BT is ON} \right] \leq Q_{inter} \tag{2.5}$$

and

$$P_m(|h^{(m)}|^2, \xi_s) \leq Q_{peak} \tag{2.6}$$

where Q_{inter} is the average interference power accepted on BR and Q_{peak} is the BS acceptable peak transmit power because of the non-linearity of amplifier. As the variance of $|q^{(m)}|$ is assumed equal to $1/d^2$, the interference constraint presented in (2.5) becomes :

$$\mathbb{E}_{|h^{(m)}|^2,\xi_s}[P_m(|h^{(m)}|^2, \xi_s)|\text{BT is ON}] \leq Q'_{inter} \tag{2.7}$$

where $Q'_{inter} = Q_{inter} d^2$. Then, the interference constraint is simplified by taking the expectation over the distribution of $|h^{(m)}|^2$.

Giving the power adaptation policy that maximizes the ergodic capacity presented in (2.4), optimal power allocation under constraints on average interference

and peak transmit power is given by [3] :

$$P_m\left(|h^{(m)}|^2,\xi_s\right)=\begin{cases} Q_{peak} & \frac{1}{|h^{(m)}|^2}\prec\frac{V(\xi_s)}{N_0B} \\ \frac{U(\xi_s)}{\lambda_s}-\frac{N_0B}{|h^{(m)}|^2} & \frac{V(\xi_s)}{N_0B}\leq\frac{1}{|h^{(m)}|^2}\leq\frac{U(\xi_s)}{\lambda_sN_0B} \\ 0 & \frac{1}{|h^{(m)}|^2}\geq\frac{U(\xi_s)}{\lambda_sN_0B} \end{cases} \tag{2.8}$$

where λ_s is the Lagrange multiplier corresponding to the constraint presented in (2.5). λ_s can be obtained by substituting (2.8) into the interference constraint in (2.5) at equality :

$$\mathbb{E}_{|h^{(m)}|^2,\xi_s}[P_m(|h^{(m)}|^2,\xi_s)|\text{BT is ON}]=Q'_{inter} \tag{2.9}$$

and the terms $U(\xi_s)$ and $V(\xi_s)$ are defined as :

$$\begin{aligned} U(\xi_s)&=c+\bar{c}\frac{f_0(\xi_s)}{f_1(\xi_s)} \\ V(\xi_s)&=\frac{U(\xi_s)}{\lambda_s}-Q_{peak} \end{aligned} \tag{2.10}$$

The solution presented in (2.8) shows that the power allocation at BS depends on $\frac{1}{|h^{(m)}|^2}$ and on $U(\xi_s)$ and $V(\xi_s)$, which confirms that the transmission power is allocated according to the BT activity detection. The optimal ergodic capacity of MR is calculated with the expression presented in (2.4) where the interference constraint is satisfied by using the bisection method [55].

2.2.3 Results and discussion

We assume that $N_0B=1$ and the number of observation samples is supposed to be $M=30$. BT is assumed to be active 50% of the time, which gives $c=0.5$. For simplicity and without loss of generality, distances in Fig. 2.1 are normalized such that $d_t=1$ and $d=3$, and the BT transmission power is normalized such that $P_b=1$. These parameters will be used throughout the remaining part of this chapter unless otherwise mentioned.

After solving (2.4), Figures 2.3 and 2.4 show respectively the variation of Lagrange multiplier λ_s and the corresponding obtained ergodic capacity in bits/s/Hz versus Q_{inter} and for different values of the constraints ratio $\rho=\frac{Q_{peak}}{Q_{inter}}$.

In Fig. 2.3, λ_s decreases when Q_{inter} increases, while it increases with the increasing values of ρ. Hence for a given value of Q_{inter} , λ_s increases as the transmit power constraint gets less stringent, and converges towards the case with no peak transmit-power constraint ($\rho\succ 2$).

The ergodic capacity in Fig. 2.4 increases with the increasing value of Q_{inter} and also increases with the increasing value of ρ, i.e. Q_{peak} for a given Q_{inter}. The

maximal ergodic capacity is achieved when no peak power constraint is considered and we can remark that the achievable rate converges toward this limit when ρ is increasing. This means that a higher Q_{peak} can be considered as an advantage for the system performance and increases the channel capacity, but after a certain value of ρ, for instance when Q_{peak} is much higher than Q_{inter} ($\rho \succ 2$), the capacity is only limited by the average interference constraint and does not increase as Q_{peak} increases.

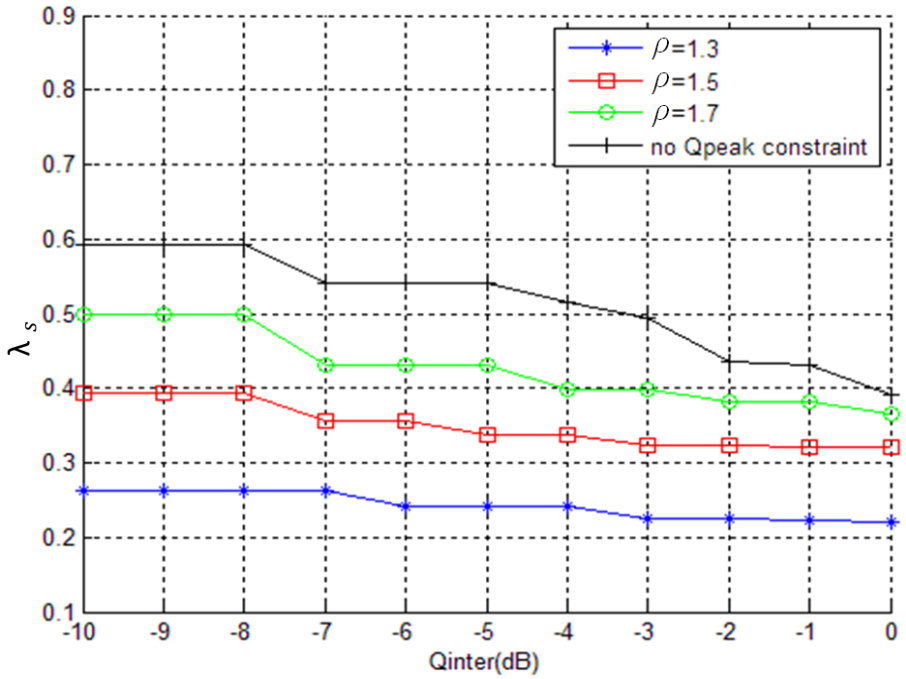

Figure 2.3 – Variation of the Lagrangian multiplier λ_s in function of Q_{inter}.

2.3 CR with Spectrum Sharing

2.3.1 System and channel models

The block diagram of SS model is presented in Fig.2.2. In this approach, BS attempts to send information to MR while using the spectrum band that is originally allocated to BT. So we have a full channel interference between these two systems. $|h^{(m)}|^2$ is the channel gain between BS and MR and $|q^{(m)}|^2$ is the channel gain between BS and BR. Moreover, $|q^{(b)}|^2$ is the interference channel gain between BT and MR that is taken into account in the SS model. All channels are considered to be flat, independent, and Rayleigh distributed with unit mean, and they include the

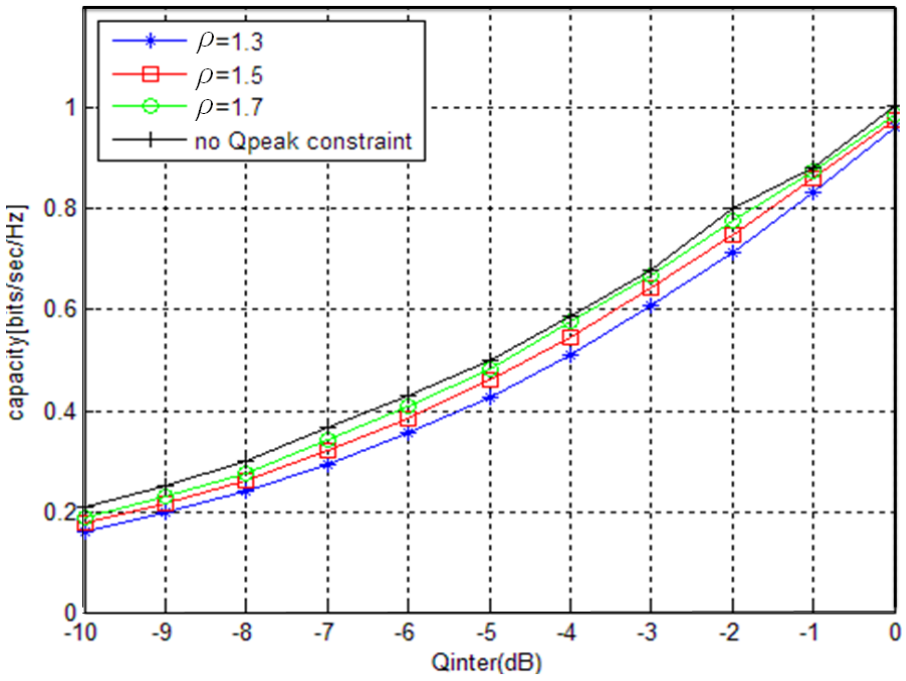

Figure 2.4 – Ergodic capacity of the secondary link under adaptive power transmission in Rayleigh fading.

path loss attenuation depending on the distances between transmitter and receiver. In Fig. 2.2, d also signifies the distance between BS and BR. The mobile secondary system uses the spectrum of the broadcast primary system and adapts its transmission power in order to maximize its ergodic capacity while respecting limitations for the primary. The received signal at MR is given by :

$$y_m = \sqrt{P_m} h^{(m)} x_m + \sqrt{P_b} q^{(b)} x_b + w_m \tag{2.11}$$

where x_b is the BT information symbol and P_b is the BT transmission power.

2.3.2 Mobile receiver received data rate

Considering that the channel is constant over one information symbol, the signal to interference plus noise ratio (SINR) of MR, averaged over the symbols, can be written as :

$$\gamma_{\mathrm{m}} = \frac{\mathbb{E}\left[\left|\sqrt{P_m} h^{(m)} x_m\right|^2\right]}{\mathbb{E}\left[\left|\sqrt{P_b} q^{(b)} x_b + w_m\right|^2\right]} = \frac{P_m \left|h^{(m)}\right|^2}{P_b \left|q^{(b)}\right|^2 + N_0 B}. \tag{2.12}$$

where $\mathbb{E}[x_m] = \mathbb{E}[x_b] = 0$ and $\mathbb{E}[|x_m|^2] = \mathbb{E}[|x_b|^2] = 1$. The achievable data rate, in bits/s, on MR can be expressed as :

$$C(P_m) = B \log_2 \left(1 + \frac{|h^{(m)}|^2 P_m}{|q^{(b)}|^2 P_b + N_0 B}\right), \tag{2.13}$$

2.3.3 Ergodic capacity maximization problem

2.3.3.1 Power constraints

We aim at maximizing the expression in (2.13) under the same constraints than previously : average interference power on BR and peak transmit power on BS [39], [40]. The average interference power is restricted below a certain level to guarantee the QoS of BT, while the peak power limitation is mainly due to the non-linearity of power amplifier in practice. We denote that the transmitted power at BS depends on the channel gain (including the path loss), i.e. $P_m(|q^{(b)}|^2, |h^{(m)}|^2)$. The average interference constraint at BR can then be expressed as [53] :

$$\mathbb{E}_{|q^{(b)}|^2, |h^{(m)}|^2}[|q^{(m)}|^2 P_m(|q^{(b)}|^2, |h^{(m)}|^2)] \leq Q_{inter} \tag{2.14}$$

The average interference constraint above is simplified by taking the expectation over the distribution of $|q^{(m)}|^2$ and can be rewritten as :

$$\mathbb{E}[P_m(|q^{(b)}|^2, |h^{(m)}|^2)] \leq Q'_{inter} \tag{2.15}$$

where $Q'_{inter} = Q_{inter} d^2$ [53]. The peak transmit power constraint is represented by :

$$P_m(|q^{(b)}|^2, |h^{(m)}|^2) \leq Q_{peak}; \forall |q^{(b)}|^2, |h^{(m)}|^2 \tag{2.16}$$

where Q_{peak} is the peak BS transmitting power limit, and $P_m(|q^{(b)}|^2, |h^{(m)}|^2) \geq 0$

2.3.3.2 Maximization problem

The performance of the secondary link is defined in terms of the ergodic capacity that can be achieved, under the aforementioned power constraints. The ergodic capacity of MR is considered under the full interference links shown in Fig. 2.2 where BT is always active. The maximal capacity will be obtained through an optimal power allocation at BS. We define the maximum secondary link capacity as :

$$C_m = \underbrace{\max}_{P_m(|q^{(b)}|^2, |h^{(m)}|^2)} \{C(P_m)\} \tag{2.17}$$

So, the optimization problem is formulated as [40] :

$$\frac{C_m}{B} = \underbrace{\max}_{P_m(|q^{(b)}|^2, |h^{(m)}|^2)} \left\{ \mathbb{E}\left[\log_2 \left(1 + \frac{P_m\left(|q^{(b)}|^2, |h^{(m)}|^2\right) |h^{(m)}|^2}{P_b |q^{(b)}|^2 + N_0 B}\right)\right]\right\} \tag{2.18}$$

subject to :

$$\mathbb{E}\left[P_m\left(|q^{(b)}|^2, |h^{(m)}|^2\right)\right] \leq Q'_{inter} \tag{2.19}$$

and

$$P_m \leq Q_{peak} \tag{2.20}$$

2.3.4 Optimal solution

2.3.4.1 Optimal power allocation

To solve the maximization problem of the ergodic capacity in (2.18) with respecting the constraints presented in (2.19) and (2.20), we adopt an approach similar to that used in [3, 40, 55]. First of all, the system is considered as an interference-limited system. So the noise term N_0B is neglected compared to the interference term $P_b|q^{(b)}|^2$ in (2.18).

The optimization problem presented in (2.18) has decoupled constraints. Hence, the problem is separated into two parts. Firstly, the Lagrangian objective function is rearranged considering the interference constraint as :

$$\begin{aligned} J(P_m(|q^{(b)}|^2, |h^{(m)}|^2), \lambda_p) &= \mathbb{E}\left[\log_2\left(1 + \frac{P_m(|q^{(b)}|^2, |h^{(m)}|^2)|h^{(m)}|^2}{P_b|q^{(b)}|^2}\right)\right] \\ &\quad -\lambda_p\left(\mathbb{E}\left[P_m(|q^{(b)}|^2, |h^{(m)}|^2)\right] - Q'_{inter}\right) \end{aligned} \tag{2.21}$$

where λ_p is the Lagrange multiplier associated with the interference constraint in (2.19). In a second time, the Lagrangian is maximized subject to the peak transmit power constraint, such as :

$$\begin{aligned} &\underbrace{\max}_{P_m(|q^{(b)}|^2, |h^{(m)}|^2)} && J\left(P_m\left(|q^{(b)}|^2, |h^{(m)}|^2\right), \lambda_p\right) \\ &\textbf{s.t} && \begin{cases} P_m \leq Q_{peak} \\ P_m \geq 0 \end{cases} \end{aligned} \tag{2.22}$$

2.3.4.2 KKT conditions

The KKT conditions corresponding to the optimization problem presented in (2.22) are given by :

$$\frac{\partial J(P_m)}{\partial P_m} = 0 \tag{2.23}$$

$$\lambda'_p(P_m - Q_{peak}) = 0 \tag{2.24}$$

where λ'_p is the Lagrange multiplier corresponding to the peak transmit power constraint. The solution of the first KKT condition in (2.23) gives :

$$P_m(|q^{(b)}|^2, |h^{(m)}|^2) = \frac{1}{\lambda_p} - P_b\frac{|q^{(b)}|^2}{|h^{(m)}|^2} \tag{2.25}$$

which represents the optimal power allocation within the range :

$$0 \leq P_m(|q^{(b)}|^2, |h^{(m)}|^2) \leq Q_{peak} \tag{2.26}$$

with the two limiting values $P_m(|q^{(b)}|^2, |h^{(m)}|^2) = Q_{peak}$ and $P_m(|q^{(b)}|^2, |h^{(m)}|^2) = 0$ obtained respectively below and above the limits in (2.26). The optimal power allocation is obtained by inserting $P_m(|q^{(b)}|^2, |h^{(m)}|^2)$ of (2.25) in (2.26), within the range :

$$\frac{1}{\lambda_p} - Q_{peak} \leq P_b \frac{|q^{(b)}|^2}{|h^{(m)}|^2} \leq \frac{1}{\lambda_p}. \tag{2.27}$$

Therefore, the optimal solution of the BS transmit power $P_m(|q^{(b)}|^2, |h^{(m)}|^2)$ is given by :

$$P_m(|q^{(b)}|^2, |h^{(m)}|^2) = \begin{cases} Q_{peak} & P_b \frac{|q^{(b)}|^2}{|h^{(m)}|^2} \prec \frac{1}{\lambda_p} - Q_{peak} \\ \frac{1}{\lambda_p} - \frac{|q^{(b)}|^2}{|h^{(m)}|^2} P_b & \frac{1}{\lambda_p} - Q_{peak} \leq P_b \frac{|q^{(b)}|^2}{|h^{(m)}|^2} \leq \frac{1}{\lambda_p} \\ 0 & P_b \frac{|q^{(b)}|^2}{|h^{(m)}|^2} \geq \frac{1}{\lambda_p} \end{cases} \tag{2.28}$$

The Lagrange multiplier λ_p is finally determined from the interference constraint at equality :

$$\mathbb{E}[P_m(|q^{(b)}|^2, |h^{(m)}|^2)] = Q'_{inter}, \tag{2.29}$$

thus completing the optimal solution in (2.28). The solution represents a water filling as in [53] and [40]. This solution is represented in Fig. 2.5 where the blue line illustrates this water level and hence shows schematically the optimal range of operation of MR which is governed by two threshold values A_{min} and A_{max} defined from (2.27) as :

$$A_{min} = \frac{1}{\lambda_p} - Q_{peak} \tag{2.30}$$

$$A_{max} = \frac{1}{\lambda_p} \tag{2.31}$$

Whenever $P_b \frac{|q^{(b)}|^2}{|h^{(m)}|^2}$ is higher than A_{max}, i.e. when the interference from BT dominates the channel gain in the secondary link, the BS optimal operation is to turn off. On the contrary, when $P_b \frac{|q^{(b)}|^2}{|h^{(m)}|^2}$ gets lower than A_{max}, the BS can transmit with increasing power level that reaches the peak power value when $P_b \frac{|q^{(b)}|^2}{|h^{(m)}|^2}$ gets lower than A_{min} as shown in Fig. 2.5.

2.3.5 Closed- form expression of the ergodic capacity of MR

2.3.5.1 Analytical solution for the Lagrange multiplier λ_p

As seen from (2.28) and (2.29), the Lagrange multiplier λ_p is contained in the expectation of the optimal allocated power $P_m(|q^{(b)}|^2, |h^{(m)}|^2)$. This latter is, in turn,

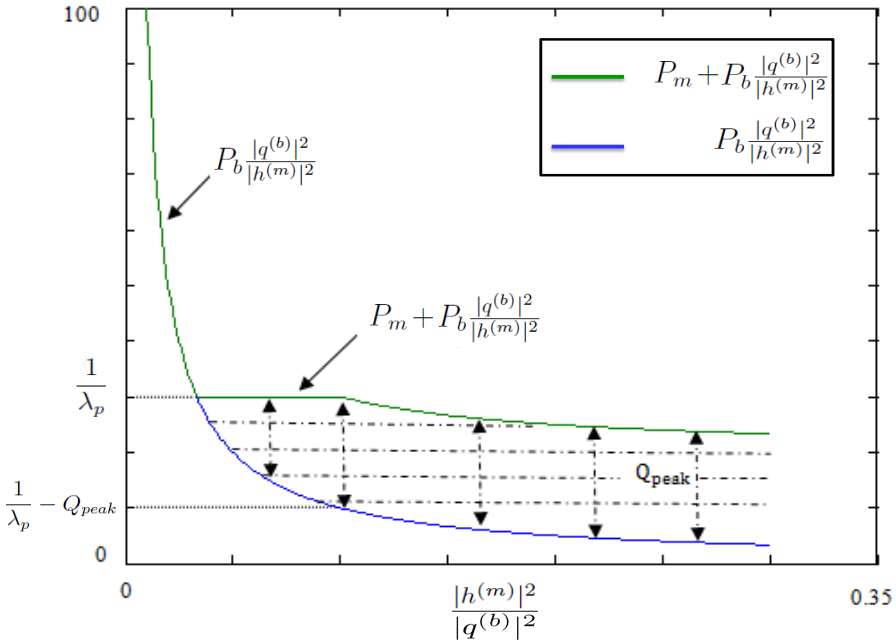

Figure 2.5 – Optimal power allocation for the secondary user

expressed in (2.28) as a function of the ratio $r = P_b \frac{|q^{(b)}|^2}{|h^{(m)}|^2}$ of channel power gains. In Rayleigh fading, the ratio r is distributed according to log-logistic probability density function [56] :

$$P_R(r) = \frac{1}{P_b \left(1 + \frac{r}{P_b}\right)^2} \tag{2.32}$$

For the sake of simplicity and without loss of generality, P_b will be in the sequel normalized to 1. For a given value of Q_{peak}, we distinguish two cases :

case 1 : $\frac{1}{\lambda_p} - Q_{peak} \succ 0$

In this case, the expectation of P_m is given by :

$$\begin{aligned} \mathbb{E}_{\frac{|q^{(b)}|^2}{|h^{(m)}|^2}}[P_m] &= \int_0^{\frac{1}{\lambda_p} - Q_{peak}} Q_{peak} \frac{1}{(1+r)^2} dr + \int_{\frac{1}{\lambda_p} - Q_{peak}}^{\frac{1}{\lambda_p}} \left(\frac{1}{\lambda_p} - r\right) \frac{1}{(1+r)^2} dr \\ &= Q_{peak} + \ln\left(1 - \frac{\lambda_p Q_{peak}}{1 + \lambda_p}\right) \end{aligned} \tag{2.33}$$

and λ_p is obtained in this case, from (2.29), as :

$$\lambda_p = \left(\frac{Q_{peak}}{1 - e^{Q'_{inter} - Q_{peak}}} - 1\right)^{-1}. \tag{2.34}$$

case 2 : $\frac{1}{\lambda_p} - Q_{peak} \prec 0$

In this case, the transmit power P_m cannot reach Q_{peak} and is only limited by the interference threshold and :

$$\mathbb{E}_{\frac{|q^{(b)}|^2}{|h^{(m)}|^2}}[P_m] = \int_0^{\frac{1}{\lambda_p}} \left(\frac{1}{\lambda_p} - r\right) \frac{1}{(1+r)^2} dr = \frac{1}{\lambda_p} + \ln\left(\frac{\lambda_p}{1+\lambda_p}\right) \tag{2.35}$$

and λ_p is deduced from (2.29) as :

$$\lambda_p = -W\left(-e^{-Q'_{inter}-1}\right) - 1 \tag{2.36}$$

where $W(.)$ is the Lambert function.

2.3.5.2 Ergodic capacity of mobile receiver

Based on the results obtained in the previous section, the optimal ergodic capacity can be achieved analytically from :

$$\frac{C_m}{B} = \mathbb{E}_{\frac{|q^{(b)}|^2}{|h^{(m)}|^2}} log_2\left(1 + P_m \frac{|h^{(m)}|^2}{|q^{(b)}|^2}\right), \tag{2.37}$$

where two cases should be considered :

case 1 : $\frac{1}{\lambda_p} - Q_{peak} \succ 0$

$$\begin{aligned} \frac{C}{B} &= \int_0^{\frac{1}{\lambda_p}-Q_{peak}} \log_2\left(1 + Q_{peak}\frac{1}{r}\right) \frac{1}{(1+r)^2} dr \\ &\quad + \int_{\frac{1}{\lambda_p}-Q_{peak}}^{\frac{1}{\lambda_p}} \log_2\left(1 + \left(\frac{1}{\lambda_p} - r\right)\frac{1}{r}\right) \frac{1}{(1+r)^2} dr \end{aligned} \tag{2.38}$$

$$\begin{aligned} \frac{C}{B} &= \log_2(1+\lambda_p) - \frac{1}{1-Q_{peak}} \left[\log_2\left(\lambda_p + 1 - \lambda_p Q_{peak}\right)\right. \\ &\quad \left. + Q_{peak}\log_2(Q_{peak})\right] \end{aligned} \tag{2.39}$$

case 2 : $\frac{1}{\lambda_p} - Q_{peak} \prec 0$

$$\begin{aligned} \frac{C}{B} &= \int_0^{\frac{1}{\lambda_p}} \log_2\left(1 + \left(\frac{1}{\lambda_p} - r\right)\frac{1}{r}\right) \frac{1}{(1+r)^2} dr \\ &= \log_2\left(\frac{\lambda_p + 1}{\lambda_p}\right) \end{aligned} \tag{2.40}$$

The closed-form expression of the ergodic capacity can be finally obtained in terms of Q_{peak} and Q'_{inter} by replacing (2.34) and (2.36) in (2.39) and (2.40) respectively.

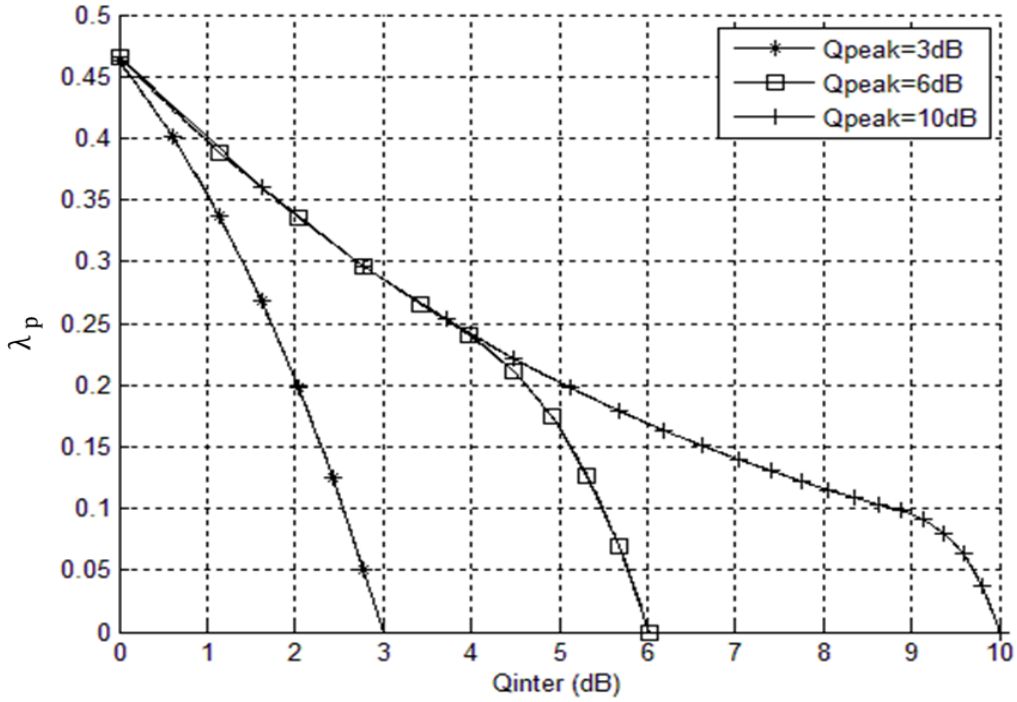

Figure 2.6 – Lagrangian multiplier λ_p in function of Q_{inter} for different values of Q_{peak}

2.4 Simulations and discussion

The simulation results obtained for optimal power allocation maximizing the ergodic capacity of BS-MR in full channel interference are presented. BT is considered to be always active. Fig. 2.6 shows the variation of λ_p in function of the interference threshold Q_{inter} for different values of Q_{peak}. It can be seen that λ_p has a decreasing behaviour when Q_{inter} increases. This observation can be interpreted thanks to Fig. 2.5 : for a given value of Q_{peak}, if λ_p decreases, the water filling area becomes larger and hence, $Q_{inter} = \mathbb{E}[P_m]$ increases. The ergodic capacity of the secondary link versus the interference threshold for different peak transmit power levels is presented in Fig. 2.7. It is clearly shown, as expected, that the capacity of BS-MR link can take benefit when Q_{inter} increases, i.e when the interference constraint is relaxed. The saturating part of the curves in Fig. 2.7 corresponds to the case where capacity is only limited by the peak power constraint.

To gain further insight on the performance of the secondary link, the variation of capacity on BS-MR link versus the MR peak power value is presented in Fig. 2.8 for different values of Q_{inter}. As expected, the ergodic capacity of the secondary link

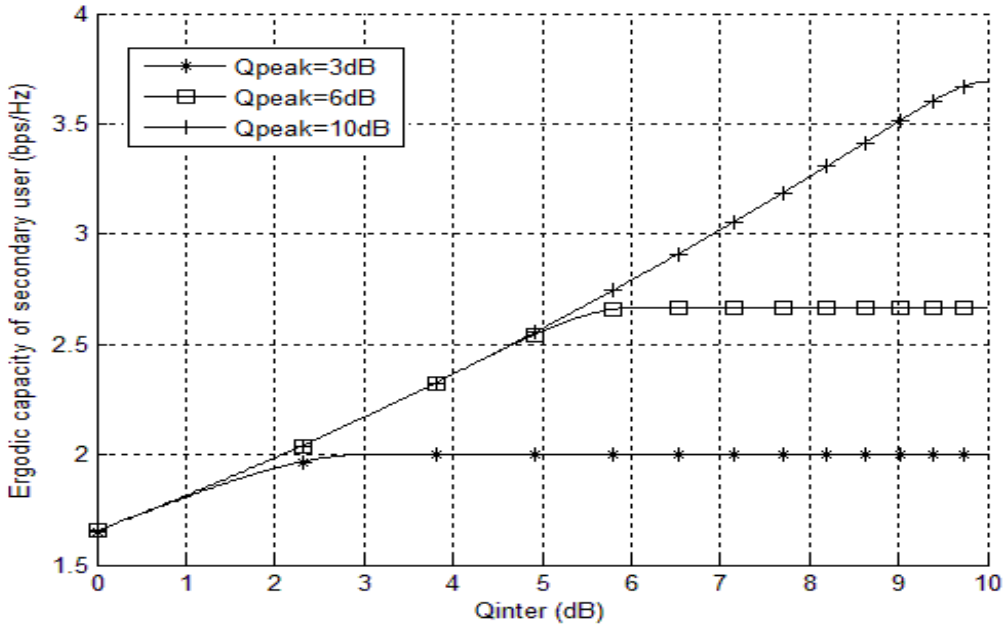

Figure 2.7 – Ergodic capacity versus Qinter for different Qpeak values.

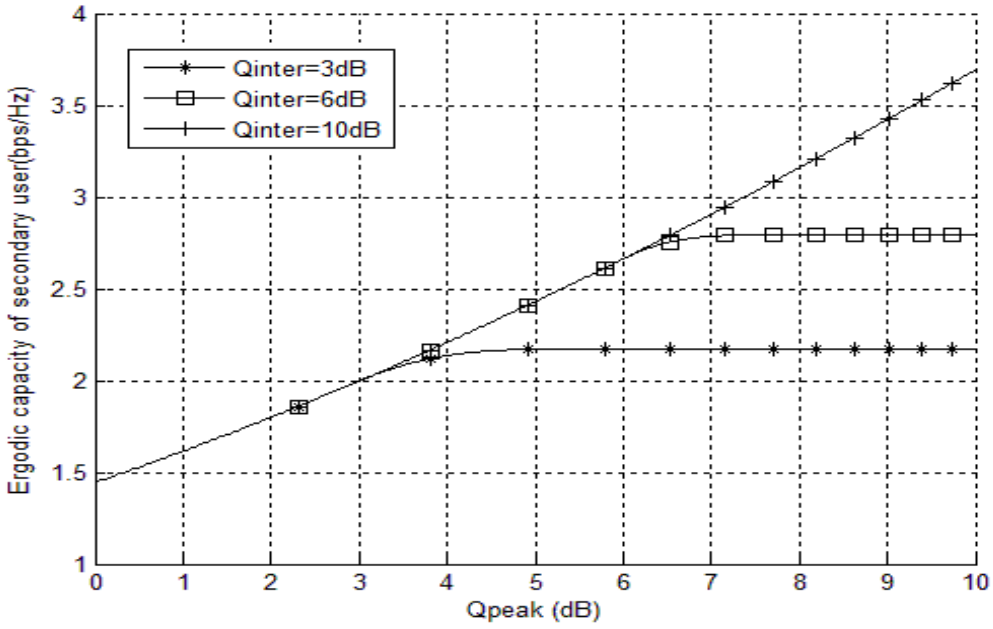

Figure 2.8 – Ergodic capacity versus Qpeak for different Qinter values.

is enhanced when Q_{peak} is getting higher values up to some saturating point where the interference constraint becomes dominant. For $Q_{inter} = 3$ dB and $Q_{inter} = 6$ dB, the saturating Q_{peak} values are equal to 4 dB and 7 dB respectively.

2.5 Opportunistic Spectrum Access versus Spectrum Sharing

As seen in this chapter, OSA and SS modes have different system models. In OSA mode, BT is considered to be active in some period. Therefore, BS uses a sensing method to detect the BT activity. The goal in OSA mode is to benefit from the non activity parts in BT bandwidth by enabling BS to use it but under severe QoS constraint, i.e. interference level. Consequently, the optimal value of the transmission power $P_m(|h^{(m)}|^2, \xi_s)$ depends on the sensing parameter ξ_s and on the BS-MR channel gain $|h^{(m)}|^2$.

Otherwise, in SS mode, BT is assumed always active to model a real sharing system with full interference. According to this, in SS mode the interfering link affecting on the MR is taken into account. The optimal power in SS mode does not depend on any sensing observation parameter, it depends on the channel gains $|h^{(m)}|^2$ and $|q^{(b)}|^2$. This means that $|q^{(b)}|^2$ is an affecting factor on the BS power allocation in SS mode, contrary to OSA mode.

In simulations, the Lagrange multipliers λ_s and λ_p, that correspond respectively to the power allocation in OSA and SS modes, react both in a same manner with Q_{inter} and Q_{peak}. In both cases, the obtained capacity increases with the increasing values of Q_{inter} and Q_{peak}. Therefore, both modes lead to the same conclusion except that it implies a different analytical resolution.

2.6 Conclusion

In this chapter, the ergodic capacity of a secondary link in a cognitive radio spectrum-sharing model under two joint power constraints and in a full cross interference Rayleigh channel is derived in closed form. The power constraints are related to the practical issues of average interference power at the primary receiver and peak transmit power at the secondary transmitter. The analytical results obtained are validated with numerical simulations. They allow finding the optimal throughput and the limits of operation of the secondary link in a CR context in different conditions. These results can be applicable in the context of convergence between networks such as DVB and LTE [36]. This chapter analysed a different contribution than the cognitive radio application explored in [3]. But, it respects always the QoS constraints which guarantee the primary network performance. In

the next chapter, the spectral coexistence of interfering multi-carriers systems such as DVB and LTE is investigated.

3

Global Ergodic Capacity Closed-Form Expression of Coexisting DVB-LTE Like systems

In this chapter, the problem of convergence between mobile and broadcast networks is analyzed differently. Here, we assume that there isn't any priority between these two networks. They transmit on the same bandwidth with specific characteristics for each of them, i.e. different sub-carrier spacings, different transmission powers, different cell radius, etc. A non-cooperative deployment of these technologies is considered in the sense that cellular and broadcast networks interfere on each other.

The idea in this chapter consists in deploying a small cell into a large broadcast cell in the framework of spectral overlap between cellular and broadcast networks. The model associated to this scenario is called the full interference channel (FIC) in which all links between different networks transmitters and receivers are considered. The main contribution consists in the derivation of the global ergodic capacity of the global system in closed-form expression with an aggressive frequency reuse and Rayleigh fading channel on each link. This derivation allows the evaluation of the system parameters influence on the received data rates in each network and on the global system. Firstly, system and signal models are discussed when DVB and LTE are OFDM-based signals. Next, the analytical form of the global ergodic capacity of the total coexistence system is calculated and a numerical study of the system performance is presented. Finally, a conclusion is drawn.

3.1 System Model

This section introduces the system model and notations used throughout the chapter. The proposed model is composed of two communication systems : the DVB broadcasting network and the LTE cellular network as described in Fig. 3.1. The broadcast network is composed of the broadcast transmitter (BT) and one Broadcast

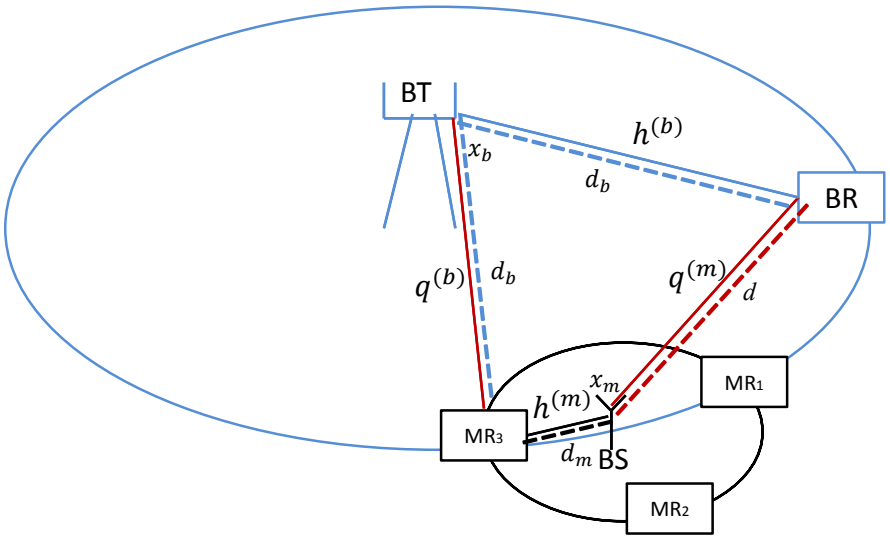

Figure 3.1 – Full interfering LTE cell in a DVB macro-cell.

Receiver (BR). The mobile network consists of a single cell of one Base Station (BS) and one Mobile Receiver (MR). It is worth noting that this model can be easily extended to multi-cells deployment considering the non-reuse of the frequency for the cellular system, leading to a single interfering cellular cell from the broadcast point of view. Moreover, it can also be easily extended to multi-user deployment considering the non-reuse of the frequency for different users, leading to a single MR from the broadcast point of view.

Both DVB and LTE are OFDM-based systems but with different physical characteristics. In addition to the links of interest, i.e. BT-BR and BS-MR, each transmission interferes on the other. Hence, the interfering links, i.e. BT-MR and BS-BR, are taken into account. All these links are considered to be as Rayleigh fading channels. In Fig. 3.1, d_m signifies the LTE cell radius and d_b signifies the DVB cell radius. Moreover, each receiver in both networks is considered located at the cell boundaries of its corresponding network, i.e. MR is located on the LTE cell edge and similarly BR is located on the DVB macro cell. Hence, the BT-BR and BS-MR distances are d_b and d_m respectively. Since $d_b \gg d_m$, MR can be assumed to be located on the DVB cell edge. Therefore, the interference distance between BT and MR is equal to d_b.

3.2 Signal model

In the FIC model, each signal interferes with the other coexisting network's signal. In the full interference case, all subcarriers in each network are similarly affected and each subcarrier is considered entirely attenuated by the interference. Hence, the system performance is studied over one subcarrier in each network.

However, as DVB and LTE systems have not the same OFDM system parameters and then their OFDM subcarriers have different spaces, the number of interfering subcarriers on each system w.r.t. the other is not equal. Indeed, an LTE subcarrier bandwidth is typically larger than the DVB one as seen in Table 1.1. Hence, for the sake of simplicity but without loss in generality, we consider that at the LTE receiver, R_b DVB subcarriers interfere with one LTE subcarrier. The value of R_b depends on the implemented modes in LTE and DVB. Contrarily, focusing on one subcarrier of the DVB receiver, only a fraction κ of one LTE subcarrier is visible on this side, leading to the signal model proposed in this chapter. Therefore, the signal received for each system is written considering one subcarrier as described below.

Cellular signal

The signal received on one subcarrier at the MR can be written in the frequency domain as the sum of the BS transmitted signal, multiplied by the channel fading and the path-loss attenuation, and the BT transmitted interfering signal, multiplied by the interfering channel fading and the path-loss attenuation. Hence, it could be written as :

$$y_m = \sqrt{p_m l_m} h^{(m)} x_m + \sum_{b=1}^{R_b} \sqrt{p_b l_{bm}} q^{(b)} x_b + w_m \tag{3.1}$$

where x_m, x_b are symbol informations of mobile and broadcast networks respectively with $\mathbb{E}[x_m] = \mathbb{E}[x_b] = 0$ and $\mathbb{E}\left[|x_m|^2\right] = \mathbb{E}\left[|x_b|^2\right] = 1$. Moreover, $h^{(m)}$ is the complex channel fading coefficient on the link BS-MR such as $h^{(m)} \sim \mathcal{CN}(0,1)$ and $q^{(b)}$ is the channel fading coefficient of the interference link BT-MR such as $q^{(b)} \sim \mathcal{CN}(0,1)$. l_m, l_{bm} are respectively their path-loss attenuations. Furthermore, p_m and p_b are the transmit power on one subcarrier at BS and BT respectively. Finally, w_m is the AWGN noise on one subcarrier at MR with power σ_m^2. Otherwise, it can be seen in (3.1) that a sum of DVB subcarriers signals are considered interfering on one LTE subcarrier signal.

Broadcast signal

On the other hand, the received signal at BR on one subcarrier in frequency domain can be written as :

$$y_b = \sqrt{p_b l_b} h^{(b)} x_b + \kappa \sqrt{p_m l_{mb}} q^{(m)} x_m + w_b \tag{3.2}$$

where $h^{(b)}$ is the complex channel fading coefficient on the link BS-MR such as $h^{(b)} \sim \mathcal{CN}(0,1)$ and $q^{(m)}$ is the channel fading coefficient of the interference link BT-MR such as $q^{(m)} \sim \mathcal{CN}(0,1)$. Moreover, l_b and l_{mb} are respectively the path-loss attenuations on the links BT-BR and BS-BR, respectively. Finally, w_b is the AWGN noise one one subcarrier at the BR with power σ_b^2. Otherwise, it can be seen in (3.2) that a ratio of one LTE subcarrier is considered interfering on one DVB subcarrier.

3.3 Global Ergodic Capacity

This section presents the derivation of the global ergodic capacity of the global mobile-broadcast coexisting system. Firstly, the signal to interference ratio (SIR) distribution is calculated to be included in the global capacity derivation.

3.3.1 SIR distribution

Considering that the channel is constant over one information symbol, the SINR of MR averaged over symbols can be written as :

$$\gamma_m = \frac{\mathbb{E}\left[\left(\sqrt{p_m l_m} h^{(m)} x_m\right)\left(\sqrt{p_m l_m} h^{(m)} x_m\right)^*\right]}{\mathbb{E}\left[\left(\sum_{b=1}^{R_b} \sqrt{p_b l_{bm}} q^{(b)} x_b + w_m\right)\left(\sum_{b=1}^{R_b} \sqrt{p_b l_{bm}} q^{(b)} x_b + w_m\right)^*\right]} \tag{3.3}$$

where $(.)^*$ denotes the corresponding conjugate. Therefore, SINR at MR becomes :

$$\gamma_m = \frac{\mathbb{E}\left[\left|\sqrt{p_m l_m} h^{(m)} x_m\right|^2\right]}{\mathbb{E}\left[\left|\sum_{b=1}^{R_b} \sqrt{p_b l_b} q^{(b)} x_b + w_m\right|^2\right]}. \tag{3.4}$$

Since the channel is considered as flat for one LTE subcarrier, it can be assumed flat over R_b DVB subcarriers on the interfering link BT-MR, i.e. $q^{(b)}$ is constant over R_b subcarriers. Moreover, l_b is also considered constant over R_b subcarriers and equal for all MRs due to the large distance between BT and MRs. For the sake of simplicity, MRs are also assumed to be positioned at the same distance from BS. Even though this assumption is considered to be strictly limiting, however, it could be seen in a way that all MRs undergo a power control scheme so that their respective received

powers are equal. Then, the average allocated power per MR and per subcarrier is uniform. The SINR of the MR is equal to :

$$\gamma_m = \frac{p_m l_m \left|h^{(m)}\right|^2}{l_{bm} \left|q^{(b)}\right|^2 \sum_{b=1}^{R_b} p_b + \sigma_m^2} \tag{3.5}$$

$$= \frac{p_m l_m \left|h^{(m)}\right|^2}{R_b p_b l_{bm} \left|q^{(b)}\right|^2 + \sigma_m^2} \tag{3.6}$$

where the step from (3.5) to (3.6) follows the assumption of equal repartition power p_b between all subcarriers. Similarly, SINR on one subcarrier at BR is given by :

$$\gamma_b = \frac{\mathbb{E}\left[\left(\sqrt{p_b l_b} h^{(b)} x_b\right)\left(\sqrt{p_b l_b} h^{(b)} x_b\right)^*\right]}{\mathbb{E}\left[\left(\kappa\sqrt{p_m l_{mb}} q^{(m)} x_m + w_b\right)\left(\kappa\sqrt{p_m l_{mb}} q^{(m)} x_m + w_b\right)^*\right]} \tag{3.7}$$

$$\gamma_b = \frac{p_b l_b \left|h^{(b)}\right|^2}{\kappa^2 p_m l_{mb} \left|q^{(m)}\right|^2 + \sigma_b^2}. \tag{3.8}$$

Since the systems are considered interference limited, the noise w.r.t. the interfering terms in SINR expressions can be neglected. The corresponding SIR expressions of MR and BR signals on one subcarrier are expressed respectively by :

$$\tilde{\gamma}_m = \frac{p_m l_m \left|h^{(m)}\right|^2}{R_b p_b l_{bm} \left|q^{(b)}\right|^2} \tag{3.9}$$

$$\tilde{\gamma}_b = \frac{p_b l_b \left|h^{(b)}\right|^2}{\kappa^2 p_m l_{mb} \left|q^{(m)}\right|^2} \tag{3.10}$$

Hence the problem turns out now to find the distributions of SIRs for the evaluation of the ergodic capacity.

Lemma 1. *In Rayleigh fading channels, the pdf of the SIR per subcarrier for the proposed interfering mobile and broadcast systems are given by :*

$$p_{\tilde{\gamma}_m}(u) = \frac{p_m p_b l_m l_{bm} R_b}{\left(p_b l_{bm} R_b u + p_m l_m\right)^2} \tag{3.11}$$

$$p_{\tilde{\gamma}_b}(u) = \frac{p_m p_b l_b l_{mb} \kappa^2}{\left(\kappa^2 p_m l_{mb} u + p_b l_b\right)^2} \tag{3.12}$$

for mobile and broadcast receivers respectively.

sketch of proof. Let us focus on the distribution of the SIR at the mobile receiver and let us define the two following random variables (r.v.) :

$$\begin{aligned} X &= p_m l_m \left|h^{(m)}\right|^2 \\ Y &= R_b p_b l_{bm} \left|q^{(b)}\right|^2 \end{aligned} \tag{3.13}$$

where their pdf follow the exponential distribution and they are defined respectively by :

$$\begin{aligned} P_X(x) &= \frac{1}{(p_m l_m)} e^{-x/p_m l_m} \\ P_Y(y) &= \frac{1}{(R_b p_b l_{bm})} e^{-y/R_b p_b l_{bm}} \end{aligned} \tag{3.14}$$

Let us consider the following change of variables :

$$\left\{ \begin{array}{lcl} U &=& \frac{X}{Y} \\ V &=& Y \end{array} \right. \Longleftrightarrow \left\{ \begin{array}{lcl} X &=& UV \\ Y &=& V \end{array} \right. \tag{3.15}$$

Thanks to the change of variable theorem, the joint pdf of the couple (U, V) can be written as :

$$P_{UV}(u,v) = P_{X,Y}\left(x\left(u,v\right), y\left(u,v\right)\right) \left|J\left(u,v\right)\right| \tag{3.16}$$

with

$$\begin{aligned} P_{X,Y}\left(x\left(u,v\right), y\left(u,v\right)\right) &= P_{X,Y}(uv, v) \\ &= P_X(uv) P_Y(v) \end{aligned} \tag{3.17}$$

because X and Y are independent. $J(u,v)$ is the Jacobian of the transformation depending on the new variables defined by :

$$J(u,v) = \left| \begin{array}{cc} \frac{\partial x(u,v)}{\partial u} & \frac{\partial x(u,v)}{\partial v} \\ \frac{\partial y(u,v)}{\partial u} & \frac{\partial y(u,v)}{\partial v} \end{array} \right| = \left| \begin{array}{cc} v & u \\ 0 & 1 \end{array} \right| = v \tag{3.18}$$

Hence, we have :

$$P_X(uv) = \frac{1}{\mathrm{E}[X]} e^{-uv/\mathrm{E}[X]} \tag{3.19}$$

$$P_Y(v) = \frac{1}{\mathrm{E}[Y]} e^{-v/\mathrm{E}[Y]} \tag{3.20}$$

where $\mathrm{E}[X]$ and $\mathrm{E}[Y]$ are respectively the mean of the numerator and the denominator of $\tilde{\gamma}_m$. $\mathrm{E}[X] = p_m l_m$ and $\mathrm{E}[Y] = R_b p_b l_{bm}$. Therefore, (3.16) becomes :

$$P_{UV}(u,v) = P_{X,Y}\left(uv, v\right)|v| = \frac{|v|}{R_b p_b p_m l_m l_{bm}} e^{-v\left(\frac{u}{p_m l_m} + \frac{1}{R_b p_b l_{bm}}\right)} \tag{3.21}$$

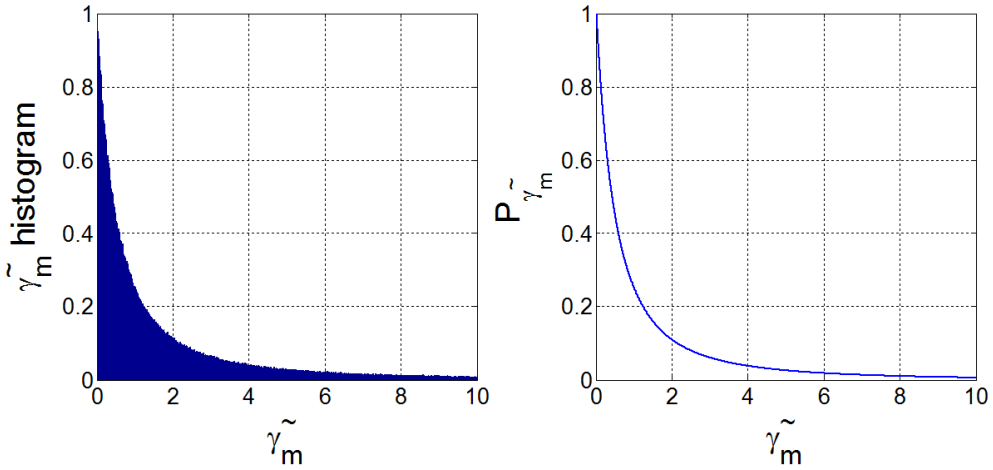

Figure 3.2 – $P_{\tilde{\gamma_m}}$ vs $\tilde{\gamma}_m$ histogram

Renaming U in $\tilde{\gamma}_m$, and integrating the joint pdf above w.r.t. the variable v, and using the following integral result [57] :

$$\int_0^{+\infty} v^{z-1} e^{-\mu v} dv = \frac{1}{\mu^z}\Gamma(z), \tag{3.22}$$

the SIR at LTE receiver can be written as :

$$p_{\tilde{\gamma}_m}(u) = \int_0^{\infty} p_{\tilde{\gamma}_m,V}(u,v)dv \tag{3.23}$$

$$= \frac{1}{E[X]E[Y]}\frac{1}{\mu^2}\Gamma(2) \tag{3.24}$$

with $\mu = \frac{u}{\mathrm{E}[X]} + \frac{1}{\mathrm{E}[Y]}$ and $\Gamma(2) = 1$. Therefore, the pdf of $\tilde{\gamma}_m$ is expressed by :

$$p_{\tilde{\gamma}_m}(u) = \frac{p_m p_b l_m l_{bm} R_b}{\left(p_b l_{bm} R_b u + p_m l_m\right)^2} \tag{3.25}$$

Following the same steps as above, the $\tilde{\gamma}_b$ pdf is obtained and the proof is complete. □

Fig. 3.2 shows the variation of the obtained pdf of $\tilde{\gamma}_m$ in (3.25) and the corresponding histogram of the ratio of two exponential distributed variables. The mean of the numerator and the denominator are normalized in these figures, i.e. $\mathrm{E}[X] = \mathrm{E}[Y] = 1$. These two figures ensure the similarity between the analytical pdf $p_{\tilde{\gamma}_m}$ and the empirical distribution of the ratio of two exponentially distributed variables.

3.3.2 Ergodic capacity

The mobile and broadcast ergodic capacities, in bits/s/Hz, are obtained respectively by averaging over all the fading distributions existing in each capacity function :

$$C_{\mathrm{m}} = \mathbb{E}_{h^{(m)},q^{(b)}}\left[\log_2\left(1+\gamma_m\left(h^{(m)},q^{(b)}\right)\right)\right] \tag{3.26}$$

$$C_{\mathrm{b}} = \mathbb{E}_{h^{(b)},q^{(m)}}\left[\log_2\left(1+\gamma_b\left(h^{(b)},q^{(m)}\right)\right)\right] \tag{3.27}$$

Moreover, it is equivalent to integrate w.r.t. the channel distribution or w.r.t. the pdf of SIR. The mobile and broadcast ergodic capacities can be re-written respectively as :

$$C_{\mathrm{m}} = \mathbb{E}_{\tilde{\gamma}_m}\left[\log_2\left(1+\tilde{\gamma}_m\right)\right] \tag{3.28}$$

$$C_{\mathrm{b}} = \mathbb{E}_{\tilde{\gamma}_b}\left[\log_2\left(1+\tilde{\gamma}_b\right)\right] \tag{3.29}$$

Using the pdf of SIRs derived in Lemma 1 in (3.28) and (3.29), the ergodic capacities are obtained in closed-form by applying the following definition :

$$\begin{aligned} C &= \mathbb{E}_u\left[\log_2(1+u)\right] \\ &= \int \log_2(1+u)p_{\tilde{\gamma}}(u)du \end{aligned} \tag{3.30}$$

$$\tag{3.31}$$

and using the following integral result [57] :

$$\int_0^\infty \frac{\log_2(1+u)}{(a_l u+b_l)^2}du = \frac{\log_2(a_l/b_l)}{a_l(a_l-b_l)} \tag{3.32}$$

Therefore, the MR and BR capacities are given respectively by :

$$C_{\mathrm{m}} = \frac{p_m l_m}{R_b p_b l_{bm} - p_m l_m}\log_2\frac{R_b p_b l_{bm}}{p_m l_m} \tag{3.33}$$

$$C_{\mathrm{b}} = \frac{p_b l_b}{\kappa^2 p_m l_{mb} - p_b l_b}\log_2\frac{\kappa^2 p_m l_{mb}}{p_b l_b} \tag{3.34}$$

The global ergodic capacity, in bits/s/Hz, is hence obtained by summing mobile and broadcast capacities. It can be written as :

$$C_{\mathrm{g}} = C_{\mathrm{m}} + C_{\mathrm{b}} \tag{3.35}$$

Therefore, the ergodic data rate in bits/s of full interfering LTE DVB-like systems can be proved to be given by the following proposition.

Proposition 1. *Considering a full interfering LTE cell on a DVB macro-cell, i.e. the mobile OFDMA symbol encompasses the OFDM symbol of a DVB signal, the global data rate in bits/s in the DVB bandwidth is :*

$$\begin{aligned} D_{\mathrm{g}}(bits/s) &= B_{min}\left(\frac{p_m l_m}{R_b p_b l_{bm} - p_m l_m}\log_2\frac{R_b p_b l_{bm}}{p_m l_m}\right. \\ &+ \left.\frac{p_b l_b}{\kappa^2 p_m l_{mb} - p_b l_b}\log_2\frac{\kappa^2 p_m l_{mb}}{p_b l_b}\right) \end{aligned} \tag{3.36}$$

where B_{min} is the smallest bandwidth among the DVB and LTE bandwidths.

Proof. According to Table 1.1, LTE can operate with different bandwidths. While in Table 1.2, it can be seen that DVB can operate in different modes, e.g. 8K and 32K modes, using actually the same bandwidth equal to 7.61 MHz in all modes. The data rate of the full interfered parts of DVB and LTE signals, is obtained by multiplying the ergodic capacity with the smallest bandwidth between B_m and B_b, i.e. $B_{min} = \min\{B_b, B_m\}$. □

3.4 Performance Discussion

In this section, the global ergodic capacity is analyzed. Firstly, the analytical expression obtained in the previous section is evaluated. Then, some simulation results are provided with real transmission parameters.

3.4.1 Analysis

The analytical expressions of the obtained ergodic capacities C_m and C_b allow to evaluate the influence of system parameters, such as mobile and broadcast transmit powers, BS-BR distance d, on the global and individual data rates. As seen in (3.36), the global capacity of the coexistence model is composed of two functions with different forms. Transmit powers, i.e. p_b and p_m, exist with contradictory effects in mobile and broadcast capacity equations, i.e. (3.33) and (3.34). Consequently, one of the capacities has a convex variation according to the power ratio $\frac{p_b}{p_m}$, while the second one has a concave variation. Therefore, when one of them increases, the second decreases. This conflict affects the global capacity attitude which is the sum of two contrary variations.

Table 3.1 – System parameters

Parameters	DVB-T2		LTE		
FFT size	8K	32K	512	1024	2048
Bandwidth (MHz)	7.61		5	10	20
Active subcarriers	6817	27265	301	601	1201
Subcarrier spacing (Hz)	1116	279	15000		
Max transmission power (W)	10000		50		
Max transmission power per subcarrier (W)	1.466	0.366	0.166	0.083	0.041
Cell radius (Km)	100		1		
Path loss exponent	2.5		3		
Path loss attenuation	$3.1623 * 10^{-13}$		10^{-9}		
Interference distance	d		d_b		
Interference path loss attenuation	$1/d^{2.5}$		$1/d_b^3$		

3.4.2 Numerical analysis

This section deals with numerical results. As the goal is to achieve a coexistence model between LTE and DVB networks, extensive simulations show the behavior of the global ergodic data rate with a full overlapping between DVB and LTE signals. Realistic parameters of DVB and LTE networks have been used for the simulations as detailed below.

System parameters

In simulations, different cases are taken into account ; DVB network operates with two different modes (8K and 32K) and LTE network operates with three different bandwidths (5, 10 and 20 MHz). The capacity functions depend on several parameters. Table 3.1 shows the chosen parameter values in all cases. The mobile and broadcast powers, i.e. p_m and p_b respectively, are normalized per subcarrier for each system. Therefore, the maximum transmit power per subcarrier is given by :

$$p = \frac{P}{N_a} \tag{3.37}$$

where P is the total transmit power and N_a is the number of active subcarriers. The

Table 3.2 – DVB -LTE subcarriers ratio with different DVB operation modes

	8K	32K
R_b	$15000/1116 = 13.44 \approx 13$	$15000/279 = 53.763 \approx 54$
$\kappa = 1/R_b$	0.0744	0.0186

path attenuations are given by (1.1). We recall that BR is situated at the limits of the DVB cell and MR is situated simultaneously at the limits of the DVB and LTE cells. The distance d between the LTE BS and DVB BR is an important parameter to be studied as it directly affects the interference level at the DVB receiver. Whatever the bandwidth value of the LTE signal, the subcarrier spacing is similar. Therefore, κ and R_b are the same in all LTE network cases in the common spectrum part of the two systems. Table 3.2 shows the values of κ and R_b in both DVB modes, i.e. 8K and 32K.

Simulations

Firstly, figures 3.3, 3.4 and 3.5 show respectively the variation of the mobile, broadcast and global data rates in bits/s w.r.t. the mobile and broadcast transmitted power per subcarrier, i.e. p_m and p_b. In these figures, DVB operates in 8K mode and the BS-BR distance is set to $d = 100$ m. Moreover, the sub-figures (a) and (b) represent the cases when the LTE bandwidth is equal respectively to 5 MHZ and 20 MHz.

In Fig. 3.4, it can be observed that in both cases the broadcast data rate sharply decreases if p_m increases due to the relatively small distance between BR and BS. As illustrated, the broadcast data rate is relatively small w.r.t. the value of the global data rate since three magnitude orders can be observed between the two surfaces in Fig. 3.5 and Fig. 3.4. Hence, the contribution of the broadcast capacity to the global data rate is relatively small w.r.t. the contribution of LTE system. This means that the performance of DVB system is strongly affected by the power of LTE network. While, the LTE system is less affected by the power of DVB network due to the large distance between BT and MR.

From Fig. 3.5, it can be immediately seen that in both cases the global data rate is not a convex function of p_m and p_b variables. Moreover, the maximum data rate would be obtained for a non-transmitting broadcast station, which is not desirable.

Furthermore, these figures show that in both cases, i.e. when $B_m = 5$ MHz and $B_m = 20$ MHz, the capacities in general have similar behaviours in function of p_m and p_b except that the achieved values when $B_m = 20$ MHz are higher that the values obtained when $B_m = 5$ MHz. This is logically due to the increasing value of the common bandwidth between both systems and then increasing value in the global received data rate. Furthermore, it can be remarked that the broadcast data rate is less curved when $B_m = 20$ MHz and this is due to the dispersion of the total mobile power over larger number of subcarriers than in the case when $B_m = 5$ MHz.

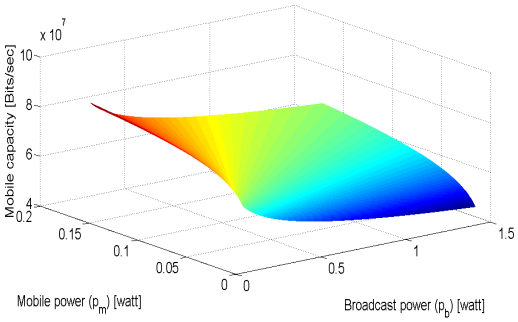

(a) $B_m = 5$ MHz, DVB mode 8K

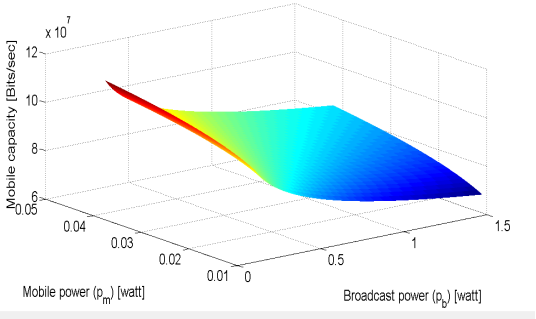

(b) $B_m = 20$ MHz, DVB mode 8K

Figure 3.3 – Mobile data rate (bits/sec) according to p_b and p_m, d = 100m.

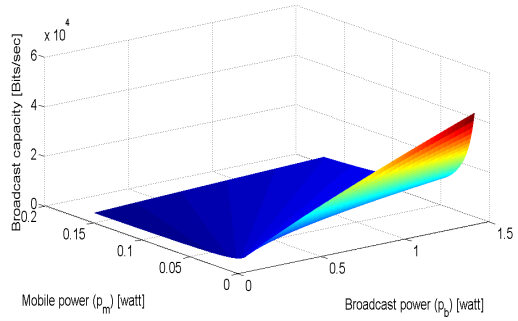

(a) $B_m = 5$ MHz, DVB mode 8K

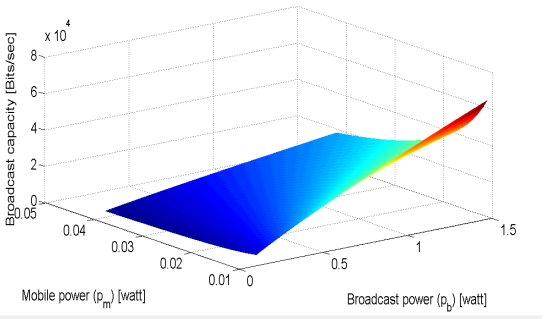

(b) $B_m = 20$ MHz, DVB mode 8K

Figure 3.4 – Broadcast data rate (bits/sec) according to p_b and p_m, d = 100m.

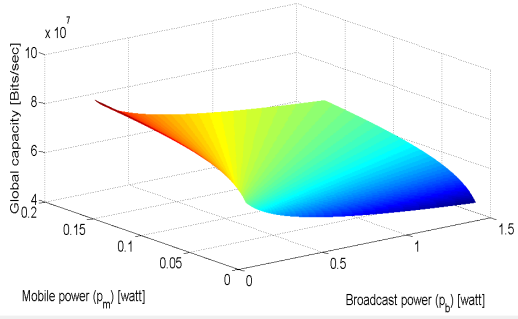

(a) $B_m = 5$ MHz, DVB mode 8K

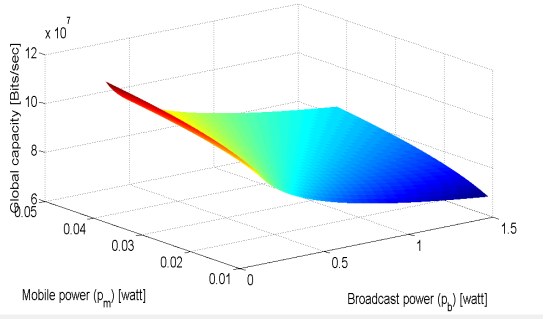

(b) $B_m = 20$ MHz, DVB mode 8K

Figure 3.5 – Global data rate (bits/sec) according to p_b and p_m, d = 100m.

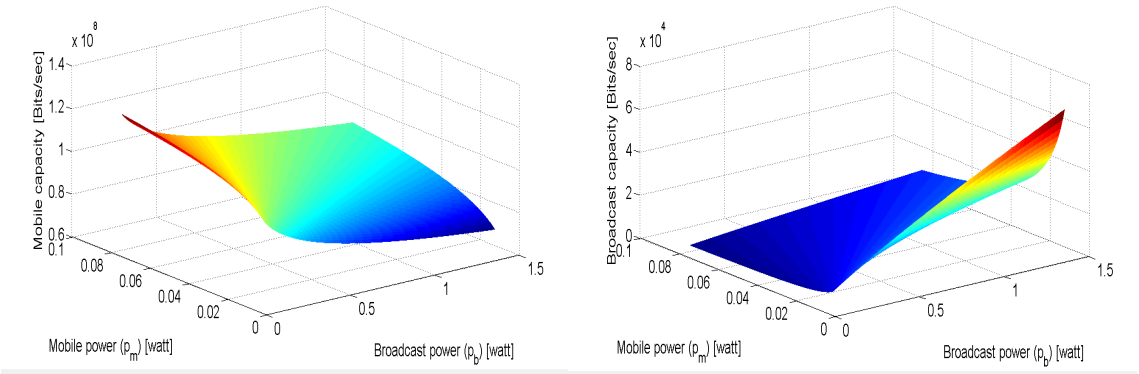

(a) Mobile data rate

(b) Broadcast data rate

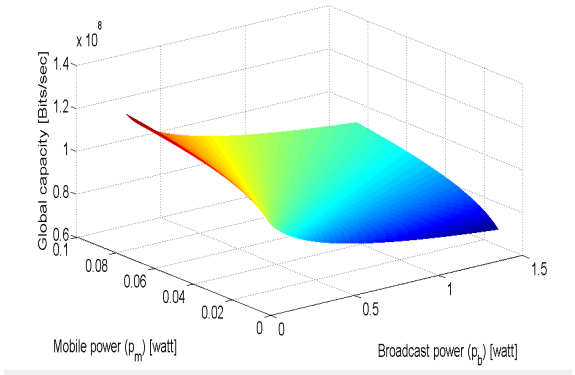

(c) Global data rate

Figure 3.6 – Data rate variation in (bits/sec) according to p_b and p_m, $B_m = 10$ MHz, DVB mode 8K, d = 100 m.

Secondly, Figures 3.6 and 3.7 show respectively the variation of the mobile, broadcast and global data rate w.r.t. the mobile and broadcast transmitted power per subcarrier, i.e. p_m and p_b, for two DVB 8K and 32K modes. In these figures, LTE operates with $B_m = 10$ MHz and BS-BR distance is set to $d = 100$ m. As illustrated in these figures, the capacities in general have similar behaviours in function of p_m and p_b in both cases, i.e. 8K mode and 32K mode. Moreover, it can be seen that the 32K mode can give higher values of mobile, broadcast and global data rates with smaller value of transmit power per DVB subcarrier. This is due to the big number of DVB subcarriers, i.e. the sum of data rates over large number of subcarriers in the DVB system and the dispersion of the interfering power over the mobile signal.

Finally, Figures 3.8 and 3.9 show respectively the broadcast and global data rates according to the mobile power, i.e. p_m, for various BS-BR distance d in both DVB operation modes 8K and 32K. The broadcast power p_b is now set to its maximum value per subcarrier, i.e. $p_b = 1.466$ Watt in 8K mode and $p_b = 0.366$ Watt in 32K

mode.

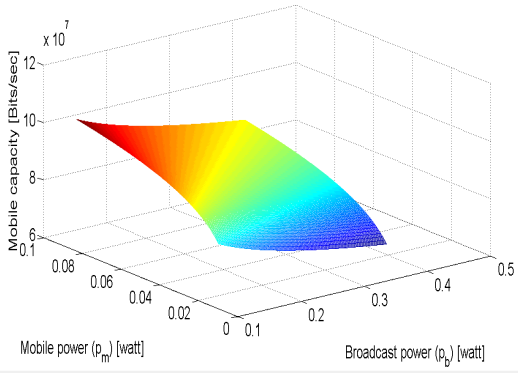

(a) $B_m = 10$ MHz, DVB mode 32K

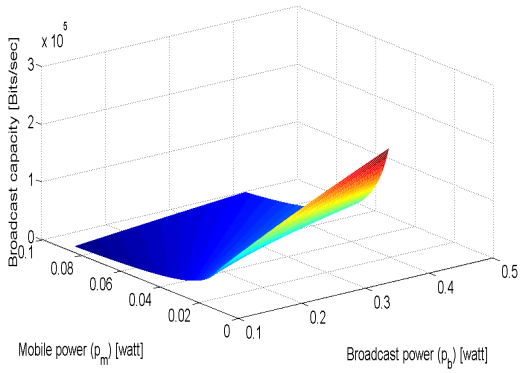

(b) $B_m = 10$ MHz, DVB mode 32K

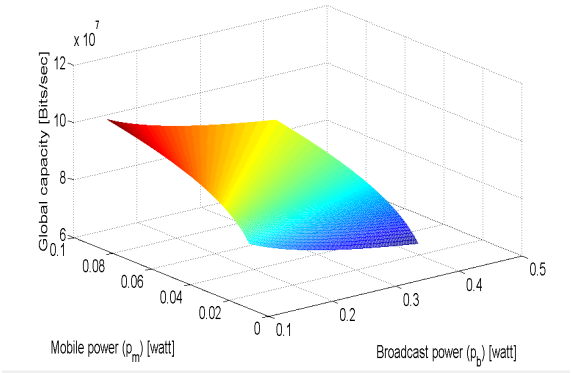

(c) $B_m = 10$ MHz, DVB mode 32K

Figure 3.7 – Data rate variation in (bits/sec) according to p_b and p_m, d = 100 m.

These figures show that the broadcast data rate decreases as p_m increases whatever the value of d. On the other hand, it is getting larger as the separation between BR and BS becomes larger as expected. Hence, the QoS of broadcast system will be strongly affected by the deployment of the LTE cell in this scenario.

However, both figures show that the global capacity is not very sensitive to d. Indeed, the global data rate curves strongly varies with p_m but the four curves, representing $d = 100, 200, 300$ and 500 m are close in both cases, i.e. 8K mode and 32K mode.

It is worth noting that the broadcast capacity in the 32K mode can get higher values than those obtained in the 8K mode when d increases. Moreover, the global data rate curves are closer in 8K mode than in 32K mode.

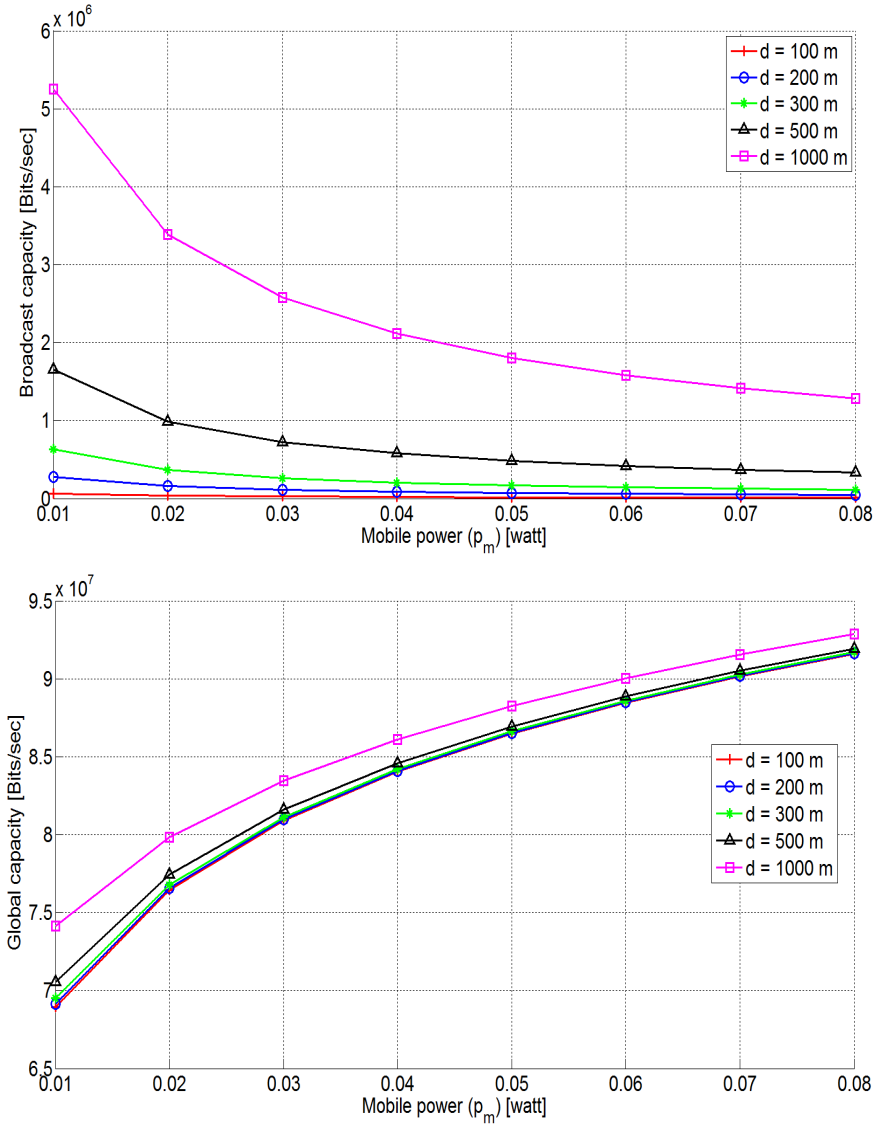

Figure 3.8 – Variation of the broadcast and the global data rate, according to the mobile power, i.e. p_m, for different values of d = 100, 200, 300, 400, 1000 m, DVB mode 8K, p_b = 1.466 W, B_m = 10 MHz.

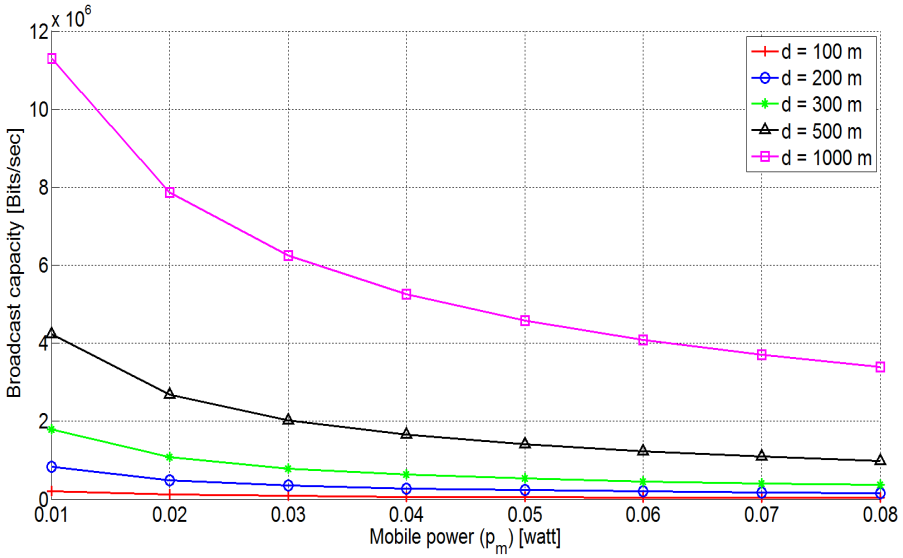

(a) (a)

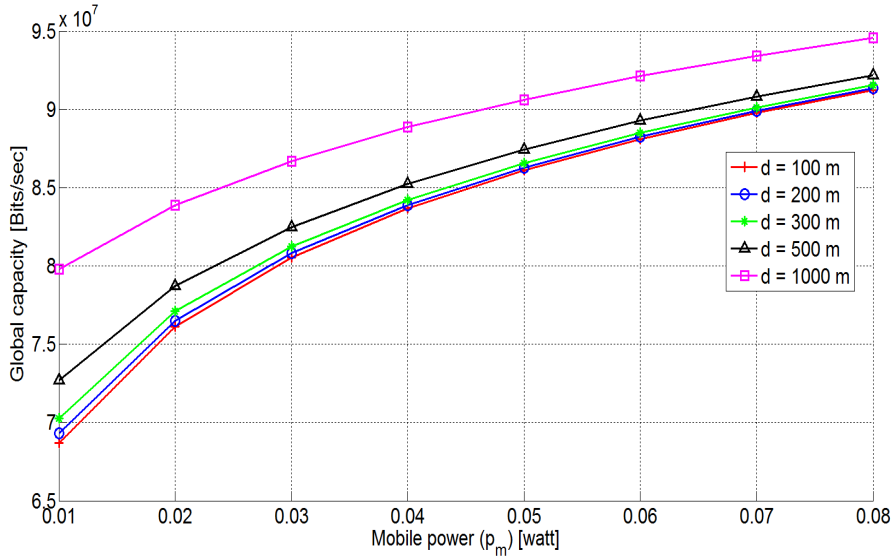

(b) (b)

Figure 3.9 – Variation of the broadcast and the global data rate, according to the mobile power, i.e. p_m, for different values of $d = 100$, 200, 300, 400, 1000 m, DVB mode 32K, $p_b = 0.366$ W, $B_m = 10$ MHz.

3.5 Conclusion

In this chapter, the problem of deploying a small LTE cell into a large broadcast cell in the spectral overlap scenario between LTE and DVB has been treated. The pdf of the SIR at both receivers, i.e. BR and MR, have been derived. From this, the global ergodic capacity of the full interfering deployment of LTE and DVB systems has been derived. The numerical results have shown that the global as well as broadcast data rate are strongly impacted by the LTE transmission power. On the other hand, the broadcast data rate is highly dependent on the separation distance between the LTE transmitter and the DVB receiver. Moreover, the global capacity is not a convex or concave function of the mobile and broadcast power.

To the best of our knowledge, the global ergodic capacity under the full interference channel in a DVB-LTE coexistence scenario has not been studied up to now. This preliminary work could be useful for mobile operators and broadcasters in the objective of merging their networks. This study gives an insight on how to deploy LTE cells overlapping the DVB bandwidth. As seen in this chapter, there is no priority between both systems sharing the same bandwidth in contrast to the previous references. Therefore, the maximization problem of global, broadcast and mobile capacities w.r.t. p_b and p_m will be tackled in the next chapter and the derived expressions of this chapter would be useful for this purpose.

4

Global Ergodic Capacity Optimization in Coexisting DVB-LTE like systems

The global ergodic capacity under the full interference channel in the DVB-LTE coexistence scenario was studied in the previous chapter, but no optimal operating conditions have been given. In this chapter, the goal is not only to evaluate the performance of two coexisting systems but also to optimize it. In Chapter 2, we proposed a closed-form expression of the ergodic capacity of the secondary link in a similar situation but with power constraints, i.e. average interference power constraint at the primary receiver and peak transmission power at the secondary transmitter. The formulation in Chapter 2 led to a completely different optimization problem with different conclusions and hence does not overlap with the present chapter in which the analytical expression of the ergodic capacity found in the previous chapter is used to solved an optimization problem with QoS constraints.

Firstly, the system and signal model are redefined briefly. Next, the global capacity maximization problem is presented and the global capacity is first shown to be a Concave Convex Procedure (CCCP) problem. The strict maximization of the global capacity is also presented and the optimal operating conditions are given as a function of the ratio of the transmit powers of both systems. The results are given in different scenarios to fit the LTE and DVB networks planning specifications. Finally, Conclusion is drawn.

4.1 System and Signal Model

The same model than in Chapter 3 for DVB and LTE systems is considered. For the sake of convenience, system model is briefly given here again and illustrated in Fig. 4.1. $h^{(b)}$, $h^{(m)}$ are the complex channel fading coefficients on BT-BR and BS-MR links respectively with $h^{(b)} \sim \mathcal{CN}(0,1)$ and $h^{(m)} \sim \mathcal{CN}(0,1)$. The received signals

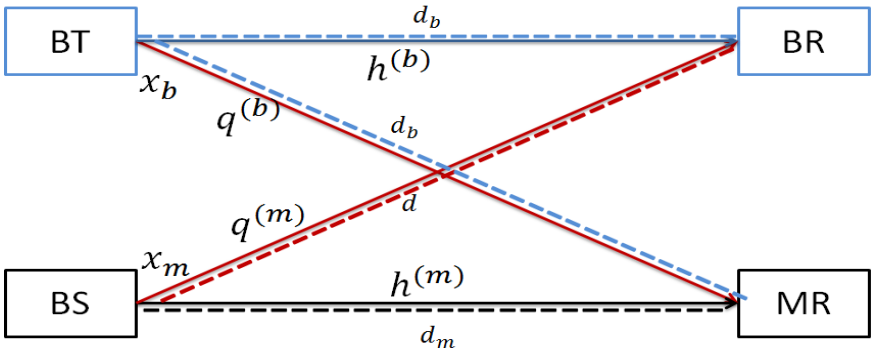

Figure 4.1 – Full interfering LTE cell in a DVB macro-cell.

on one subcarrier on MR and BR are respectively given by :

$$y_m = \sqrt{p_m l_m} h^{(m)} x_m + \sum_{b=1}^{R_b} \sqrt{p_b l_{bm}} q^{(b)} x_b + w_m \tag{4.1}$$

$$y_b = \sqrt{p_b l_b} h^{(b)} x_b + R_m \sqrt{p_m l_{mb}} q^{(m)} x_m + w_b \tag{4.2}$$

where p_m, p_b, l_m, l_b, x_m and x_b are reminded to be respectively the BS, BT transmit power per subcarrier, the path-loss attenuation in the BS-MR and BT-BR links, the information symbols of mobile and broadcast transmission. Moreover, R_b is the number of DVB subcarriers interfering with one LTE subcarrier and R_m is the ratio of the bandwidth of the DVB and LTE subcarriers. $q^{(b)}$ and $q^{(m)}$ are respectively the channel coefficients of BT-MR and BS-BR links, assumed to be complex Gaussian distributed. The path-loss attenuations on these links are respectively noted l_{bm} and l_{mb}. Finally, $w_m \sim \mathcal{CN}(0, \sigma_m^2)$ and $w_b \sim \mathcal{CN}(0, \sigma_b^2)$ represent the AWGN on one subcarrier at LTE and DVB receiver respectively.

4.2 Optimization problem

The objective of a common deployment between broadcasters and cellular operators would be to maximize the system data rate under strict data constraints for each system. To improve the system performance, the ergodic capacity of the mobile-broadcast system must be maximized by optimizing the power allocation mechanism of the LTE and DVB networks.

4.2.1 Objective function

According to Chapter 3, the global ergodic capacity in bits/s/Hz of the system model described in 4.1 can be expressed as :

$$C_g(p_b, p_m) = \frac{p_m l_m}{R_b p_b l_{bm} - p_m l_m} \log_2 \frac{R_b p_b l_{bm}}{p_m l_m} + \frac{p_b l_b}{R_m^2 p_m l_{mb} - p_b l_b} \log_2 \frac{R_m^2 p_m l_{mb}}{p_b l_b} \quad (4.3)$$

where the first term of the sum represents the cellular network capacity, i.e. $C_m(p_b, p_m)$ and the second term stands for the broadcast network capacity, i.e. $C_b(p_b, p_m)$. In this equation, the SIR is being targeted as we assume that the interference from one system on the other one will not be highly affecting if it is below the noise power threshold. As seen in (4.3), the transmission powers p_m and p_b exist in the terms $\frac{R_b p_b l_{bm}}{p_m l_m}$ and $\frac{R_m^2 p_m l_{mb}}{p_b l_b}$. Thanks to the following change of variables :

$$\beta = \frac{R_b p_b l_{bm}}{p_m l_m} \quad (4.4)$$

$$A = \frac{l_{mb} l_{bm}}{R_b l_b l_m} \quad (4.5)$$

the global ergodic capacity can be expressed as :

$$\begin{aligned} C_g(\beta) &= C_m(\beta) + C_b(\beta) \\ &= \frac{1}{\beta - 1} \log_2 \beta + \frac{1}{\frac{A}{\beta} - 1} \log_2 \frac{A}{\beta} \end{aligned} \quad (4.6)$$

where

$$C_m(\beta) = \frac{1}{\beta - 1} \log_2 \beta \quad (4.7)$$

$$C_b(\beta) = \frac{1}{\frac{A}{\beta} - 1} \log_2 \frac{A}{\beta} \quad (4.8)$$

and

$$\frac{A}{\beta} = \frac{R_m^2 p_m l_{mb}}{p_b l_b} \quad (4.9)$$

where (4.6) is defined for $\beta \in]0, \infty[\setminus \{1, A\}$. The broadcast and cellular transmit powers, i.e. p_b and p_m, act in a ratio which is caught in the variable β. The variable β relies in $]0, \infty[$ since neither p_b nor p_m are allowed to be strictly zero.

4.2.2 Maximization problem

To guarantee the QoS of the mobile-broadcast coexistence system, the optimization problem is defined and resolved with two different manners. First of all, the goal is to maximize the global ergodic capacity, i.e. C_g, which is the sum of the mobile and the broadcast capacities. The terms C_m and C_b can be shown to be convex and concave in β respectively which will be verified later. Instead of optimizing the global ergodic capacity over p_m and p_b, it will be maximized by choosing the optimal β which reflects the ratio between these two powers. After finding the optimal β, the optimal p_m and p_b can be chosen. Hence, the maximization problem can be written as :

$$\begin{aligned} \max_{\beta} \quad & C_g(\beta) \\ \text{s.t.} \quad & \begin{cases} C_m(\beta) \geq C_{mth} \\ C_b(\beta) \geq C_{bth} \end{cases} \end{aligned} \tag{4.10}$$

where C_{mth} and C_{bth} are the given threshold values to be respected. The constraints on C_m and C_b aim to preserve the QoS requirements of cellular and broadcast systems when optimizing the global capacity. The main issue in this maximization problem is that C_m and C_b are varying in an opposite way with β. From (4.7), β can be expressed in function of C_m :

$$\beta(C_m) = -\frac{\mathrm{W}(-2^{-C_m} C_m \log(2))}{C_m \log(2)} \tag{4.11}$$

where W(.) is the Lambert function. Therefore, the broadcast capacity C_b can be expressed in function of C_m as :

$$C_b(C_m) = \frac{1}{\frac{A}{\beta(C_m)} - 1} \log_2 \left(\frac{A}{\beta(C_m)} \right) \tag{4.12}$$

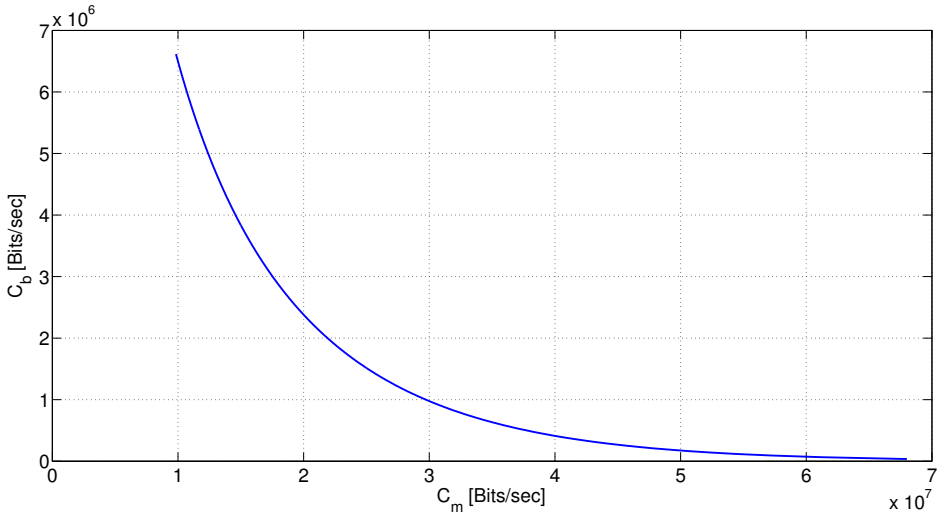

Figure 4.2 – C_b in function of C_m, d=100 m

The maximization problem in this chapter is treated in the worse case, i.e. when DVB network operates with the 8K mode. The chosen LTE bandwidth is 10 MHz. As explained in the previous chapter, the bandwidth of the global full spectral overlapped systems is the minimum bandwidth among the DVB and LTE bandwidths. Therefore, the bandwidth of the interfering systems is 7.61 MHz. The DVB and LTE cell radius are 100 km and 1 km respectively. Due to the small dimension of the LTE cell w.r.t. the macro DVB cell, the distance from the BT to the MR is also approximately to 100 km. The distance d between BS and BR, is a variable parameter of simulations. The path-loss attenuation l_m, l_b, l_{mb} and l_{bm} are calculated such that the attenuation exponent η is equal to 2.5 for the broadcast system and 3 for the LTE system. Fig. 4.2 represents the variation of C_b in function of C_m with $d = 100$ m. This figure shows that C_m and C_b vary in opposite ways. Therefore, to maximize the global ergodic capacity, two opposites functions, i.e. C_m and C_b, should also be maximized. Two different methods or rather with two different priorities will be used in the solution. The first one consists in getting a compromise between the maximum of the two capacities. The second one consists in getting the maximum of C_g while respecting the constraints over C_m and C_b. These two problems have different priorities and different goals and then solved with different algorithms. Firstly, the CCCP is used to give a compromise between C_m and C_b. Then, we propose an algorithm to maximize the global ergodic capacity. The two methods are detailed below.

4.3 Optimal Power Allocation for Global Ergodic Capacity

In this section, the resolution methods of the problem presented in (4.10) are detailed. Firstly CCCP is applied. Secondly, a maximization procedure (MP) is explained and discussed.

4.3.1 Concave convex procedure

As explained in Chapter 1, CCCP is applied on an optimization problem where the objective function is a sum of concave and convex functions. The procedure actually converges to an equilibrium point of the objective function. The objective function C_g in (4.6) is composed of two functions, i.e. C_m and C_b. As seen in Fig. 4.3, C_m is a convex function of β and C_b is a concave function of β [1]. Therefore, the initial condition of CCCP is satisfied and an equilibrium point can be found on C_g. The Lagrangian function of (4.10) is firstly defined as :

$$L(\beta, \lambda, \nu) = (1+\lambda)C_m(\beta) + (1+\nu)C_b(\beta) - \lambda C_{mth} - \nu C_{bth} \tag{4.13}$$

with $\lambda \geq 0$ and $\nu \geq 0$ are the Lagrange multipliers associated to the constraints on C_m and C_b respectively. L in (4.13) is composed of two terms :

$$\text{convex term} : L_{\text{vex}}(\beta) = (1+\lambda)C_m(\beta) - \lambda C_{mth} \tag{4.14}$$

and

$$\text{concave term} : L_{\text{cave}}(\beta) = (1+\nu)C_b(\beta) - \nu C_{bth} \tag{4.15}$$

According to [2], the procedure consists of an iterative algorithm where at each iteration we have :

$$\nabla_\beta L_{\text{vex}}(\beta^{t+1}) = -\nabla_\beta L_{\text{cave}}(\beta^t) \tag{4.16}$$

where ∇_β stands for the derivative w.r.t. β and β^t, β^{t+1} are the current and next values of β respectively. From (4.16) and (4.13), β^{t+1} is expressed in an implicit form in function of β^t :

$$\nabla_\beta C_m\left(\beta^{t+1}\right) = -\frac{1+\nu}{1+\lambda}\nabla_\beta C_b\left(\beta^t\right). \tag{4.17}$$

The main difficulty here is that the closed-form expressions giving the Lagrange multipliers, i.e. λ and ν according to β^t do not exist, which could be useful for the implementation of CCCP. In order to realize the iterative procedure described by (4.17), we firstly propose Algorithm 1 which can be applied without having an explicit form of λ and ν in function of β.

1. Of course, this can be shown in a formal way easily.

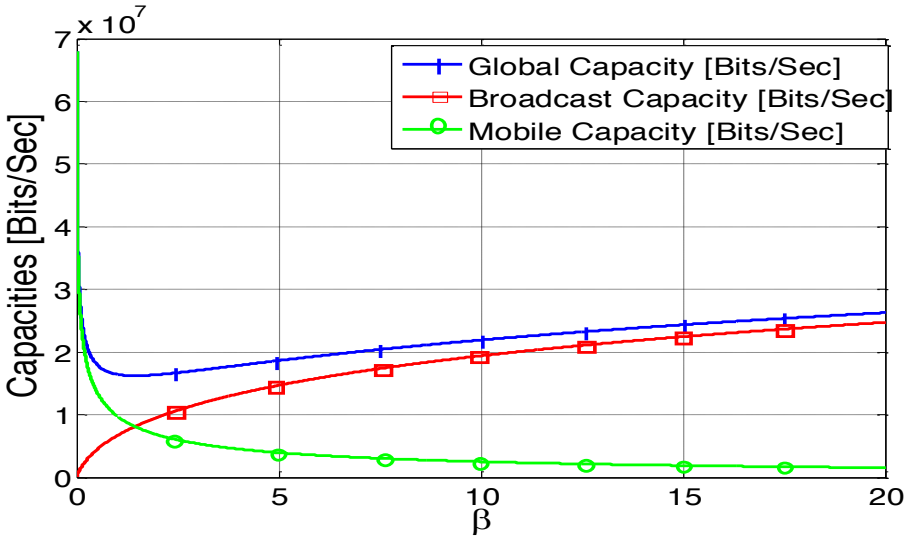

Figure 4.3 – Variation of global, mobile and broadcast capacities, d=100m

First of all, in Algorithm 1, the lower and upper bounds of λ, λ_{min} and λ_{max} respectively, are initialized. Similarly the lower and upper bounds of ν, ν_{min} and ν_{max} respectively, are initialized. Moreover, we also initialize $\beta = \beta_0$ and we define the convergence parameter ϵ with very small value. Algorithm 1 consists of three loops as shown below. In step 5, the loop iterates until the convergence on β and the constraints in the problem (4.10) are satisfied. The loop in step 8 tries to converge toward the optimal Lagrange multiplier λ for a given β and iterates until C_m satisfies the constraint on the mobile capacity. The loop in step 17 tries to converge toward the optimal Lagrange multiplier ν for a given β and iterates until C_b satisfies the constraint on the broadcast capacity. This algorithm leads to an equilibrium point that gives fairness purposes between C_m and C_b.

4.3.2 Maximization procedure

The global ergodic capacity is unbounded as it is illustrated in Fig. 4.3. Hence, the strict maximum of the global capacity without any constraint would consist of drawing β toward 0, i.e. equivalent to turn off the DVB system, or drawing β toward infinity, i.e. turn off mobile system. However, since the mobile system capacity is varying in an opposite way to the DVB system capacity, the maximum global capacity should lie on the boundaries of β defined by both system capacities with the intersection of the constraints, i.e. C_{mth} and C_{bth}. Algorithm 2 presents the procedure maximizing the global capacity.

Algorithm 1 CCCP for global capacity optimization

Require : $C_{mth} > 0$, $C_{bth} > 0$,
Ensure : Return the optimal (CCCP sense) transmit power ratio β^* between DVB and LTE

Initialize $\epsilon > 0$, $\lambda_{\min}$, $\lambda_{\max}$, $\nu_{\min}$, $\nu_{\max}$ and β^0
$\lambda \leftarrow (\lambda_{\min} + \lambda_{\max})/2$, $\nu \leftarrow (\nu_{\min} + \nu_{\max})/2$
Update β^{t+1} with (4.17), $\beta_1 \leftarrow \beta^{t+1}$
Update $C_m(\beta^{t+1})$ and $C_b(\beta^{t+1})$
while $|\beta^{t+1} - \beta^t| > \epsilon$ or $C_m < C_{mth}$ or $C_b < C_{bth}$ **do**
  $\beta^t \leftarrow \beta_1$ and update β^{t+1} with (4.17)
  Update $C_m(\beta^{t+1})$ and $C_b(\beta^{t+1})$
  while $\lambda_{\max} - \lambda_{\min} > \epsilon$ **do**
    if $C_m < C_{mth}$ **then**
      $\lambda_{\max} \leftarrow \lambda$
    else
      $\lambda_{\min} \leftarrow \lambda$
    end if
    $\lambda \leftarrow (\lambda_{\min} + \lambda_{\max})/2$
    $\beta^t \leftarrow \beta_1$ and update β^{t+1} with (4.17)
    Update $C_m(\beta^{t+1})$ and $C_b(\beta^{t+1})$
    while $\nu_{\max} - \nu_{\min} > \epsilon$ **do**
      if $C_b < C_{bth}$ **then**
        $\nu_{\max} \leftarrow \nu$
      else
        $\nu_{\min} \leftarrow \nu$
      end if
      $\nu \leftarrow (\nu_{\min} + \nu_{\max})/2$
      $\beta^t \leftarrow \beta_1$ and update β^{t+1} with (4.17)
      Update $C_m(\beta^{t+1})$ and $C_b(\beta^{t+1})$
    end while
  end while
end while
$\beta^* \leftarrow \beta^{t+1}$

Algorithm 2 MP for global capacity maximization

Require : $C_{mth} > 0$, $C_{bth} > 0$,
Ensure : Return the optimal transmit power ratio β^* between DVB and LTE giving the maximum global capacity
1 : Initialize $\beta_{\min}$, $\beta_{\max}$, $\epsilon > 0$, $\delta > 0$
2 : Update $C_m(\beta_{\min})$ and $C_b(\beta_{\min})$
3 : **while** $C_m < C_{mth}$ or $C_b < C_{bth}$ **do**
4 : $\beta_{min} \leftarrow \beta_{min} + \epsilon$
5 : Update $C_m(\beta_{\min})$ and $C_b(\beta_{\min})$
6 : **end while**
7 : Store $C_g(\beta_{\min})$
8 : **while** $C_m < C_{mth}$ or $C_b < C_{bth}$ **do**
9 : $\beta_{max} \leftarrow \beta_{max} - \delta$
10 : Update $C_m(\beta_{\max})$ and $C_b(\beta_{\max})$
11 : **end while**
12 : Store $C_g(\beta_{\max})$
13 : Compare $C_g(\beta_{\min})$ and $C_g(\beta_{\max})$ and pick the maximum value
14 : Return β^*

In Algorithm 2, β_{min} and β_{max}, i.e. the upper and lower bounds of β are initialized. Moreover, the convergence parameters ϵ and δ are defined by taking very small values. Algorithm 2 consists of two loops. In both loops, i.e. steps 3 and 8, we iterate until the satisfaction of the two constraints of the problem presented in (4.10). C_g is maximum for $\beta \to 0$ and $\beta \to \infty$ as it can be seen on Fig. 4.3. In step 3, β is iteratively incremented until the constraints are satisfied. In that case, the mobile capacity C_m tends to its maximum value while the broadcast capacity C_b tends to its minimum value and β takes its right minimum value β_{min}, i.e. the lower bound of the range of the acceptable β values according to the constraints in (4.10). In step 8, β is iteratively decremented until the constraints are satisfied. As seen in Fig. 4.3, the broadcast capacity C_b tends to its maximum value while the mobile capacity C_m tends to its minimum value. In this case, β takes its right maximum value β_{max}, i.e. the upper bound of the range of the acceptable β values according to the constraints. Therefore, the range $]\beta_{min}, \beta_{max}[$ contains all β satisfying the constraints on C_m and C_b in (4.10).

After satisfying the constraints and specifying β_{min} and β_{max}, it remains to choose β^* which gives the maximum value of C_g respecting the constraints. As illustrated in Fig. 4.3, $C_g(\beta^*)$ must be in the right or in the left side according to the given parameter values of the system. Comparing $C_g(\beta_{min})$ and $C_g(\beta_{max})$, $C_g(\beta^*)$ is specified and β^* is selected among β_{min} and β_{max}.

4.4 Results & Discussion

Firstly, the simulation results are presented to compare the CCCP and MP algorithms and then evaluate the advantages of each of them. Next, an analyse of the results is carried out to choose the optimal value for β and then for the transmission powers p_m and p_b.

4.4.1 Simulation results

In this section, the results of the algorithms given in Section 4.3 are illustrated. Realistic parameter values of DVB and LTE networks are used in these simulations. We recall that, the bandwidth of the interfering systems is 7.61 MHz. The DVB and LTE cell radius are 100 km and 1 km respectively. The distance from BT to MR is 100 km. The distance d between BS and BR, in this section, is a parameter of simulations ranging from 100 m to 500 m.

Fig. 4.4 gives the optimal β w.r.t. the BS-BR distance d and for equal constraints case $C_{mth} = C_{bth} = 0.37$ bits/sec/Hz when CCCP algorithm is run. It can be seen that β is first decreasing for small range of d values but it slightly increases in the $50 - 180$ m range and finally decreases for larger d. Hence the behavior of β in function of d is not intuitive as it could be first thought. This is due to the effect of p_m and p_b in β expression.

In Fig. 4.5, the global, mobile and broadcast capacities are depicted according to the mobile capacity constraint, i.e. C_{mth} for a fixed value of the broadcast capacity constraint $C_{bth} = 0.5$ bit/s/Hz, when MP algorithm is run. The broadcast capacity and the mobile capacity are varying in an opposite way and remain constant for $C_{mth} \geq 0.5$ bit/s/Hz. As noticed, the mobile capacity and the broadcast capacity are reversed for $C_{mth} \leq 0.5$. The mobile capacity increases to take a constant value while the broadcast capacity decreases to take a constant value less than the mobile capacity. Interestingly, the global capacity is decreasing for $C_{mth} \leq 0.5$ and remains constant for higher values of the constraint on the mobile system. This result is very important as it concludes that if the mobile system is allowed to operate with low data rate (C_m less than 0.3 bits/sec/Hz), the broadcast receivers will be slightly affected. It is not the case if we increase the requirements on the QoS for the mobile.

In Fig. 4.6, C_g, C_m and C_b are plotted according to β for $d = 100$ m. In this figure, an example of the capacities thresholds, i.e. C_{mth} and C_{bth} values, is given. The horizontal red lines stand for capacity constraint for each system, e.g. $C_{mth} = 0.5$ bit/s/Hz and $C_{bth} = 1$ bit/s/Hz. The intersections of these lines with C_m and C_b gives the boundaries for the search of β^*. The difference between the optimal value of C_g is shown in case of using the CCCP algorithm and the MP algorithm. As illustrated in Fig. 4.6, the horizontal red lines representing C_{mth} and C_{bth} values intersect with the mobile and the broadcast capacity. Between these two intersection

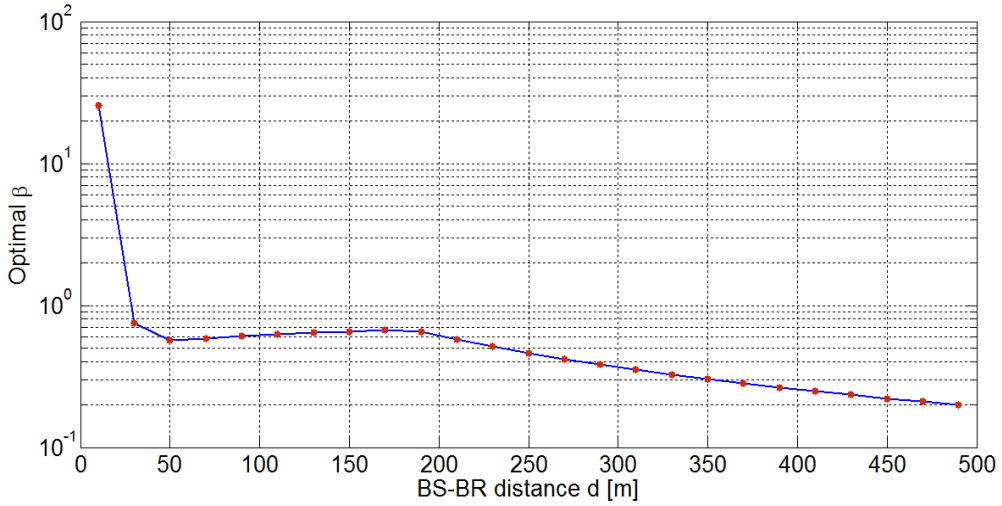

Figure 4.4 – β^* according to the BS-BR distance b and $C_{mth} = C_{bth} = 0.37$ bits/s/Hz.

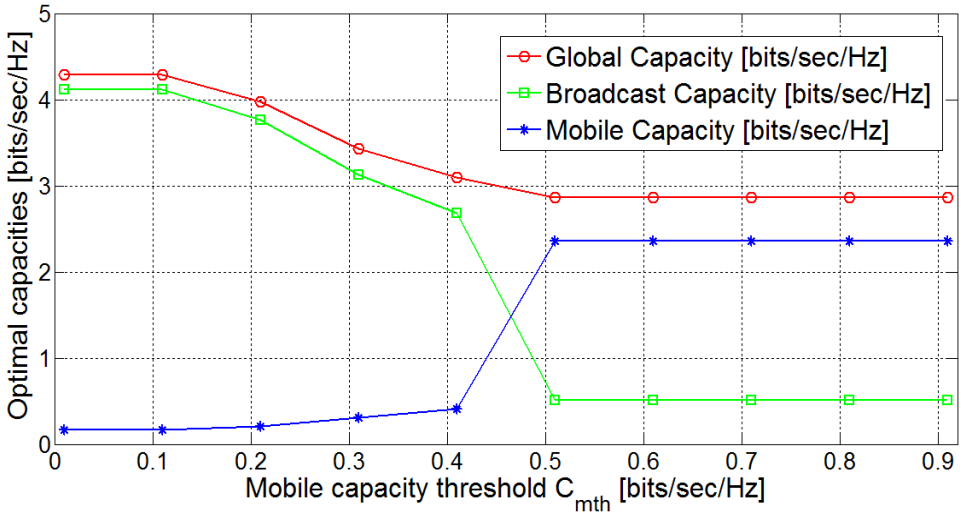

Figure 4.5 – C_g, C_m and C_b according to C_{mth} for $d = 100$ m and $C_{bth} = 0.5$ bit/s/Hz.

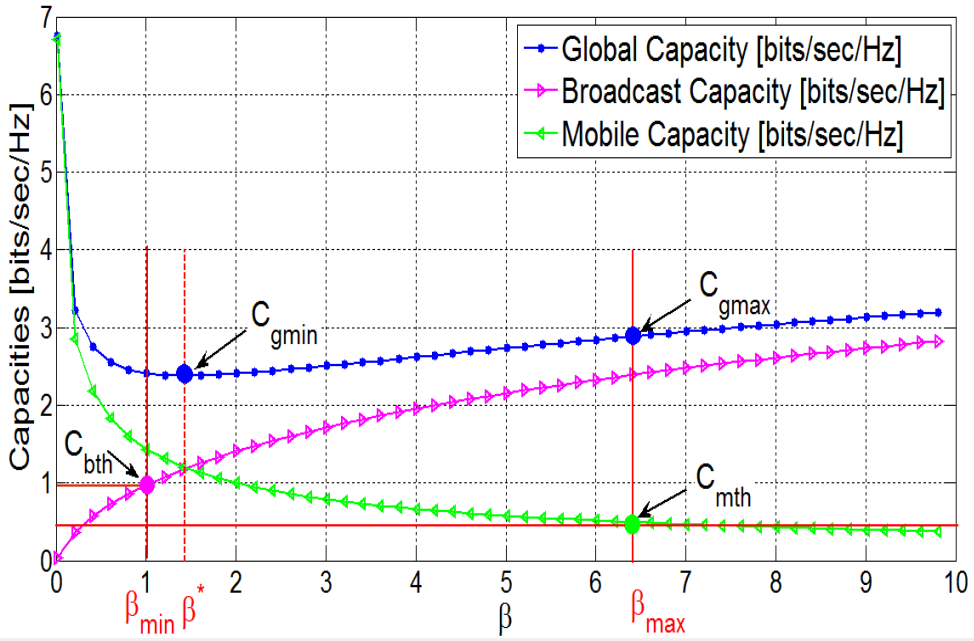

Figure 4.6 – C_g, C_m and C_b according to β for $d = 100$ m, $C_{mth} = 0.5$ and $C_{bth} = 1$ bit/s/Hz.

points, the constraints in (4.10) are respected because C_m and C_b have a monotonic behaviour in this interval. Algorithm 1 tends toward β^* giving the minimum value of the global capacity, i.e. C_{gmin} value, when CCCP is run. It can be also remarked that β^* obtained with CCCP corresponds to the β leading to the intersection between C_b and C_m curves. On the other hand, Algorithm 2 finds the strict maximum of the global capacity while satisfying the constraints and hence β tends toward $\beta^*_{\max}$, i.e. β_{max} in this simulation case, which gives the maximum value of C_g, i.e. C_{gmax}. To summarize, CCCP gives the minimum value of C_g but provides a certain fairness between C_m and C_b while the proposed MP gives the maximum value of C_g which can be at the right or left side of the interval containing the acceptable values of β according to (4.10). In the later case, one system is necessarily favoured over the other.

Moreover, Fig. 4.7 gives the global, mobile and broadcast capacities for the optimal β obtained with Algorithm 1 and 2 when d is varying.

All capacities globally increase with d for both algorithms (except mobile capacity for MP algorithm which remains constant while d is varying). As known, Algorithm 2 gives the maximum value of C_g which is at one of the two extremities according to the system parameter values and requested constraints. Furthermore, the obtained C_m and C_b values are affected by the choice of the maximum of the

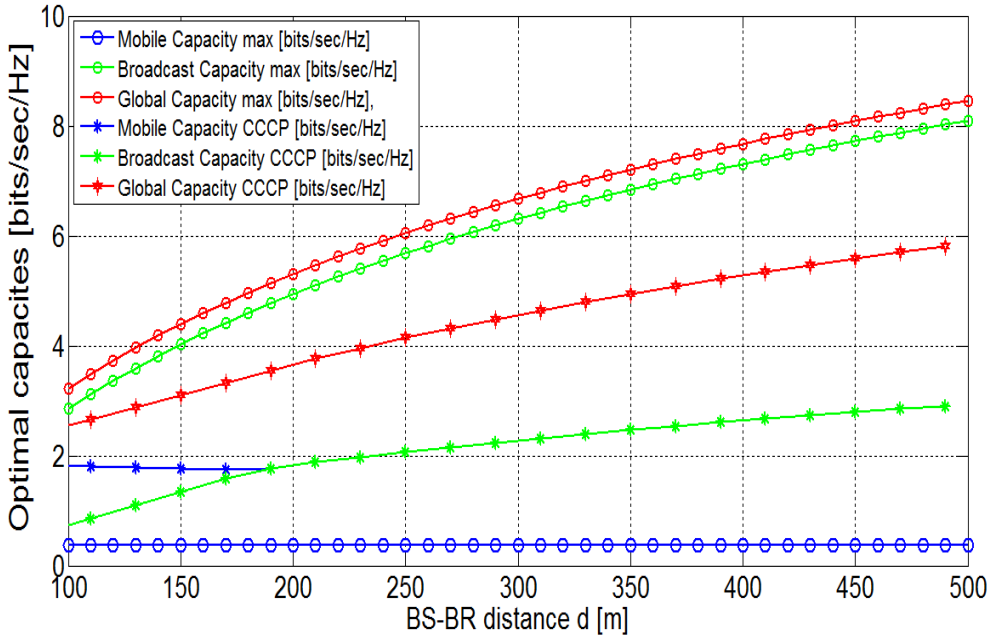

Figure 4.7 – C_g, C_m and C_b achieved with Algorithm 1 and Algorithm 2 and according to d, $C_{mth} = C_{bth} = 0.36673$ bits/sec/Hz.

global capacity, which is in its turn affected by d. Hence, the mobile capacity may have this stable behavior only for the case of these given parameters and constraint values. Indeed, the mobile system strongly affects the achievable capacity in the DVB link due to the small values of d compared to the DVB cell radius. Hence, when d increases, the DVB system becomes interference-free and hence contributes to the increase of the global capacity.

Second, the capacities achieved with Algorithm 2 are higher than the ones achieved with Algorithm 1. Indeed, the global capacity at β^*, i.e. $C_g(\beta^*)$, for CCCP corresponds to the minimum of the global capacity. This can be explained by the fact that CCCP naturally goes toward the stable energy point of a function. In our case, this corresponds to the junction between the convex and concave part of the Lagrangian of the problem in (4.10) as illustrated in Fig. 4.6.

4.4.2 Optimal choice

As seen in the previous section, CCCP procedure does not lead to the strict maximum of the global ergodic capacity but to an equilibrium point between mobile and broadcast capacities. Moreover, MP algorithm, i.e. Algorithm 2, leads to the strict maximum of the global capacity but it maximizes simultaneously the capacity

of one of the two coexisting systems and minimizes the other. This depends on the given parameter values. Each algorithm responds to specific priorities ; either the priority is for the performance of the global coexistence system, either the priority is to balance both coexisting systems.

Despite Algorithm 1 gives the minimum value of the global capacity, it remains interesting because it gives the maximum capacity for both systems, i.e. LTE and DVB, in a fair way as it can be seen in Fig. 4.6. Hence, Algorithm 1 can be used for fairness purposes between the two coexisting systems. Moreover, it can be noticed that CCCP allows the three capacities increase while Algorithm 2 keeps C_m constant with the constraint chosen. Moreover, the two algorithms are interesting as they are complementary to each other. Therefore, the optimal choice between the results of the two algorithms is selected according to the point of view of the needs and the requirements.

The optimization is realized in function of the variable β. The actual transmitted powers can be recovered by fixing one of the power, i.e. p_m or p_b, and compute the remaining power thanks to β and the variables existing in β in (4.4).

4.5 Conclusion

In this chapter, the maximization of the global ergodic capacity of spectrally fully-overlapping DVB and LTE systems is studied. The global ergodic capacity is made of a convex part, i.e. LTE system capacity, and a concave part, i.e. DVB system capacity, and moreover, it only depends on the ratio of the transmitted powers and not on the absolute values of them. The problem has hence been solved using CCCP algorithm leading to an equilibrium point of the global capacity, corresponding to the minimum of the global capacity, but to the maximum of each individual data rate. In order to strictly maximize the global capacity, an another simple algorithm is proposed allowing to achieve the boundaries of the global data rate while respecting the QoS constraints. This solution favors one system over the other, and hence achieves an higher throughput than the one obtained with the CCCP solution. This study can be useful for operators interested in dense network deployment scenarios to decide the operating point of resources allocated in a very aggressive frequency reuse pattern.

Finally, we should say that our study in this chapter does not rely on a particular spectrum sensing principle. Indeed, in the proposed model, the two systems are considered active at the same time on the same frequency and hence interferences are not sought to be avoided. In this chapter, the optimization has been studied in case of continuous activity and full interference of the two systems over the entire spectrum differently than the chapter 2 case. In the next chapter, the spectral coexistence between LTE and DVB systems will be studied according to the variation of the

spectral overlap ratio between their bandwidths and with a more realistic signal model.

5

Spectral Efficiency of DVB and LTE Networks in Function of Frequency Overlap

In the previous chapters, the spectral coexistence between DVB and LTE is analyzed in case of full spectral overlap. The subcarriers are supposed all affected in the same way. In this chapter, we consider that the frequency overlap ratio between the DVB and the LTE bandwidths varies and according to this variation, we study the effect over the spectral efficiency of the global coexistence system. Consequently, the subcarriers of each bandwidth are not affected in the same way in this chapter when the frequency overlap ratio is varying. Therefore, the main contribution of this chapter is to derive the interfering signal variance according to the frequency overlap and taking into account carefully the difference between the characteristics of the LTE and DVB networks, especially the OFDM subcarrier spacing and hence the OFDM symbol duration.

First of all, the system model is described and the signal model is given. Then, the expression of the sampled signal on each sub-carrier is given taking into account the interference experienced. The variance of the interfering system, i.e. DVB over LTE and LTE over DVB, is derived by averaging over symbols, asynchronism and channel coefficients. The spectral efficiency of the global system containing the DVB and LTE networks is then expressed. Next, the variation of this global spectral efficiency in function of the overlap ratio is evaluated and the optimal condition is selected. Finally, a conclusion is drawn.

5.1 System Model

This section introduces the system model and notations used throughout the chapter. Both systems, i.e. DVB and LTE, are allowed to spectrally overlap as illustrated in Fig. 5.1. In this figure B and B' are the bandwidth of LTE and DVB

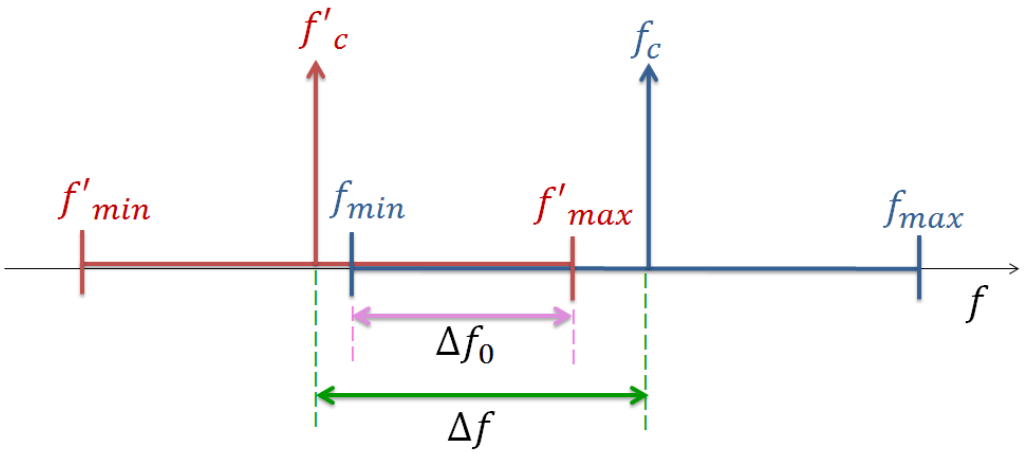

Figure 5.1 – Spectral overlap presentation

respectively, Δf_0 expresses the spectral overlap between B and B' and f_c and f'_c are the central frequencies such as $\Delta f = f_c - f'_c$. Moreover, the spectral overlap ratio is defined by :

$$\alpha = \frac{\Delta f_0}{B_{min}} = \frac{1+\chi}{2\chi} - \frac{\Delta f}{B_{\min}} \tag{5.1}$$

where χ is defined by $\chi = \frac{B_{\min}}{B_{\max}}$ and $B_{\min} = \min\{B, B'\}$ and $B_{\max} = \max\{B, B'\}$.

Both systems, i.e. LTE and DVB, have different characteristics such as different subcarrier spacing and sampling frequency. Consequently, the interference arising between both bandwidths depends on the frequency shift between them and takes into account the non orthogonality between the subcarriers. Fig. 5.2 shows how the useful data in a specific subcarrier is affected by the interference coming from the signal waveform of other subcarriers when a frequency shift exists between bandwidths.

5.2 Signal model

In this section, we introduce the OFDM signal model for LTE and DVB systems using bank filters formalism. We first introduce some notations concerning LTE and DVB characteristics. Let us define $T_s^{(L/D)}$, $T_g^{(L/D)}$, $N^{(L/D)}$ the OFDM symbol and cyclic prefix (CP) durations and the number of subcarriers of LTE and DVB systems respectively and $T^{(L/D)} = T_s^{(L/D)} + T_g^{(L/D)}$. Moreover, $\xi = \frac{T^{(D)}}{T^{(L)}} = \frac{T_s^{(D)}}{T_s^{(L)}} = \frac{T_g^{(D)}}{T_g^{(L)}} > 1$, such as $\xi \in \mathbb{Q}$, the rational number set.

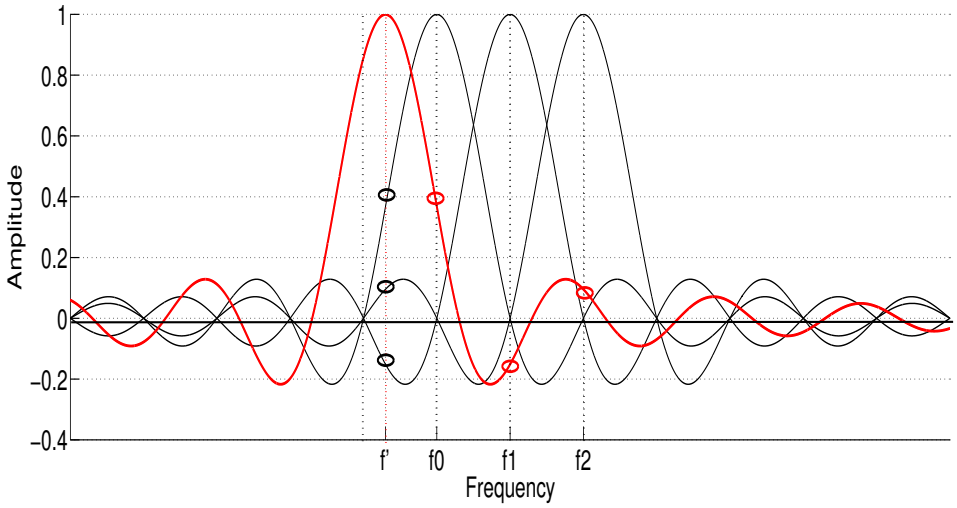

Figure 5.2 – OFDM signal waveform with frequency offset

5.2.1 LTE received signal

The OFDM signal waveform generated by the LTE BS is given by :

$$s^{(L)}(t) = \frac{1}{\sqrt{T_s^{(L)}}} \sum_{l\in\mathbb{Z}} \sum_{k=0}^{N^{(L)}-1} X_k^{(L)}[l] e^{j2\pi \frac{k}{T_s^{(L)}} t} \Pi\left(\frac{t - lT^{(L)}}{T_s^{(L)}}\right) \tag{5.2}$$

where $X_k^{(L)}[l]$ is the symbol of the $l-$th OFDM data block transmitted over the $k-$th LTE subcarrier. $\Pi(t)$ is the rectangular pulse shaping function defined by :

$$\Pi(t) = \text{rect}(t) = \begin{cases} 1 & 0 \leq t \leq 1 \\ 0 & \text{otherwise} \end{cases} \tag{5.3}$$

Before being transmitted, CP is added to the signal which can be written as :

$$s^{(L)}(t) = \frac{1}{\sqrt{T_s^{(L)}}} \sum_{l\in\mathbb{Z}} \sum_{k=0}^{N^{(L)}-1} X_k^{(L)}[l] e^{j2\pi \frac{k}{T_s^{(L)}} t} \Pi\left(\frac{t - lT^{(L)} + T_g^{(L)}}{T^{(L)}}\right) \tag{5.4}$$

The signal passes through a multipath channel, and the received signal on the LTE receiver is :

$$r^{(L)}(t) = \frac{1}{\sqrt{T_s^{(L)}}} \sum_{l\in\mathbb{Z}} \sum_{k=0}^{N^{(L)}-1} \sum_{n=1}^{L} X_k^{(L)}[l] h_n^{(L)} e^{j2\pi \frac{k}{T_s^{(L)}} \left(t-\tau_n^{(L)}\right)} \Pi\left(\frac{t - \tau_n^{(L)} - lT^{(L)} + T_g^{(L)}}{T^{(L)}}\right) \tag{5.5}$$

where $h_n^{(L)}$, $\tau_n^{(L)}$ are the channel coefficient complex Gaussian distributed and the delay of the $n-$th path of LTE channel. Moreover, LTE channel contains L paths. The channel frequency response on the $k-$th subcarrier is given by

$$H_k^{(L)} = \sum_{n=1}^{L} h_n^{(L)} e^{-j2\pi \frac{k}{T_s^{(L)}} \tau_n} \tag{5.6}$$

The LTE received signal on the $p-$th subcarrier and over the $n-$th OFDM data bloc is given by :

$$\tilde{X}_p^{(L)}[m] = \int_{\mathbb{R}} r^{(L)}(t) \phi_{p,m}^{(L)}(t) dt \tag{5.7}$$

where $\phi_{p,m}^{(L)}(t)$ is the reception filter defined by :

$$\phi_{p,m}^{(L)}(t) = \frac{1}{\sqrt{T_s^{(L)}}} e^{-j2\pi \frac{p}{T_s^{(L)}} t} \Pi\left(\frac{t - mT^{(L)}}{T_s^{(L)}}\right) \tag{5.8}$$

Therefore, the received LTE signal becomes :

$$\begin{aligned} \tilde{X}_p^{(L)}[m] &= \frac{1}{T_s^{(L)}} \int_{\mathbb{R}} \sum_{l \in \mathbb{Z}} \sum_{k=0}^{N^{(L)}-1} \sum_{n=1}^{L} X_k^{(L)}[l] h_n^{(L)} e^{j2\pi \frac{k}{T_s^{(L)}} \left(t - \tau_n^{(L)}\right)} e^{-j2\pi \frac{p}{T_s^{(L)}} t} \\ &\quad \Pi\left(\frac{t - mT^{(L)}}{T_s^{(L)}}\right) \Pi\left(\frac{t - \tau_n^{(L)} - lT^{(L)} + T_g^{(L)}}{T^{(L)}}\right) dt \end{aligned} \tag{5.9}$$

The integration over t depends on the term $\Pi\left(\frac{t-mT^{(L)}}{T_s^{(L)}}\right) \Pi\left(\frac{t-\tau_n^{(L)}-lT^{(L)}+T_g^{(L)}}{T^{(L)}}\right)$ where :

$$\Pi\left(\frac{t - mT^{(L)}}{T_s^{(L)}}\right) \neq 0 \leftrightarrow \begin{cases} m = l \\ t \in \left[mT_s^{(L)} + mT_g^{(L)}, (m+1)T_s^{(L)} + mT_g^{(L)}\right] \end{cases} \tag{5.10}$$

Therefore :

$$\begin{aligned} \tilde{X}_p^{(L)}[m] &= \frac{1}{T_s^{(L)}} \sum_{k=0}^{N^{(L)}-1} \sum_{n=1}^{L} X_k^{(L)}[m] h_n^{(L)} e^{-j2\pi \frac{k}{T_s^{(L)}} \tau_n^{(L)}} \int_{mT^{(L)}}^{mT^{(L)} + T_s^{(L)}} e^{j2\pi \frac{k-p}{T_s^{(L)}} t} dt \\ &= \sum_{k=0}^{N^{(L)}-1} \sum_{n=1}^{L} X_k^{(D)}[m] h_n^{(L)} e^{-j2\pi \frac{k}{T_s^{(L)}} \tau_n^{(L)}} \operatorname{sinc}(k-p) e^{j\pi(k-p)} e^{j2\pi \frac{(k-p)}{T_s^{(L)}} mT^{(L)}} \end{aligned} \tag{5.11}$$

where :

$$\operatorname{sinc}(k-p) = \begin{cases} 1 & \text{if } k = p \\ 0 & \text{otherwise} \end{cases} \tag{5.12}$$

We conclude that when the transmitter and the receiver are perfectly synchronized, the received signal becomes :

$$\tilde{X}_p^{(L)}[m] = X_p^{(L)}[m] H_p^{(L)}[m] \tag{5.13}$$

5.2.1.1 DVB interfering signal

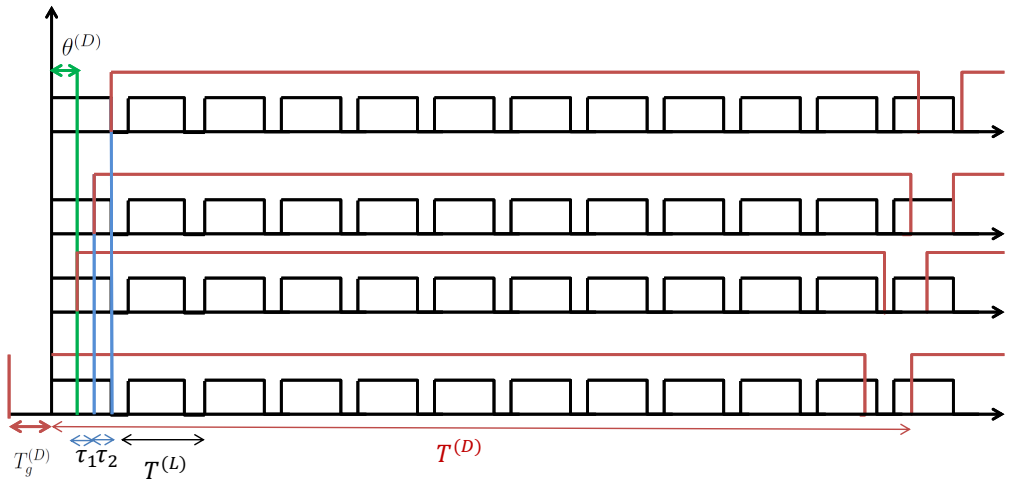

Figure 5.3 – Interfering DVB symbols over LTE symbol

DVB signal is also OFDM based and hence, the transmitted OFDM DVB signal with CP is expressed as

$$s^{(D)}(t) = \frac{1}{\sqrt{T_s^{(D)}}} \sum_{l' \in \mathbb{Z}} \sum_{k'=0}^{N^{(D)}-1} X_{k'}^{(D)}[l'] e^{j2\pi \frac{k'}{T_s^{(D)}} t} \Pi\left(\frac{t - l'T^{(D)} + T_g^{(D)}}{T^{(D)}}\right) \tag{5.14}$$

where $X_{k'}^{(D)}[l']$ is the DVB QAM symbol of the $l'-$th OFDM data block over the $k'-$th DVB subcarrier.

The broadcasted DVB signal passes through a multipath channel before being received by LTE receiver. Fig. 5.3 presents the interference of the DVB symbol over the LTE symbols. It shows that from LTE receiver point of view, DVB is delayed with an unknown and random asynchronism $\theta^{(D)}$ and hence DVB interfering symbols interferes the LTE signal with several delayed copies. Moreover, DVB is frequency shifted w.r.t. LTE. The DVB interfering signal received by LTE before sampling can

be expressed as :

$$r^{(D)}(t) = \frac{e^{j2\pi\Delta f^{(D)}t}}{\sqrt{T_s^{(D)}}} \sum_{l'\in\mathbb{Z}} \sum_{k'=0}^{N^{(D)}-1} \sum_{n'=1}^{L'} X_{k'}^{(D)}[l'] e^{-j2\pi\frac{k'}{T_s^{(D)}}\theta^{(D)}t} q_{n'}^{(D)} e^{j2\pi\frac{k'}{T_s^{(D)}}\left(t-\tau_{n'}^{(D)}\right)} \Pi\left(\frac{t-\tau_{n'}^{(D)}-l'T^{(D)}+T_g^{(D)}-\theta^{(D)}}{T^{(D)}}\right) \quad (5.15)$$

where $q_{n'}^{(D)}$, $\tau_{n'}^{(D)}$ are the channel coefficient complex Gaussian distributed and the delay of the $n'-$th path of DVB channel. Moreover, DVB channel contains L' paths. The channel frequency response on the $k'-$th subcarrier is given by

$$Q_{k'}^{(D)} = \sum_{n'=1}^{L'} q_{L'}^{(D)} e^{-j2\pi\frac{k'}{T_s^{(D)}}\tau_{n'}} \quad (5.16)$$

LTE receiver decomposes the interfering DVB signal on its own basis. Hence, the interference received on the $p-$th subcarrier and during the $m-$th LTE OFDM data block is given by :

$$I_p^{(D)}[m] = \int_{\mathbb{R}} r^{(D)}(t)\phi_{p,m}^{(L)}(t)dt \quad (5.17)$$

Therefore, we obtain :

$$I_p^{(D)}[m] = \frac{1}{\sqrt{T_s^{(D)}T_s^{(L)}}} \sum_{k'=0}^{N^{(D)}-1} e^{-j2\pi\frac{k'}{T_s^{(D)}}\theta^{(D)}t} \sum_{l'\in\mathbb{Z}} X_{k'}^{(D)}[l'] \sum_{n'=1}^{L'} q_{n'}^{(D)} e^{-j2\pi\frac{k'}{T_s^{(D)}}\tau_{n'}^{(D)}} \times \int_{\mathbb{R}} e^{j2\pi\left(\Delta_f+\frac{k'}{T_s^{(D)}}-\frac{p}{T_s^{(L)}}\right)t} \Pi\left(\frac{t-mT^{(L)}}{T_s^{(L)}}\right) \Pi\left(\frac{t-l'T^{(D)}+T_g^{(D)}-\theta^{(D)}-\tau_{n'}^{(D)}}{T^{(D)}}\right) dt \quad (5.18)$$

The integration over t depends on the term $\Pi\left(\frac{t-mT^{(L)}}{T_s^{(L)}}\right)\Pi\left(\frac{t-\tau_{n'}^{(D)}-l'T^{(D)}+T_g^{(D)}-\theta^{(D)}}{T^{(D)}}\right)$.
We have :

$$\Pi\left(\frac{t-mT^{(L)}}{T_s^{(L)}}\right) = 1 \quad \text{iff} \quad mT^{(L)} \le t \le mT^{(L)} + T_s^{(L)} \quad (5.19)$$

$$\Pi\left(\frac{t-\tau_{n'}^{(D)}-l'T^{(D)}+T_g^{(D)}-\theta^{(D)}}{T^{(D)}}\right) = 1 \quad \text{iff} \quad l'T^{(D)}+\tau_{n'}^{(D)}-T_g^{(D)}+\theta^{(D)} \le t \le (l'+1)T^{(D)}+\tau_{n'}^{(D)}-T_g^{(D)}+\theta^{(D)} \quad (5.20)$$

Re-expressing the non-null conditions of (5.19) in terms of DVB characteristics, the DVB interference has non null value for t such that :

$$\begin{aligned} m\frac{T^{(D)}}{\xi} \leq \quad t \quad &\leq \frac{1}{\xi}\left(mT^{(D)} + T_s^{(D)}\right) \\ l'T^{(D)} + \tau_{n'}^{(D)} - T_g^{(D)} + \theta^{(D)} \leq \quad t \quad &\leq (l'+1)T^{(D)} + \tau_{n'}^{(D)} - T_g^{(D)} + \theta^{(D)} \end{aligned} \tag{5.21}$$

In (5.21), the DVB asynchronism θ is uniformly distributed over the entire OFDM symbol duration such that : $\theta^{(D)} \sim \mathcal{U}([0, T^{(D)}])$. According to (5.21), two cases exist :

case 1 : One symbol interferes : $X_{k'}^{(D)}[l'-1]$. If $\forall n'$, we have :

$$\begin{aligned} m\frac{T^{(D)}}{\xi} \quad &> \quad l'T^{(D)} + \tau_{n'}^{(D)} - T_g^{(D)} + \theta^{(D)} \\ \frac{1}{\xi}\left(mT^{(D)} + T_s^{(D)}\right) \quad &\leq \quad (l'+1)T^{(D)} + \tau_{n'}^{(D)} - T_g^{(D)} + \theta^{(D)} \end{aligned} \tag{5.22}$$

one symbol interferes. This condition is reached when :

$$\left(\frac{m}{\xi} - l' - 1\right)T^{(D)} + \frac{T_s^{(D)}}{\xi} + T_g^{(D)} - \tau_{n'}^{(D)} \leq \theta^{(D)} \leq \left(\frac{m}{\xi} - l'\right)T^{(D)} + T_g^{(D)} - \tau_{n'}^{(D)} \tag{5.23}$$

case 2 : Two symbols interfere : $X_{k'}^{(D)}[l'-1]$ and $X_{k'}^{(D)}[l']$. This case is more complex than the first one and includes three sub-cases :

1. $\exists A$ such that $\forall n' < A$, we have :

$$\begin{aligned} m\frac{T^{(D)}}{\xi} \quad &> \quad l'T^{(D)} + \tau_{n'}^{(D)} - T_g^{(D)} + \theta^{(D)} \\ \frac{1}{\xi}\left(mT^{(D)} + T_s^{(D)}\right) \quad &\leq \quad (l'+1)T^{(D)} + \tau_{n'}^{(D)} - T_g^{(D)} + \theta^{(D)} \end{aligned} \tag{5.24}$$

2. $\exists B$ such that $\forall n'$, $A \leq n' < B$:

$$\begin{aligned} m\frac{T^{(D)}}{\xi} \quad &\leq \quad l'T^{(D)} + \tau_{n'}^{(D)} - T_g^{(D)} + \theta^{(D)} \\ \frac{1}{\xi}\left(mT^{(D)} + T_s^{(D)}\right) \quad &\geq \quad l'T^{(D)} + \tau_{n'}^{(D)} - T_g^{(D)} + \theta^{(D)} \end{aligned} \tag{5.25}$$

3. $\forall n' \geq B$

$$\begin{aligned} m\frac{T^{(D)}}{\xi} \quad &\geq \quad (l'-1)T^{(D)} + \tau_{n'}^{(D)} - T_g^{(D)} + \theta^{(D)} \\ \frac{1}{\xi}\left(mT^{(D)} + T_s^{(D)}\right) \quad &\leq \quad l'T^{(D)} + \tau_{n'}^{(D)} - T_g^{(D)} + \theta^{(D)} \end{aligned} \tag{5.26}$$

In fact, this reformulation includes the first case of one interfering symbol where we have finally $A \geq L'$. Rewriting these conditions of the three cases over $\theta^{(D)}$, we obtain :

1. $\exists A$ such that $\forall n' < A$ and $A \leq L'$, therefore one symbol interferes such as :

$$\left(\frac{m}{\xi} - l' - 1\right) T^{(D)} + \frac{T_s^{(D)}}{\xi} + T_g^{(D)} - \tau_{n'}^{(D)} \leq \theta^{(D)} \leq \left(\frac{m}{\xi} - l'\right) T^{(D)} + T_g^{(D)} - \tau_{n'}^{(D)} \tag{5.27}$$

2. $\exists B$ such that $\forall n' \in [A, B[$ and $B \leq L'$:

$$\left(\frac{m}{\xi} - l'\right) T^{(D)} + T_g^{(D)} - \tau_{n'}^{(D)} \leq \theta^{(D)} \leq \left(\frac{m}{\xi} - l'\right) T^{(D)} + \frac{T_s^{(D)}}{\xi} + T_g^{(D)} - \tau_{n'}^{(D)} \tag{5.28}$$

3. $\forall n' \geq B$ and $n' \leq L'$:

$$\left(\frac{m}{\xi} - l'\right) T^{(D)} + \frac{T_s^{(D)}}{\xi} + T_g^{(D)} - \tau_{n'}^{(D)} \leq \theta^{(D)} \leq \left(\frac{m}{\xi} - l' + 1\right) T^{(D)} + T_g^{(D)} - \tau_{n'}^{(D)} \tag{5.29}$$

Therefore the interference can be written as :

$$\begin{aligned}
I_p^{(D)}[m] \;=\; & \frac{1}{\sqrt{T_s^{(D)} T_s^{(L)}}} \sum_{k'=0}^{N^{(D)}-1} e^{-j2\pi \frac{k'}{T_s^{(D)}} \theta^{(D)}} \times \\
& \left\{ \sum_{n'=1}^{A-1} q_{n'}^{(D)} e^{-j2\pi \frac{k'}{T_s^{(D)}} \tau_{n'}^{(D)}} X_{k'}^{(D)}[l'-1] \int_{\frac{m}{\xi} T^{(D)}}^{\frac{1}{\xi}(mT^{(D)} + T_s^{(D)})} e^{j2\pi \left(\Delta f^{(D)} + \frac{k'}{T_s^{(D)}} - \frac{p}{T_s^{(L)}} \right) t} dt \right. \\
& + \sum_{n'=A}^{B-1} q_{n'}^{(D)} e^{-j2\pi \frac{k'}{T_s^{(D)}} \tau_{n'}^{(D)}} \left[X_{k'}^{(D)}[l'-1] \int_{\frac{m}{\xi} T^{(D)}}^{l' T^{(D)} - T_g^{(D)} + \tau_{n'}^{(D)} + \theta^{(D)}} e^{j2\pi \left(\Delta f^{(D)} + \frac{k'}{T_s^{(D)}} - \frac{p}{T_s^{(L)}} \right) t} dt \right. \\
& \qquad \left. + X_{k'}^{(D)}[l'] \int_{l' T^{(D)} - T_g^{(D)} + \tau_{n'}^{(D)} + \theta^{(D)}}^{\frac{1}{\xi}(mT^{(D)} + T_s^{(D)})} e^{j2\pi \left(\Delta f^{(D)} + \frac{k'}{T_s^{(D)}} - \frac{p}{T_s^{(L)}} \right) t} dt \right] \\
& \left. + \sum_{n'=B}^{L'} q_{n'}^{(D)} e^{-j2\pi \frac{k'}{T_s^{(D)}} \tau_{n'}^{(D)}} X_{k'}^{(D)}[l'-1] \int_{\frac{m}{\xi} T^{(D)}}^{\frac{1}{\xi}(mT^{(D)} + T_s^{(D)})} e^{j2\pi \left(\Delta f^{(D)} + \frac{k'}{T_s^{(D)}} - \frac{p}{T_s^{(L)}} \right) t} dt \right\}
\end{aligned} \tag{5.30}$$

$$I_p^{(D)}[m] = \frac{1}{\sqrt{T_s^{(D)}T_s^{(L)}}} \sum_{k'=0}^{N^{(D)}-1} e^{-j2\pi\frac{k'}{T_s^{(D)}}\theta^{(D)}} \left\{ \sum_{n'\in L_b} q_{n'}^{(D)} e^{-j2\pi\frac{k'}{T_s^{(D)}}\tau_{n'}^{(D)}} \left(X_{k'}^{(D)}[l'] + X_{k'}^{(D)}[l'-1]\right) \times \int_{\frac{m}{\xi}T^{(D)}}^{\frac{1}{\xi}(mT^{(D)}+T_s^{(D)})} e^{j2\pi\left(\Delta f^{(D)}+\frac{k'}{T_s^{(D)}}-\frac{p}{T_s^{(L)}}\right)t} dt + \sum_{n'=A}^{B-1} q_{n'}^{(D)} e^{-j2\pi\frac{k'}{T_s^{(D)}}\tau_{n'}^{(D)}} \left[X_{k'}^{(D)}[l'-1] \int_{\frac{m}{\xi}T^{(D)}}^{l'T^{(D)}-T_g^{(D)}+\tau_{n'}^{(D)}+\theta^{(D)}} e^{j2\pi\left(\Delta f^{(D)}+\frac{k'}{T_s^{(D)}}-\frac{p}{T_s^{(L)}}\right)t} dt + X_{k'}^{(D)}[l'] \int_{l'T^{(D)}-T_g^{(D)}+\tau_{n'}^{(D)}+\theta^{(D)}}^{\frac{1}{\xi}(mT^{(D)}+T_s^{(D)})} e^{j2\pi\left(\Delta f^{(D)}+\frac{k'}{T_s^{(D)}}-\frac{p}{T_s^{(L)}}\right)t} dt \right] \right\} \quad (5.31)$$

with $L_b = \{1,..,L'\}\backslash\{A,..,B-1\}$. Hence, the interference variance is obtained by averaging over $X_{k'}^{(D)}$, $q_{n'}^{(D)}$ then $\theta^{(D)}$.

In practice, the maximum channel delay $\tau_{max}^{(D)} \approx 5\mu s << T_s^{(L)}$. Consequently, we consider that the probability that $\theta^{(D)}$ is such that $\exists A$ and B leading to the situation previously described is negligible. Therefore, only two cases of the DVB interference over the LTE signal are considered :

case 1 : The time interval boundaries are described in (5.21), (5.22), (5.23) $\forall n'$. In such a case, only one DVB symbol, i.e. $X_{k'}^{(D)}[l']$ is interfering with the current LTE symbol, hence interference on the $p-$th subcarrier of the $m-$th OFDM symbol is given by :

$$I_p^{(D)}[m] = \frac{1}{\sqrt{T_s^{(D)}T_s^{(L)}}} \sum_{k'=0}^{N^{(D)}-1} X_{k'}^{(D)}[l'] \sum_{n'=1}^{L'} q_{n'}^{(D)} e^{-j2\pi\frac{k'}{T_s^{(D)}}\left(\tau_{n'}^{(D)}+\theta^{(D)}\right)} \int_{m\frac{T^{(D)}}{\xi}}^{\frac{1}{\xi}\left(mT^{(D)}+T_s^{(D)}\right)} e^{j2\pi\left(\Delta f^{(D)}+\frac{k'}{T_s^{(D)}}-\frac{p}{T_s^{(L)}}\right)t} dt \quad (5.32)$$

which gives :

$$I_p^{(D)}[m] = \sqrt{\frac{1}{\xi}} \sum_{k'=0}^{N^{(D)}-1} X_{k'}^{(D)}[l'] e^{-j2\pi\frac{k'}{T_s^{(D)}}\theta^{(D)}} Q_{k'}^{(D)} \mathrm{sinc}\left(\pi\left(\frac{\Delta f^{(D)}T_s^{(D)}}{\xi} + \frac{k'}{\xi} - p\right)\right) \times e^{j2\pi\frac{mT^{(D)}}{\xi}\left(\Delta f^{(D)}+\frac{k'}{T_s^{(D)}}-\frac{p}{T_s^{(L)}}\right)} e^{j\pi\left(\frac{\Delta f^{(D)}T_s^{(D)}}{\xi}+\frac{k'}{\xi}-p\right)} \quad (5.33)$$

Averaging $I_p^{(D)}[m]$ over the symbols $X_{k'}^{(D)}$ and the channel $q_{n'}^{(D)}$ [1], we obtain :

$$\mathbb{E}^{(1)}_{X_{k'},q_{n'}}\left[|I_p^{(D)}[m]|^2\right] = \frac{1}{\xi}\sum_{k'=0}^{N^{(D)}-1}\left|\text{sinc}\left(\pi\left(\frac{\Delta f^{(D)}T_s^{(D)}}{\xi}+\frac{k'}{\xi}-p\right)\right)\right|^2\sum_{n'=1}^{L'}\Omega_{n'}^{(D)} \tag{5.34}$$

where $\Omega_{n'}^{(D)} = \mathbb{E}[|q_{n'}^D|^2]$.

case 2 : The time interval boundaries in (5.21) are such that $\forall n'$:

- For $m\frac{T^{(D)}}{\xi} \leq t \leq l'T^{(D)}+\tau_{n'}^{(D)}-T_g^{(D)}+\theta^{(D)} \rightarrow X_{k'}^{(D)}[l'-1]$ interferes.
- For $l'T^{(D)}+\tau_{n'}^{(D)}-T_g^{(D)}+\theta^{(D)} \leq t \leq \frac{1}{\xi}\left(mT^{(D)}+T_s^{(D)}\right) \rightarrow X_{k'}^{(D)}[l']$ interferes.

which implies that :

$$\left(\frac{m}{\xi}-l'\right)T^{(D)}-\tau_{n'}^{(D)}+T_g^{(D)} < \theta < \left(\frac{m}{\xi}-l'\right)T^{(D)}-\tau_{n'}^{(D)}+T_g^{(D)}+\frac{T_s^{(D)}}{\xi} \tag{5.35}$$

In this case, two DVB symbols $X_{k'}^{(D)}[l']$ and $X_{k'}^{(D)}[l'-1]$ interfere over the $p-$th subcarrier of the $m-$th LTE OFDM data bloc, and hence the broadcast interference is given by :

$$\begin{aligned} I_p^{(D)}[m] \;=\; & \frac{1}{\sqrt{T_s^{(D)}T_s^{(L)}}}\sum_{k'=0}^{N^{(D)}-1} e^{-j2\pi\frac{k'}{T_s^{(D)}}\theta^{(D)}}\sum_{n'=1}^{L'} q_{n'}^{(D)} e^{-j2\pi\frac{k'}{T_s^{(D)}}\tau_{n'}^{(D)}} \\ & \left[X_{k'}^{(D)}[l'-1]\int_{m\frac{T^{(D)}}{\xi}}^{l'T^{(D)}+\tau_{n'}^{(D)}-T_g^{(D)}+\theta^{(D)}} e^{j2\pi\left(\Delta f^{(D)}+\frac{k'}{T_s^{(D)}}-\frac{p}{T_s^{(L)}}\right)t}dt\right. \\ & \left. +X_{k'}^{(D)}[l']\int_{l'T^{(D)}+\tau_{n'}^{(D)}-T_g^{(D)}+\theta^{(D)}}^{\frac{1}{\xi}\left(mT^{(D)}+T_s^{(D)}\right)} e^{j2\pi\left(\Delta f^{(D)}+\frac{k'}{T_s^{(D)}}-\frac{p}{T_s^{(L)}}\right)t}dt\right] \end{aligned} \tag{5.36}$$

Let us define the following variables $A(k') = \Delta f^{(D)}+\frac{k'}{T_s^{(D)}}-\frac{p}{T_s^{(L)}}$ and $B(n',\theta) =$

1. Delays are considered as deterministic values.

$l'T^{(D)} - T_g^{(D)} + \tau_{n'}^{(D)} + \theta^{(D)}$. Calculating integrals, we obtain :

$$\begin{aligned} I_p^{(D)}[m] &= \frac{1}{\sqrt{T_s^{(D)} T_s^{(L)}}} \sum_{k'=0}^{N^{(D)}-1} \frac{e^{-j2\pi \frac{k'}{T_s^{(D)}} \theta^{(D)}}}{\pi A\left(k'\right)} e^{j\pi A(k') \frac{mT^{(D)}}{\xi}} \sum_{n'=1}^{n'} q_{n'}^{(D)} e^{-j2\pi \frac{k'}{T_s^{(D)}} \tau_{n'}^{(D)}} \times \\ & e^{j\pi A(k') B(n',\theta)} \left\{ -X_{k'}^{(D)}[l'-1] \sin\left(\pi A(k') \left(\frac{mT^{(D)}}{\xi} - B(n',\theta)\right)\right) \right. \\ & \left. + X_{k'}^{(D)}[l'] e^{j\pi A(k') \frac{T_s^{(D)}}{\xi}} \sin\left(\pi A(k') \left(\frac{1}{\xi}\left(mT^{(D)} + T_s^{(D)}\right) - B(n',\theta)\right)\right)\right\} \end{aligned} \tag{5.37}$$

We aim at computing the average interference created by DVB system over LTE by averaging over symbols, channel coefficient and asynchronism [2]. Averaging DVB interference over the symbols, we obtain :

$$\begin{aligned} \mathbb{E}_{X_{k'}}^{(2)} \left[\left|I_p^{(D)}[m]\right|^2\right] &= \frac{1}{T_s^{(D)} T_s^{(L)}} \sum_{k'=0}^{N^{(D)}-1} \frac{1}{\pi^2 A(k')^2} \\ & \left\{ \left| \sum_{n'=0}^{L'} q_{n'}^{(D)} e^{-j2\pi \frac{k'}{T_s^{(D)}} \tau_{n'}^{(D)}} e^{j\pi A(k') B(n',\theta)} \times \right. \right. \\ & \left. \sin\left(\pi A(k') \left(\frac{1}{\xi}\left(mT^{(D)} + T_s^{(D)}\right) - B(n',\theta)\right)\right) \right|^2 + \\ & \left. \left| \sum_{n'=0}^{L'} q_{n'}^{(D)} e^{-j2\pi \frac{k'}{T_s^{(D)}} \tau_{n'}^{(D)}} e^{j\pi A(k') B(n',\theta)} \sin\left(\pi A(k') \left(\frac{mT^{(D)}}{\xi} - B(n',\theta)\right)\right) \right|^2 \right\} \end{aligned} \tag{5.38}$$

where the mean of the double products give null value because of the independence of the symbols. Averaging $\mathbb{E}_{X_{k'}}^{(2)} \left[\left|I_p^{(D)}[m]\right|^2\right]$ over the channel, we obtain :

$$\begin{aligned} \mathbb{E}_{X_{k'},q_{n'}}^{(2)} \left[\left|I_p^{(D)}[m]\right|^2\right] &= \frac{1}{T_s^{(D)} T_s^{(L)}} \sum_{k'=0}^{N^{(D)}-1} \frac{1}{\pi^2 A(k')^2} \\ & \left\{ \sum_{n'=0}^{L'} \left|\Omega_{n'}^{(D)}\right|^2 \sin^2\left(\pi A(k') \left(\frac{1}{\xi}\left(mT^{(D)} + T_s^{(D)}\right) - B(n',\theta)\right)\right) + \right. \\ & \left. \sum_{n'=0}^{L'} \left|\Omega_{n'}^{(D)}\right|^2 \sin^2\left(\pi A(k') \left(\frac{mT^{(D)}}{\xi} - B(n',\theta)\right)\right) \right\} \end{aligned} \tag{5.39}$$

2. The averaging order is not important, however this one leads to the simplest derivations.

where the expectation of the double products is zero because of the independence between coefficients $q_{n'}$.

As explained above, the asynchronism term $\theta^{(D)}$ leads either to the case 1 either to the case 2. The variance of DVB interference should take into account both cases and hence the previous interference expression should be averaged over $\theta^{(D)}$. Asynchronism is assumed to be uniformly distributed over $\left[0, T^{(D)}\right[$ and its pdf is :

$$f_{\theta^{(D)}} = \begin{cases} \frac{1}{T^{(D)}} & \forall\theta \in \left[0, T^{(D)}\right[\\ 0 & \text{elsewhere} \end{cases} \tag{5.40}$$

The variation domain of θ leading to case 2 is such as $\theta^D \in \left[0, \frac{T_s^{(D)}}{\xi}\right]$. Therefore, the DVB interference over the LTE signal in case 2 averaged by $\theta^{(D)}$ is given by :

$$\mathbb{E}^{(2)}_{x_{k'},q_{n'},\theta}[|I_p^{(D)}[m]|^2] = \frac{1}{T_s^{(D)}/\xi}\int_0^{T_s^{(D)}/\xi} \mathbb{E}^{(2)}_{X_{k'},q_{n'}}\left[\left|I_p^{(D)}[m]\right|^2\right] d\theta \tag{5.41}$$

After trigonometric considerations and tedious calculation, the interference variance for case 2 is obtained as :

$$\begin{aligned}
\mathbb{E}^{(2)}_{x_{k'},\theta,q_{n'}}[|I_p^{(D)}[m]|^2] \;=\; & \frac{\xi}{\left(T_s^{(D)}\right)^2 T_s^{(L)}} \sum_{k'=0}^{N^{(D)}-1} \frac{1}{\pi^2 A(k')^2} \sum_{n'}^{L'} \frac{\Omega_{n'}}{2} \left\{ 2\frac{T_s^{(D)}}{\xi} \right. \\
& + \frac{\sin\left(2\pi A(k')\left(\frac{mT^{(D)}}{\xi} + \frac{T_s^{(D)}}{\xi} - B(n', \frac{Ts^{(D)}}{\xi})\right)\right)}{2\pi A(k')} \\
& - \frac{\sin\left(2\pi A(k')\left(\frac{mT^{(D)}}{\xi} + \frac{T_s^{(D)}}{\xi} - B(n', 0)\right)\right)}{2\pi A(k')} \\
& \frac{\sin\left(2\pi A(k')\left(\frac{mT^{(D)}}{\xi} - B(n', \frac{Ts^{(D)}}{\xi})\right)\right)}{2\pi A(k')} \\
& \left. - \frac{\sin\left(2\pi A(k')\left(\frac{mT^{(D)}}{\xi} - B(n', 0)\right)\right)}{2\pi A(k')} \right\}
\end{aligned} \tag{5.42}$$

For case 1, the interference variance expression depends on $\theta^{(D)}$ *implicitly*. The probability that case 1 occurs is equal to the probability that θ belongs to $\left[T_s^{(D)}/\epsilon, T^{(D)}\right[$. Therefore the DVB interference variance taking into account both cases is obtained by :

$$V^{(D)} = \left(1 - \frac{T_s^{(D)}}{\xi T^{(D)}}\right) \mathbb{E}^{(1)}_{x_{k'},q_{n'}}[|I_p^{(D)}[m]|^2] + \mathbb{E}^{(2)}_{x_{k'},q_{n'},\theta}[|I_p^{(D)}[m]|^2] \tag{5.43}$$

5.2.2 DVB received signal

In the DVB network, the signal transmitted by the BR over the k'-th subcarrier of the l'-th OFDM symbol is given by :

$$r^{(D)}(t) = \frac{1}{\sqrt{T_s^{(D)}}} \sum_{l' \in \mathbb{Z}} \sum_{k'=0}^{N^{(D)}-1} \sum_{n'=1}^{L'} X_{k'}^{(L)}[l'] h_{n'}^{(D)} e^{j2\pi \frac{k'}{T_s^{(D)}} \left(t - \tau_{n'}^{(D)}\right)} \Pi \left(\frac{t - \tau_{n'}^{(D)} - l' T^{(D)} + T_g^{(D)}}{T^{(D)}} \right) \tag{5.44}$$

where $h_{n'}^{(D)}$ is the channel coefficient complex Gaussian distributed of the BT-BR link. The channel frequency response on the $k'-$th subcarrier is given by

$$H_{k'}^{(D)} = \sum_{n'=1}^{L'} h_{n'}^{(D)} e^{-j2\pi \frac{k'}{T_s^{(D)}} \tau_{n'}} \tag{5.45}$$

Projecting over the base functions, the received signal at the BR on the $p'-$th DVB subcarrier and over the $m'-$th OFDM data symbol is given by :

$$\tilde{X}_{p'}^{(D)}[m'] = \int_{\mathbb{R}} r^{(D)}(t) \phi_{p',m'}^{(D)}(t) dt \tag{5.46}$$

where $\phi_{p',m'}^{(D)}(t)$ is the reception filter defined by :

$$\phi_{p',m'}^{(D)}(t) = \frac{1}{\sqrt{T_s^{(D)}}} e^{-j2\pi \frac{p'}{T_s^{(D)}} t} \Pi \left(\frac{t - m' T^{(D)}}{T_s^{(D)}} \right) \tag{5.47}$$

Applying the same calculation steps as in LTE case, the received DVB signal can be written as :

$$\tilde{X}_{p'}^{(D)}[m'] = X_{p'}^{(D)}[m'] H_{p'}^{(D)}[m'] \tag{5.48}$$

5.2.2.1 LTE interfering signal

As shown above, the transmitted LTE signal is given by :

$$s^{(L)}(t) = \frac{1}{\sqrt{T_s^{(L)}}} \sum_{l \in \mathbb{Z}} \sum_{k=0}^{N^{(L)}-1} X_k^{(L)}[l] e^{j2\pi \frac{k}{T_s^{(L)}} t} \Pi \left(\frac{t - l T^{(L)} + T_g^{(L)}}{T^{(L)}} \right) \tag{5.49}$$

The transmitted LTE signal passes through the multipath channel of BS-BR interference link before being received by DVB receiver. Moreover, from the DVB receiver point of view, LTE is frequency shifted and delayed with an unknown and random asynchronism $\theta^{(L)}$. The LTE interfering signal received by BR before sampling can

be expressed as :

$$r^{(L)}(t) = \frac{e^{j2\pi\Delta f^{(L)}t}}{\sqrt{T_s^{(L)}}} \sum_{l\in\mathbb{Z}} \sum_{k=0}^{N^{(L)}-1} \sum_{n=1}^{L} X_k^{(L)}[l] q_n^{(L)} e^{j2\pi \frac{k}{T_s^{(L)}}(t-\tau_l^{(L)}-\theta^{(L)})} \Pi\left(\frac{t-\tau_l^{(L)}-lT^{(L)}+T_g^{(L)}-\theta^{(L)}}{T^{(L)}}\right) \quad (5.50)$$

DVB receiver decomposes the interfering LTE signal on its own basis. Hence, the interference received on the $p'-$th subcarrier and during the $m'-$th LTE OFDM data block is given by

$$I_{p'}^{(L)}[m'] = \int_{\mathbb{R}} r^{(L)}(t)\phi_{p',m'}^{(D)}(t)dt \quad (5.51)$$

Therefore, we obtain :

$$I_{p'}^{(L)}[m'] = \frac{1}{\sqrt{T_s^{(D)}T_s^{(L)}}} \int_t e^{j2\pi\Delta f^{(L)}t} \sum_{l\in\mathbb{Z}} \sum_{k=0}^{N^{(L)}-1} \sum_{n=1}^{L} X_k^{(L)}[l] q_n^{(L)} e^{j2\pi \frac{k}{T_s^{(L)}}(t-\tau_l^{(L)}-\theta^{(L)})} e^{-j2\pi\frac{p'}{T_s^{(D)}}t} \Pi\left(\frac{t-m'T^{(D)}}{T_s^{(D)}}\right) \Pi\left(\frac{t-\tau_l^{(L)}-lT^{(L)}+T_g^{(L)}-\theta^{(L)}}{T^{(L)}}\right) \quad (5.52)$$

where the integration over t depends on the term $\Pi\left(\frac{t-m'T^{(D)}}{T_s^{(D)}}\right) \Pi\left(\frac{t-\tau_n^{(L)}-lT^{(L)}+T_g^{(L)}-\theta^{(L)}}{T^{(L)}}\right)$ such that :

$$\begin{aligned} \Pi\left(\frac{t-m'T^{(D)}}{T_s^{(D)}}\right) = 1 \quad \text{iff} \quad & \begin{cases} m'T^{(D)} \le t \le m'T^{(D)} + T_s^{(D)} \\ m'\xi T^{(L)} \le t \le \xi(m'T^{(L)} + T_s^{(L)}) \end{cases} \\ \Pi\left(\frac{t-\tau_n^{(L)}-lT^{(L)}+T_g^{(L)}-\theta^{(L)}}{T^{(L)}}\right) = 1 \quad \text{iff} \quad & lT^{(L)} + \tau_n^{(L)} - T_g^{(L)} + \theta^{(L)} \le t \\ & \le (l+1)T^{(L)} + \tau_n^{(L)} - T_g^{(L)} + \theta^{(L)} \end{aligned} \quad (5.53)$$

Where in (5.53), the LTE asynchronism $\theta^{(L)}$ is such that : $\theta^{(L)} \sim \mathcal{U}([0, T^{(L)}])$. Moreover, the DVB OFDM symbol duration is larger than the LTE OFDM symbol duration and is not a multiple of it. The numbers of LTE symbols interfering on DVB symbol is :

$$\xi' \triangleq \frac{T_s^{(D)}}{T^{(L)}} = \xi\frac{T_s^{(D)}}{T^{(D)}} \quad (5.54)$$

Therefore, $\lfloor\xi'\rfloor$ LTE symbols interfere entirely over DVB symbol : $X_k^{(L)}[l], X_k^{(L)}[l+1], X_k^{(L)}[l+2]..., X_k^{(L)}[\lfloor\xi'\rfloor - 1]$. Moreover, the $(l-1)$-th and $\lfloor\xi'\rfloor$-th LTE symbols interfere partially respectively at the beginning and the end of DVB symbol. Hence,

the received interference over the p'-th DVB subcarrier and the m'-th data block can be written as :

$$\begin{aligned} I_{p'}^{(L)}[m'] &= \frac{1}{\sqrt{T_s^{(D)}T_s^{(L)}}} \sum_{k=0}^{N^{(L)}-1} e^{-j2\pi\frac{k}{T_s^{(L)}}\theta^{(L)}} \sum_{n=1}^{L} q_n^{(L)} e^{-j2\pi\frac{k}{T_s^{(L)}}\tau_l^{(L)}} \\ &\quad \left\{ X_k^{(L)}[l] \int_{m'\xi T^{(L)}}^{lT^{(L)}-T_g^{(L)}+\tau_n^{(L)}+\theta^{(L)}} e^{j2\pi\left(\Delta f+\frac{k}{T_s^{(L)}}-\frac{p'}{T_s^{(D)}}\right)t} dt \right. \\ &+ \sum_{b=0}^{\lfloor\xi'\rfloor-1} X_k^{(L)}[l+b] \int_{(l+b)T^{(L)}-T_g^{(L)}+\tau_n^{(L)}+\theta^{(L)}}^{(l+b+1)T^{(L)}-T_g^{(L)}+\tau_n^{(L)}+\theta^{(L)}} e^{j2\pi\left(\Delta f+\frac{k}{T_s^{(L)}}-\frac{p'}{T_s^{(D)}}\right)t} dt \\ &+ \left. X_k^{(L)}[\lfloor\xi'\rfloor] \int_{(l+\lfloor\xi'\rfloor)T^{(L)}-T_g^{(L)}+\tau_n^{(L)}+\theta^{(L)}}^{\xi(m'T^{(L)}+T_s^{(L)})} e^{j2\pi\left(\Delta f+\frac{k}{T_s^{(L)}}-\frac{p'}{T_s^{(D)}}\right)t} dt \right\} \end{aligned} \tag{5.55}$$

Applying the same calculation steps than those presented in the case of DVB interfering signal over LTE signal, we obtain :

$$\begin{aligned} I_{p'}^{(L)}[m'] &= \frac{1}{\sqrt{T_s^{(D)}T_s^{(L)}}} \sum_{k=0}^{N^{(L)}-1} e^{-j2\pi\frac{k}{T_s^{(L)}}\theta^{(L)}} \times \\ &\quad \left\{ -X_k^{(L)}[l-1] e^{j\pi C(k) m\xi T^{(L)}} \sum_{n=1}^{L} q_n^{(L)} e^{-j\pi\left(C(k)G(n,\theta^{(L)})+2\frac{k}{T_s^{(L)}}\tau_n^{(L)}\right)} \right. \\ &\qquad \left. \frac{\sin\left(\pi C(k)\left(m\xi T^{(L)} - G(n,\theta^{(L)})\right)\right)}{\pi C(k)} \right. \\ &+ \left(T^{(L)} \sin\left(\pi C(k) T^{(L)}\right) e^{j2\pi C(k)T^{(L)}} \sum_{b=0}^{\lfloor\xi'\rfloor-1} X_k^{(L)}[l+b] e^{j2\pi C(k) b T^{(L)}} \right) \\ &\qquad \sum_{n=1}^{L} q_n^{(L)} e^{-j2\pi\left(C(k)G(n,\theta^{(L)})-\frac{k}{T_s^{(L)}}\tau_n^{(L)}\right)} \\ &+ X_k^{(L)}[\lfloor\xi'\rfloor] e^{j\pi C(k)\left(\lfloor\xi'\rfloor T^{(L)}+\xi m T^{(L)}+\xi T_s^{(L)}\right)} \sum_{n=1}^{L} q_n^{(L)} e^{-j\pi\left(C(k)G(n,\theta^{(L)})+2\frac{k}{T_s^{(L)}}\tau_n^{(L)}\right)} \\ &\qquad \left. \left. \frac{\sin\left(\pi C(k)\left(\xi\left(mT^{(L)}+T_s^{(L)}\right) - \lfloor\xi'\rfloor T^{(L)} - G\left(n,\theta^{(L)}\right)\right)\right)}{\pi C(k)} \right\} \end{aligned} \tag{5.56}$$

where $C(k) = \Delta f^{(L)} + \frac{k}{T_s^{(L)}} - \frac{p'}{T_s^{(D)}}$ and $G\left(n, \theta^{(L)}\right) = lT^{(L)} - T_g^{(L)} + \tau_n^{(L)} + \theta^{(L)}$. Applying the same steps than above, i.e. averaging over the symbols, channel and asynchronism, we obtain :

$$\begin{aligned} V^{(L)} &= \mathbb{E}_{X_k,h_n,\theta}\left[|I_{p'}^{(L)}[m']|^2\right] \\ &= \frac{1}{T_s^{(D)}T_s^{(L)}T^{(L)}} \sum_{k=0}^{N^{(L)}-1} \sum_{n=1}^{L} \Omega_n^{(L)} \left(\frac{1}{\pi^2 C(k)^2}(T1+T2) + \lfloor \xi' \rfloor (T^{(L)})^3 \mathrm{sinc}^2\left(\pi C(k) T^{(L)}\right)\right) \end{aligned} \tag{5.57}$$

where $T1$ and $T2$ are defined by :

$$T1 = \frac{1}{2}T^{(L)} + \frac{\sin\left(2\pi C(k)\left(m\xi T^{(L)} - G(n, T^{(L)})\right)\right) - \sin\left(2\pi C(k)\left(m\xi T^{(L)} - G(n,0)\right)\right)}{4\pi C(k)} \tag{5.58}$$

$$\begin{aligned} T2 &= \frac{1}{2}T^{(L)} + \frac{\sin\left(2\pi C(k)\left(\xi\left(mT^{(L)} + T_s^{(L)}\right) - \lfloor \xi' \rfloor T^{(L)} - G\left(n, T^{(L)}\right)\right)\right)}{4\pi C(k)} \\ &\quad - \frac{\sin\left(2\pi C(k)\left(\xi\left(mT^{(L)} + T_s^{(L)}\right) - \lfloor \xi' \rfloor T^{(L)} - G\left(n,0\right)\right)\right)}{4\pi C(k)} \end{aligned} \tag{5.59}$$

5.3 Spectral efficiency

In this section, we calculate the spectral efficiency of the received signal in both networks LTE and DVB. Then we calculate the spectral efficiency of the total spectral overlap system.

5.3.1 Uniform power allocation

The power is first assumed to be equally allocated to each subcarrier in both systems whatever the interfering subcarriers are. The achievable data rates of LTE and DVB systems are given by :

$$D^{(L)} = \sum_{p=0}^{N^{(L)}} w_p^{(L)} \log_2(1 + \gamma_p^{(L)}) \tag{5.60}$$

$$D^{(D)} = \sum_{p'=0}^{N^{(D)}} w_{p'}^{(D)} \log(1 + \gamma_{p'}^{(D)}) \tag{5.61}$$

where $w_p^{(L/D)}$ is the LTE (DVB) subcarrier spacing respectively, and $\gamma_p^{(L)}$, $\gamma_{p'}^{(D)}$ are the SINR of LTE and DVB over the $p-$th and $p'-$th subcarrier respectively. The

SINR expressions are given by :

$$\gamma_p^{(L)} = \frac{p^{(L)} l_m |H_p^{(L)}|^2}{p^{(D)} l_{bm} V^{(D)} + N_0^{(L)} w_p^{(L)}} \tag{5.62}$$

$$\gamma_{p'}^{(D)} = \frac{p^{(D)} l_m |H_{p'}^{(D)}|^2}{p^{(D)} l_{mb} V^{(L)} + N_0^{(D)} w_p^{(D)}} \tag{5.63}$$

where $p^{(L)}$ and $p^{(D)}$ are respectively the transmit power per LTE and DVB subcarrier. We recall that l_m, l_b, l_{bm} and l_{mb} are the path loss attenuations of the BS-MR, BT-BR, BT-MR and BS-BR links respectively. Moreover, $N_0^{(L/D)}$ is the noise spectral density per one LTE (DVB) subcarrier. Therefore, the LTE (DVB) spectral efficiency is given by :

$$S^{(L/D)} = \frac{D^{(L/D)}}{B^{(L/D)}} \tag{5.64}$$

where $B^{(L/D)}$ is the total bandwidth of LTE (DVB) system respectively.

The global spectral efficiency is the sum data rate over the bandwidth used. The total bandwidth is the sum of the DVB and LTE bandwidths and varies with the overlap ratio α such that :

$$B_T(\alpha) = B_{min}\,(1-\alpha) + B_{max} \tag{5.65}$$

Therefore, the spectral efficiency of the total bandwidth can be written as :

$$S_T(\alpha) = \frac{1}{B_T(\alpha)}(D^{(D)} + D^{(L)}) \tag{5.66}$$

5.3.2 Interference-aware power allocation

Based on the observation that, the more power affected in good channels, i.e. without interference, the larger the achievable data rate, we assume the systems have the ability to allocate power differently on the interfering and non-interfering parts. Typically, the power allocated to the interfering part should be less than the power allocated in interference-free part in order to increase the spectral efficiency. Hence, the total transmission power in each system is composed as :

$$P_T = (1-\alpha)P_T + \alpha P_T \tag{5.67}$$

with P_T is the total transmission power over the bandwidth, then $(1-\alpha)P_T$ is the portion of power dedicated to the overlapped part and αP_T is for interference free part. Therefore, the transmission powers per subcarrier in the interfering and non-interfering parts are :

$$p_I = \frac{(1-\alpha)P_T}{K_I} \tag{5.68}$$

$$p = \frac{\alpha P_T}{K} \tag{5.69}$$

with $K_I = \alpha N$ and $K = (1-\alpha)N$ and N the total number of subcarriers in each system. We should note here that the values of K_I and K depends on α. The transmission power per one subcarrier can be re-written as :

$$p_I = \frac{1-\alpha}{\alpha} p_t \tag{5.70}$$

$$p = \frac{\alpha}{1-\alpha} p_t \tag{5.71}$$

with $p_t = P_T/N$ is the given transmission power value per subcarrier in case of uniform power allocation.

The SINR expressions on the overlapped and non-overlapped LTE and DVB subcarriers are respectively given by :

$$\tilde{\gamma}_p^{(L)} = \frac{p_I^{(L)} l_m |H_p^{(L)}|^2}{l_{bm}\left(p_I^{(D)} V_I^{(D)} + p^{(D)} V^{(D)}\right) + N_0^{(L)} w_p^{(L)}} \tag{5.72}$$

$$\gamma_p^{(L)} = \frac{p^{(L)} l_m |H_p^{(L)}|^2}{l_{bm}\left(p_I^{(D)} V_I^{(D)} + p^{(D)} V^{(D)}\right) + N_0^{(L)} w_p^{(L)}} \tag{5.73}$$

$$\tilde{\gamma}_{p'}^{(D)} = \frac{p_I^{(D)} l_b |H_{p'}^{(D)}|^2}{l_{mb}\left(p_I^{(L)} V_I^{(L)} + p^{(L)} V^{(L)}\right) + N_0^{(D)} w_{p'}^{(D)}} \tag{5.74}$$

$$\gamma_{p'}^{(D)} = \frac{p^{(D)} l_b |H_{p'}^{(D)}|^2}{l_{mb}\left(p_I^{(L)} V_I^{(L)} + p^{(L)} V^{(L)}\right) + N_0^{(D)} w_{p'}^{(D)}} \tag{5.75}$$

In this work, we have considered that DVB occupies a lower spectral range than LTE. Consequently, the rightmost subcarriers of DVB and the leftmost subcarriers of LTE are the more affected by the frequency overlap as seen in Fig. 5.1. Therefore, the received data rates of LTE and DVB networks in this allocations strategy can be given by :

$$\tilde{D}^{(L)} = \sum_{p=0}^{K_I^{(L)}-1} w_p^{(L)} \log(1+\tilde{\gamma}_p^{(L)}) + \sum_{p=K_I^{(L)}}^{N^{(L)}-1} w_p^{(L)} \log(1+\gamma_p^{(L)}) \tag{5.76}$$

$$\tilde{D}^{(D)} = \sum_{p'=0}^{K_I^{(D)}-1} w_{p'}^{(D)} \log(1+\gamma_{p'}^{(D)}) + \sum_{p'=K_I^{(D)}}^{N^{(D)}-1} w_{p'}^{(D)} \log(1+\tilde{\gamma}_{p'}^{(D)}) \tag{5.77}$$

The global spectral efficiency w.r.t. α can be hence written as :

$$S_T(\alpha) = \frac{1}{B_T(\alpha)} (\tilde{D}^{(D)} + \tilde{D}^{(L)}) \tag{5.78}$$

If receivers have interference-cancellation abilities, the interference effect can be reduced and hence the overlap ratio could be enhanced while maintaining a high QoS. Let us assume that each receiver can remove a proportion of the interference signal by multiplying it by the term I_R. Consequently, we can prove that LTE and DVB SINR expressions can be written respectively as :

$$\tilde{\Gamma}_{p/p'}^{(L/D)} = \frac{p_I^{(L/D)} l_{m/b} |H_{p/p'}^{(L/D)}|^2}{|1 - I_R|^2 l_{bm/mb} \left(p_I^{(D/L)} V_I^{(D/L)} + p^{(D/L)} V^{(D/L)} \right) + N_0^{(L/D)} w_{p/p'}^{(L/D)}} \tag{5.79}$$

$$\Gamma_{p/p'}^{(L/D)} = \frac{p^{(L/D)} l_{m/b} |H_{p'}^{(L/D)}|^2}{|1 - I_R|^2 l_{bm/mb} \left(p_I^{(D/L)} V_I^{(D/L)} + p^{(D/L)} V^{(D/L)} \right) + N_0^{(L/D)} w_{p/p'}^{(L/D)}} \tag{5.80}$$

The achievable data rate and spectral efficiency can be obtained by substituting the SINR expressions in (5.79), (5.80) in (5.76), (5.77) and (5.66) respectively.

5.4 Numerical results

Table 5.1 presents the parameters used throughout this section. The transmit power per subcarrier is obtained by dividing the maximum transmission power in each system by its total number of active subcarriers. Moreover, the LTE receiver is located at the limits of the LTE cell while the protection distance d between the LTE transmitter and the DVB receiver is a variable parameter.

Table 5.1 – Given system parameters

Parameters	**DVB-T2**	**LTE-3GPP**
Bandwidth	7.6 MHz	10 MHz
Subcarrier spacing	1.116 KHz	15 KHZ
Number of active subcarriers	6817	601
Symbol period	$896\mu s$	66.7 μs
Guard interval time	$T_s^{(D)}/4 = 224\mu s$	$T_s^{(L)}/4 = 16.675\mu s$
Cell radius	100Km	1Km
Max transmission power	10KW	50W
Transmit power/subcarrier	1.395W	0.075W
Noise spectral density	-165 dBm	-165 dBm
Path loss exponent	2.5	3

Tables 5.2 and 5.3 present respectively the power delay profiles, i.e. normalized average path power and path delays, of the Typical Urban (TUx) LTE 3GPP channel and the Typical Urban 6 (TU-6) DVB channel that are used respectively as the BT-MR and BS-BR channel interference models.

Table 5.2 – Power delay profile of 3GPP TUx channel model

Tap	1	2	3	4	5	6	7	8	9
Average power (db)	-5.7	-7.6	-10.1	-10.2	-10.2	-11.5	-13.4	-16.3	-16.9
$\tau_n^{(L)}$ **(ns)**	0	217	512	514	517	674	882	1230	1287

10	11	12	13	14	15	16	17	18	19	20
-17.1	-17.4	-19	-19	-19.8	-21.5	-21.6	-22.1	-22.6	-23.5	-24.3
1311	1349	1533	1535	1622	1818	1836	1884	1943	2048	2140

First of all, Figures 5.4 and 5.5 present respectively the LTE and DVB received data rates w.r.t. α labeled on the BS-BR distance d. Both $D^{(L)}$ and $D^{(D)}$ decrease when the spectral overlap ratio α increases. Obviously, $D^{(L)}$ is not affected by the distance BS-BR at contrary of DVB which is very sensitive to the protection distance between BS and BR. When d increases, DVB data rate increases as per DVB becomes less affected by the LTE interference.

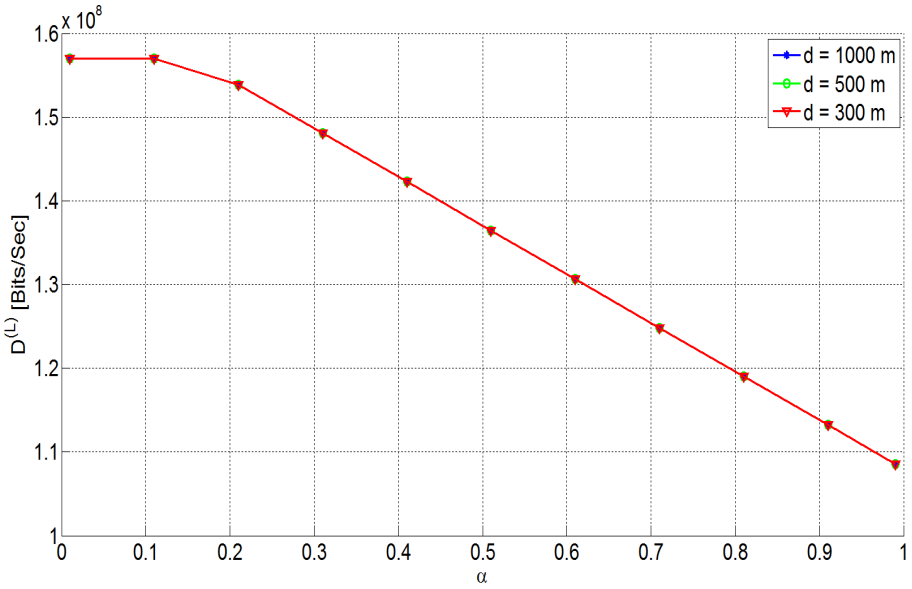

Figure 5.4 – LTE received data rate in [Bits/sec]

Table 5.3 – Power delay profile of DVB-T2 TU-6 channel model

Tap	1	2	3	4	5	6
Average power (db)	-3	0	-2	-6	-8	-10
$\tau_{n'}^{(D)} \mu s$	0	0.2	0.5	1.6	2.3	5

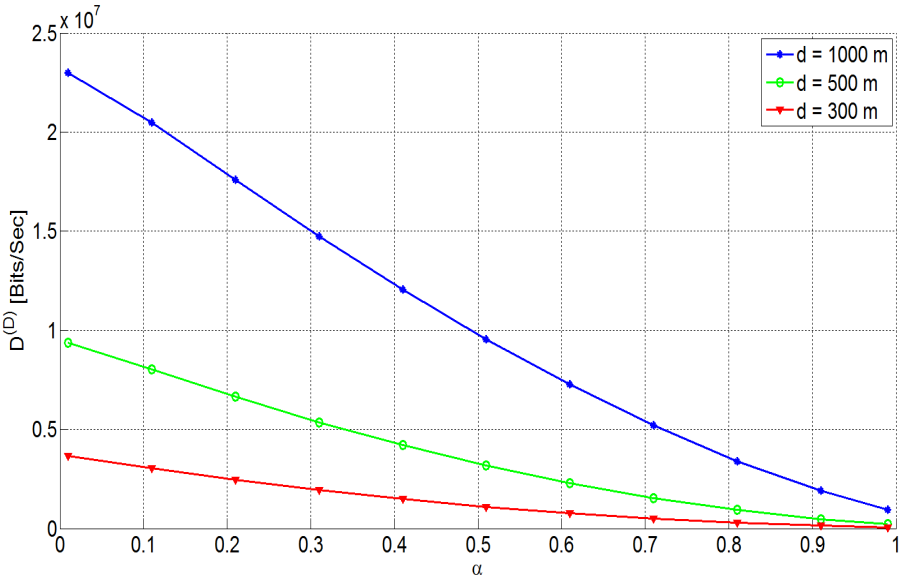

Figure 5.5 – DVB received data rate in [Bits/sec]

Fig. 5.6 shows the global spectral efficiency w.r.t α and labeled on d. As illustrated, the total spectral efficiency increases when the overlap ratio α increases despite the interference increases. However, the used bandwidth is reduced as shown in (5.65) leading to an increase in SE as in (5.66) and moreover, SE of LTE is largely greater than DVB. Moreover, the total spectral efficiency increases when d increases due to the increasing of $D^{(D)}$.

Secondly, Figures 5.7 and 5.8 draw the LTE and DVB data rates respectively labeled on $I_r = |1 - I_R|^2$ when the power allocation is different between the overlapped and non overlapped subcarriers as presented in (5.70) and (5.71). There is an optimal overlap ratio where the DVB data rate is maximal because DVB is the most sensitive to the overlap. For $\alpha = 1$, the entire DVB band is interfered. At the contrary, LTE data rates are maximal when the overlap is maximal because of the larger LTE bandwidth. The LTE bandwidth is not entirely disturbed by DVB and hence, more power can be allocated to non-interfering part, largely increasing the achievable data rate. The optimal α for DVB is varying according to the interference-rejection ability, e.g. $\alpha^* = 0.50$ without interference rejection and $\alpha = 0.4$ when 70% of the interference is rejected. Paradoxically, the optimal overlapping is reduced when interference-cancellation and power allocation are jointly allowed for DVB. This can be explained by the fact that interference-aware power allocation consists in allocated less power to interfering band. However, interference rejection abilities would rather favour high interfering signals in order to be able to remove it properly (in successive interference cancellation SIC scheme). We can however observe that the achievable DVB data rate globally improves when interference rejection ability is

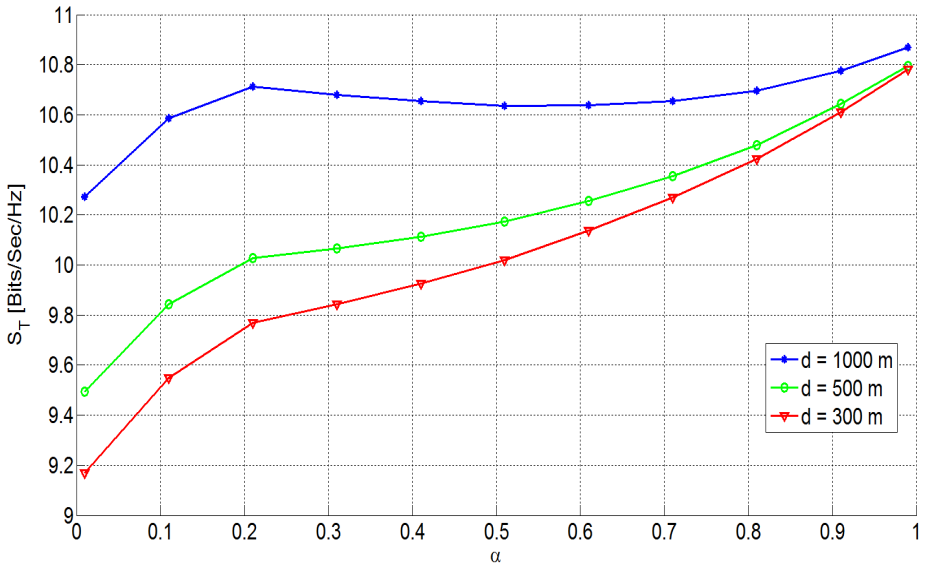

Figure 5.6 – Total spectral efficiency w.r.t. α and labeled on d.

allowed. One can remark that interference-aware power allocation and interference rejection jointly allow to increase the overlap between systems and hence the total spectral efficiency. Beyond the optimal overlap, the DVB data rates decreases due to the interference created.

In Fig. 5.9 the total spectral efficiency w.r.t. the overlap ratio α is plotted labeled on interference rejection coefficient. Spectral efficiency is continuously increasing with α contrarily to the same power allocation case. This is due to the fact that SE of LTE system is largely greater than DVB even for large frequency overlapping scenario. 70% of interference-cancellation ability allows to improve the total spectral efficiency. However, a full interfering system, i.e. $\alpha = 1$ is not beneficial to DVB system which experiment a data rate approaching zero, since no more power is used for it. Hence, a tradeoff can be found between the individual achievable data rate and the enhancement of the global spectral efficiency. Indeed, it can be remarked that an overlap between 0.3 and 0.4 may be beneficial to both systems.

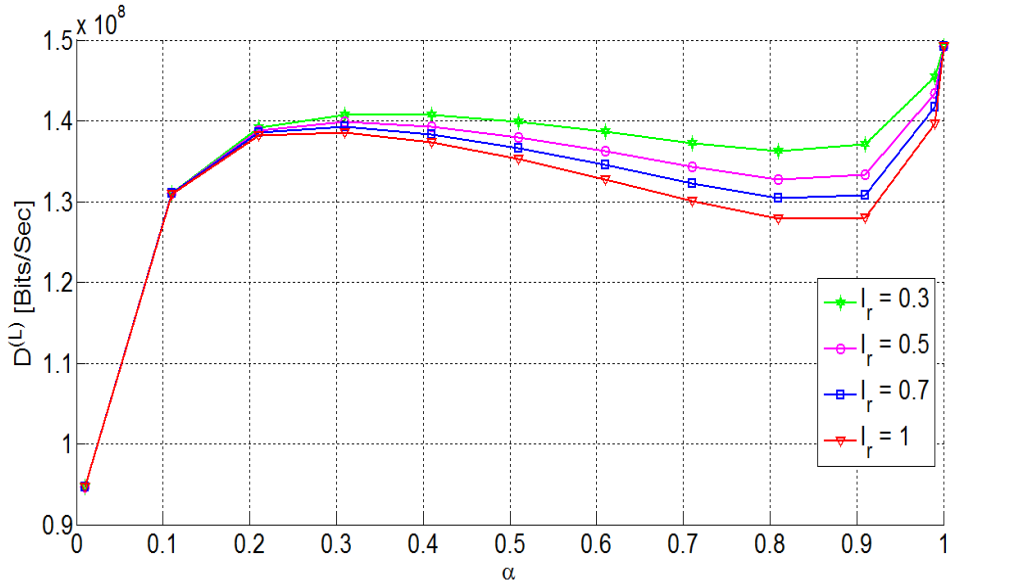

Figure 5.7 – LTE data rate w.r.t. α labeled on interference-cancellation coefficient and $d = 1000$ m.

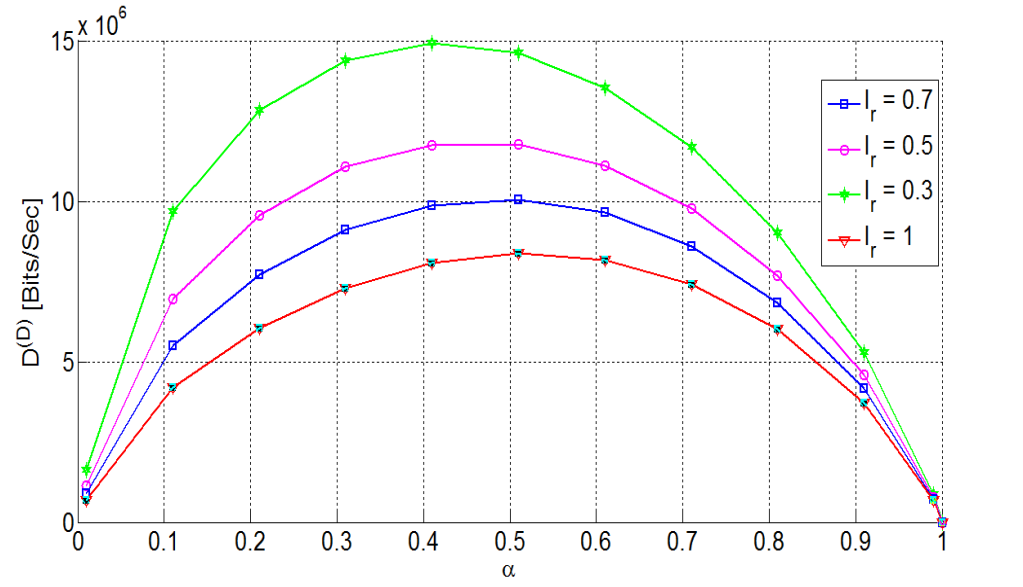

Figure 5.8 – DVB data rate w.r.t. α labeled on interference-cancellation coefficient and $d = 1000$ m.

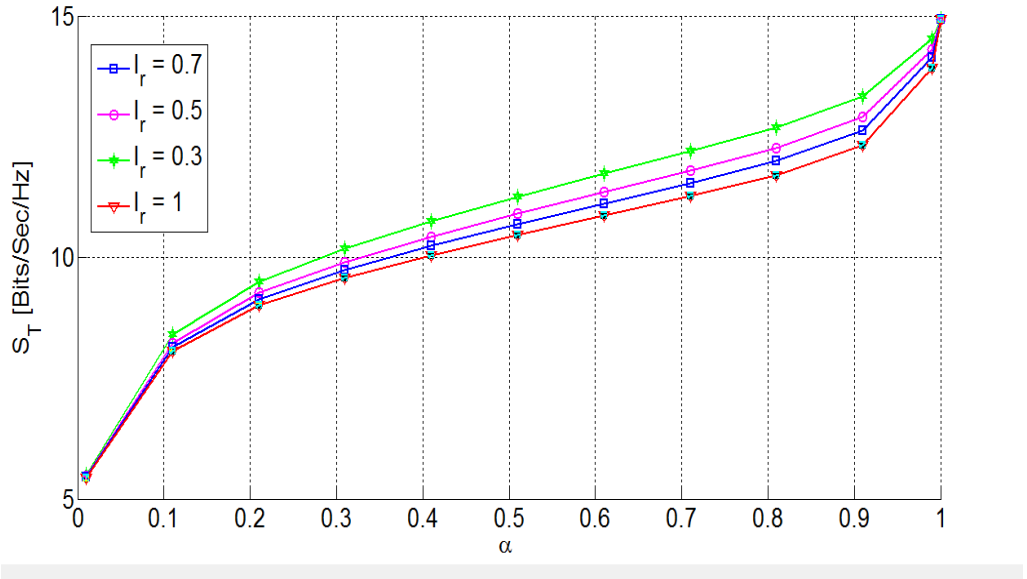

Figure 5.9 – Total spectral efficiency w.r.t. α labeled on interference-cancellation coefficient and $d = 1000$ m.

5.5 Conclusion

In this chapter, the spectral overlap ratio between DVB and LTE has been studied and its impact over the global system performance has been investigated. The interfering signal received on a given receiver, i.e. LTE or DVB, has been carefully derived based on a continuous-time formulation. The interference has been expressed w.r.t. LTE and DVB characteristics and random asynchronism between them. The interference signal has been shown to be asymmetric between LTE and DVB systems, mainly due to the differences between OFDM signal characteristics. The interference powers have been derived by successively deriving w.r.t. symbols, channel and asynchronism. Individual data rates and global spectral efficiency have then been investigated according to the overlap ratio when first the allocated power is the same on all subcarriers. Due to the high SE of LTE compared to DVB, one should increase the spectral overlap to increase the global SE. However, global SE value remains relatively stable with α in that case. When interference-aware power allocation is allowed, i.e. higher power is allocated to non-interfering parts than interfering frequency range, DVB data rates exhibits an optimal overlap ratio for which it is maximal. In order to increase the achievable performance, an advanced interference rejection ability has been assumed at receivers in order to maximize the global capacity and find an optimal spectral overlap ratio.

Further researches could be done on this basis. Indeed, we could search for the

optimal power and frequency sharing between systems in order to maximize both system capacities under a global, i.e. LTE+DVB, power constraint. This could be interesting to characterize the optimal functioning point.

Conclusions and prospects

Conclusions

In this thesis, we studied the spectral convergence between DVB and LTE networks. We focused in our study on the performance evaluation of the coexisting networks that spectrally overlap without cooperation

First of all, we presented the DVB and LTE networks basics and the circumstances leading up to the possibility of spectral overlap existence between their bandwidths. It has been shown that both technologies present some similarities, mainly both use orthogonal frequency division multiplexing (OFDM) waveform (in downlink for LTE), but technical characteristics remain rather different between those. This presentation performed good reference for the further works based on the LTE and DVB characteristics and parameters.

The coexistence DVB - LTE problem being analog to the Primary User (PU) - Secondary User (SU) coexistence in overlay scenario, the ergodic capacity of the secondary link in a cognitive radio spectrum-sharing model under two joint power constraints and in a full cross interference Rayleigh channel was derived in closed form. Hence, the analytical and numerical results presented the optimal throughput and the limits of operation of the secondary link under the practical average interference power at the primary receiver and the peak transmit power at the secondary transmitter. Consequently, the solution respected the QoS constraints that guarantee the primary network performance.

Secondly, SU and PU are considered to be LTE and DVB respectively. The problem of deploying a small LTE cell into a large broadcast cell in the spectral overlap scenario between LTE and DVB was treated. The PDF of the signal to interference ratio (SIR) at both receivers, i.e. Broadcast Receiver (BR) and Mobile Receiver (MR), have been derived leading to the derivation of the global ergodic

capacity. It was shown by numerical analysis that the global and the broadcast capacities are strongly affected by the LTE transmission power. Moreover, it was seen that the broadcast data rate is highly dependent on the interference distance between the LTE transmitter and the DVB receiver. Furthermore, it was illustrated that the global capacity is not a convex or concave function of the mobile and broadcast transmit power.

Moreover, the global ergodic capacity in the spectrally fully-overlapping DVB and LTE scenario was optimized by finding the optimal LTE-DVB power ratio. It was shown that the global ergodic capacity is made of a convex part, i.e. the LTE system capacity, and a concave part, i.e. the DVB system capacity, and further, it only depends on the ratio of the transmitted powers and not on the absolute values of them. The global capacity was optimized while respecting severe constraints over the DVB and the LTE capacities that guarantee the DVB and LTE QoS. On one hand, the global capacity was optimized using a convex-concave procedure leading to the minimum of the global capacity but to balanced capacity on individual links. On the other hand, the global capacity was maximized leading to favor one system over the other. We showed that the proposed MP algorithm achieves an higher throughput of the global system than the one obtained with the CCCP solution.

Finally, we studied the variation effect of the spectral overlap ratio between the DVB and the LTE networks over the global system performance. The global spectral efficiency was derived while taking carefully the difference between DVB and LTE characteristics into account in order to evaluate accurately the interference effect over both networks. In this study, an interference-aware power allocation strategy at transmitters and advanced interference rejection abilities at receivers have been assumed in order to increase the global capacity and find an optimal spectral overlap ratio for each individual system.

This preliminary work could be useful for mobile operators and broadcasters giving an insight, mainly at the theoretical level, on how to deploy LTE cells overlapping the DVB bandwidth. The different contributions in this work have led to three international conferences where one of them has received the Best Paper Award at the International Conference on Ultra Modern Telecommunications and Control Systems (ICUMT-2014, IEEE). Another paper on contributions of the fifth chapter is under progress.

Prospects

There are numerous open prospects which could be addressed in future works :

— Extension for multi-user case with block resource allocation for the LTE system.

— Explicit integration of the reduction interference techniques by using multiple

antennas for example.

— Performances of spectral overlapping when DVB and LTE cooperate.

The last one seems to be very important. In fact, both networks have similar contents and services but for the moment, their convergence remains theoretical. For example, in order to increase the performance presented in this thesis, which present two interfering systems, an interference coding with "dirty paper coding" between both systems would provide the possibility to increase the achievable data rate, since this scheme is capacity-achieving for broadcast channel. This would consist to study the needed informations that should be exchanged between both systems and specify the goals and the priorities of their cooperation.

Bibliography

[1] S. Boyd and L. Vandenberghe, *Convex Optimization*. United Kingdom : Cambridge University Press, 2004.

[2] A. Yuille and A. Rangarajan, "The Concave-Convex Procedure," *Neural Computation*, vol. 15, no. 15, pp. 915–936, April 2003.

[3] V. Asghari and S. Aissa, "Resource Management in Spectrum-Sharing Cognitive Radio Broadcast Channels : Adaptive Time and Power Allocation," *IEEE Transactions on Communications*, vol. 59, no. 5, pp. 1446–1457, 2011.

[4] H. Urkowitz, "Energy detection of unknown deterministic signals," in *proc. IEEE*, vol. 55, no. 4, Apr. 1967, pp. 523–53.

[5] J. G. Proakis, *Digital Communications*, 4th ed. McGraw-Hill, 2001.

[6] CEPT, "The identification of common and minimal (least restrictive) technical conditions for 790 - 862 MHz for the digital dividend in the European Union," Electronic Communications Committee (ECC) within the European Conference of Postal and Telecommunications Administrations (CEPT), Tech. Rep., October 2009.

[7] P. Barsocchi, "Channel models for terrestrial wireless communications : a survey," National Research Council ? ISTI Institute, Tech. Rep.

[8] D. Tse and P. Viswanath, *Fundamentals of wireless Communications*. Cambridge University Press, 2005.

[9] J. R. Shewchuk, "An Introduction to the Conjugate Gradient Method Without the Agonizing Pain," August 1994.

[10] A. Company, "LTE Resource Guide," 2009. [Online]. Available : www.us.anritsu.com

[11] M. Nohrborg, "LTE Overview." [Online]. Available : http://www.3gpp.org/technologies/keywords-acronyms/98-lte

[12] J. Wannstrom, "LTE Advanced." [Online]. Available : http://www.3gpp.org/technologies/keywords-acronyms/97-lte-advanced

[13] T.-Y. Lee, "An introduction of 3GPP Long Term Evolution(LTE)." [Online]. Available : http://wenku.baidu.com/view/e521af81d4d8d15abe234e21.html

[14] telesystem innovations, "LTE in a Nutshell : The physical Layer," 2010.

[15] E. T. S. I. (ETSI), "Digital Video Broadcasting (DVB) ; Frame structure channel coding and modulation for a second generation digital terrestrial television broadcasting system (DVB-T2)," 4 2012, eTSI EN 302 755 V1.3.1.

[16] DVB-T2, "2nd Generation Terrestrial - The world's Most Advanced Digital Terrestrial TV System," December 2013, dVB.

[17] Rohde&Schwarz, "Coexistence Digital TV and LTE," Tech. Rep.

[18] "3rd Generation Partnership Project ; Technical Specification Group Radio Access Network ; Evolved Universal Terrestrial Radio Access (E-UTRA) ; Relay architectures for E-UTRA (LTE-Advanced) (Release 9)," march 2010.

[19] S. E. Nai, T. Quek, and M. Debbah, "Shadowing time-scale admission and power control for small cell networks," in *Wireless Personal Multimedia Communications (WPMC), 2012 15th International Symposium on*, 2012, pp. 628–632.

[20] A. A. Razzac, S. E. Elayoubi, T. Chahed, and B. E. Hassan, "Comparaison of LTE eMBMS and DVB-NGH mobile TV solutions from ana energy consumption perspective," in *Workshop on End-to-End Green Cellular Networks, IEEE 24th International Symposium on Personal, Indoor and Mo ?bile Radio communications*, 2013.

[21] A. Razzac, S. Elayoubi, T. Chahed, and B. El-Hassan, "Impact of LTE and DVB-NGH cooperation on QoS of Mobile TV users," in *Communications (ICC), 2013 IEEE International Conference on*, 9-13 June 2013, pp. 3672,3677.

[22] A. Razzac, S. Elayoubi, T. Chahed, and B. ElHassan, "Dimensioning and Profit Sharing in Hybrid LTE/DVB Systems to Offer Mobile TV Services," in *Wireless Communications, IEEE Transactions on*, vol. 12, no. 12, December 2013, pp. 6314,6327.

[23] K. Ben Fredj, S. Aissa, and L. Musavian, "Ergodic and outage capacities of relaying channels in spectrum-sharing constrained systems," *Communications, IET*, vol. 7, pp. 98,109, January 22 2013.

[24] L. Li and A. Goldsmith, "Capacity and optimal resource allocation for fading broadcast channels – part i : Ergodic capacity," *IEEE Transactions on Information Theory*, vol. 47, no. 3, pp. 1083–1102, 2001.

[25] R. Zhang, S. Cui, and Y.-C. Liang, "On Ergodic Sum Capacity of Fading Cognitive Multiple-Access and Broadcast Channels," *IEEE Transactions on Information Theory*, vol. 55, no. 11, pp. 5161–5178, 2009.

[26] L. Musavian and S. Aissa, "Ergodic and Outage Capacities of Spectrum-Sharing Systems in Fading Channels," in *Global Telecommunications Conference, 2007. GLOBECOM '07. IEEE*, 26-30 Nov. 2007, pp. 3327,3331.

[27] T. N. IT and A. M. Telecom Agency (NITA), DotEcon, "800MHz auction : Coexistence of LTE systems in 790-862 MHz with Digital Terrestrial Television ," August 2011.

[28] A. Aloisi, M. Celidonio, L. Pulcini, and A. Rufini, "Experimental study on Protection Distances between LTE and DVB-T stations operating in adjacent UHF frequency bands," in *Wireless Telecommunications Symposium (WTS) 2011*, 13-15 April 2011, pp. 1–7.

[29] ——, "A simulation study of broadband mobile systems interference on DVB-T systems operating in the UHF frequency band," in *Future Network & Mobile Summit (FutureNetw), 2011*, 15-17 June 2011, pp. 1–8.

[30] K. Sakic and S. Grgic, "The influence of the LTE system on DVB-T reception," in *ELMAR, 2010 PROCEEDINGS*, 15-17 Sept. 2010, pp. 235,238.

[31] W. Wang, W. Wang, Z. Lv, W. Huang, and Y. Zhang, "Analysis of interference from digital terrestrial television broadcast to lte tdd in digital dividend spectrum," in *Network Infrastructure and Digital Content, 2010 2nd IEEE International Conference on*, Sept 2010, pp. 692–697.

[32] W. Li, J. Chen, H. Long, and B. Wu, "Performance and analysis on lte system under adjacent channel interference of broadcasting system," in *Computer and Information Technology (CIT), 2012 IEEE 12th International Conference on*, Oct 2012, pp. 290–294.

[33] A. Guidotti, D. Guiducci, M. Barbiroli, C. Carciofi, P. Grazioso, and G. Riva, "Coexistence and mutual interference between mobile and broadcasting systems," in *Vehicular Technology Conference (VTC Spring), 2011 IEEE 73rd*, May 2011, pp. 1–5.

[34] D.-H. Kim, S.-J. Oh, and J. Woo, "Coexistence analysis between imt system and dtv system in the 700mhz band," in *ICT Convergence (ICTC), 2012 International Conference on*, Oct 2012, pp. 284–288.

[35] Z. Shamsan, "Lte-advanced compatibility with digital broadcasting receiver at 800 mhz," in *Electronics, Communications and Photonics Conference (SIECPC), 2013 Saudi International*, April 2013, pp. 1–4.

[36] L. Polak, O. Kaller, L. Klozar, and J. Prokopec, "Exploring and measuring the co-existence between lte and dvb-t2-lite services," in *Telecommunications and*

Signal Processing (TSP), 2013 36th International Conference on, July 2013, pp. 316–320.

[37] S. Srinivasa and S. Jafar, "How much spectrum sharing is optimal in cognitive radio networks ?" *IEEE Transactions on Wireless Communications*, vol. 7, no. 10, pp. 4010–4018, 2008.

[38] H. Yao, Z. Zhou, H. Liu, and L. Zhang, "Optimal power allocation in joint spectrum underlay and overlay cognitive radio networks," in *Cognitive Radio Oriented Wireless Networks and Communications, 2009. CROWNCOM '09. 4th International Conference on*, 2009, pp. 1–5.

[39] A. T. Hoang and Y.-C. Liang, "Downlink Channel Assignment and Power Control for Cognitive Radio Networks," *IEEE Transactions on Wireless Communications*, vol. 7, no. 8, pp. 3106–3117, 2008.

[40] M. Khojastepour and B. Aazhang, "The capacity of average and peak power constrained fading channels with channel side information," in *Wireless Communications and Networking Conference, 2004. WCNC. 2004 IEEE*, vol. 1, 21-25 March 2004, pp. 77,82.

[41] J. Mietzner, L. Lampe, and R. Schober, "Distributed transmit power allocation for multihop cognitive-radio systems," *IEEE Transactions on Wireless Communications*, vol. 8, no. 10, pp. 5187–5201, 2009.

[42] G. Baruffa, M. Femminella, F. Mariani, and G. Reali, "Protection Ratio and Antenna Separation for DVB-T/LTE Coexistence Issues," *Communications Letters, IEEE*, vol. 17, no. 8, pp. 1588–1591, August 2013.

[43] I.-K. Cho, I.-K. Lee, and Y. ok Park, "Study on Coexistence between Long Term Evolution and Digital Broadcasting services," *International Journal of Advances Science and Technology*, vol. 38, January 2012.

[44] P. Mary, J.-M. Gorce, G. Villemaud, M. Dohler, and M. Arndt, "Performance Analysis of Mitigated Asynchronous Spectrally-Overlapping WLAN Interference," in *Wireless Communications and Networking Conference (WCNC 2007), 2007 IEEE*, 2007, pp. 2097–2102.

[45] ——, "Reduced Complexity MUD-MLSE Receiver for Partially-Overlapping WLAN-Like Interference," in *Vehicular Technology Conference (VTC Spring'07), 2007 IEEE 65th*, 2007, pp. 1876–1880.

[46] S. Sangtarash, H. Sadeghi, W. Hassan, H. King, and T. Rahman, "Using cognitive radio interference mitigation technique to enhance coexistence and sharing between DVB-T and LTE system," *Future Network & Mobile Summit (FutureNetw) 2012*, pp. 1–9, 4-6 July 2012.

[47] J. Mitola and J. Maguire, G.Q., "Cognitive radio : making software radios more personal," *Personal Communications, IEEE*, vol. 6, no. 4, p. 13, 18, Aug 1999.

[48] L. Doyle, *Essentials of cognitive radio*. Cambridge University Press, 2009.

[49] A. Goldsmith and P. Varaiya, "Capacity of fading channels with channel side information," *Information Theory, IEEE Transactions on*, vol. 43, no. 6, pp. 1986,1992, Nov 1997.

[50] L. Paura and R. Savoia, "Mobility-aware sensing enabled capacity in Cognitive Radio networks," in *in Measurements and Networking Proceedings (M&N), 2013 IEEE International Workshop*, Oct 2013, pp. 179,183.

[51] A. S. Cacciapuoti, I. F. Akyildiz, and L. Paura, "Optimal primary-user mobility aware spectrum sensing design for cognitive radio networks," *IEEE J. Sel. Areas Commun.*, vol. 31, no. 11, pp. 2161–2172, Nov 2013.

[52] B. Wang, , and K. J. Liu, "Advance in cognitive radio networks : A Survey," *IEEE J. Sel. Areas Commun.*, vol. 5, no. 1, pp. 5–23, Jan 2011.

[53] V. Asghari and S. Aissa, "Adaptive Rate and Power Transmission in Spectrum-Sharing Systems," *IEEE Transactions on Wireless Communications*, vol. 9, no. 10, pp. 3272–3280, 2010.

[54] X. Kang, Y.-C. Liang, H. K. Garg, and L. Zhang, "Sensing-Based Spectrum Sharing in Cognitive Radio Networks," in *Global Telecommunications Conference, 2008. IEEE GLOBECOM 2008. IEEE*, Nov.30 2008-Dec.4 2008 2009, pp. 1,5.

[55] W. Yu, "sum capacity computation for the Gaussian vector Broadcast channel via Dual decomposition," *IEEE Trans. Inform. Theory*, vol. 52, no. 2, Feb. 2006.

[56] A. Ghasemi and E. Sousa, "Fundamental limits of spectrum-sharing in fading environments," *Wireless Communications, IEEE Transactions on*, vol. 6, no. 2, pp. 649,658, Feb. 2007.

[57] I. S. Gradshteyn and I. M. Ryzhik, *Table of Integrals, Series, and Products*, 7th ed., A. Jeffrey and D. Zwillinger, Eds. Academic Press, Mar. 2007.

[58] 3GPP, "Utra-utran long term evolution (lte) and 3gpp system architecture evolution (sae)." [Online]. Available : ftp://ftp.3gpp.org/Inbox/2008_web_files/LTA_Paper.pdf

[59] H. Bawab, P. Mary, J. F. H ???lard, Y. Nasser, and O. Bazzi, "Ergodic capacity optimization in coexisting DVB-LTE-like systems," in *Ultra Modern Telecommunications and Control Systems and Workshops (ICUMT), 2014 6th International Congress on*, 6-8 Oct. 2014, pp. 54,59.

[60] H. Bawab, P. Mary, J. F. çois Hélard, Y. Nasser, and O. Bazzi, "Global Ergodic Capacity Closed-Form Expression of Coexisting DVB-LTE-Like Systems," in *Vehicular Technology Conference (VTC Spring'14), 2014 IEEE 79th*, 2014, pp. 1–5.

[61] M. L. BELHOUCHET and M. H. EBDELLI, "LTE Technology," in *ITU/BDT Arab Regional Workshop on ?4G Wireless Systems ?, Session3 : LTE Overview-Design Targets and Multiple Access Technologies*, 27-29January 2010.

[62] S. Boyd, S.-J. Kim, L. Vandenberghe, and A. Hassibi, "A tutorial on geometric programming," *Optimization and Engineering*, vol. 8, no. 1, pp. 67–127, 2007.

[63] J.-P. Chaib, "Technical overview of the DVB-T2 switchover planning, cases studies," in *ATDI, Digital Broadcasting Switchover Forum, Johannesburg, South Africa*, 11 Feb. 2013.

[64] ——, "Coexistence between Digital TV and LTE," in *ATDI, Middle East Spectrul Conference*, 2012.

[65] C. A. C. Coello, G. B. Lamont, and D. A. V. Veldhuizen, *Evolutionary Algorithms for Solving Multi-Objective Problems (Genetic and Evolutionary Computation)*. Secaucus, NJ, USA : Springer-Verlag New York, Inc., 2006.

[66] M. Ehrgott., *Multicriteria Optimization*. Berlin : Springer, 2005.

[67] M. Ghanem, H. Bawab, O. Bazzi, Y. Nasser, P. Mary, and J. F. Hélard, "Closed-Form Expression of the Ergodic Capacity in a Cognitive Radio Link under Power Constraints," in *ICUMT 2014*, 2014.

[68] J. Gibson, *The Mobile Communications Handbook*. CRC Press, 1996.

[69] P. Glover, I. ; Grant, *Digital communications*, 2nd ed. Pearson Education Ltd.l, 2004.

[70] J. Proaksis, *Digital communications*, 4th ed. McGraw-Hill, 2001.

[71] V. Konei, L. Yang, L. Yang, B. Zhao, and H. Zheng, "On the Feasibility of Effective Opportunistic Spectrum Access," in *IMC '10 Proceedings of the 10th ACM SIGCOMM conference on Internet measurement*, vol. 14, no. 14, November 2010.

[72] T.-Y. Lee, "Long Term Evolution-Evolved Packet Core S1 Interface Conformance Test Plan," MultiService Forum. [Online]. Available : http://www.msforum.org/techinfo/testplans/msf-p0044.031.pdf

[73] P. Mary, I. Fijalkow, and C. Poulliat, "Adaptive Rate Allocation Scheme for Uplink TH-UWB Networks," in *IEEE International Conference on Communications (ICC)*, June 2011.

[74] R. van Nee and R. Prasad, *OFDM for wireless Multimedia Communications, Norwood)*, 1st ed., ser. Artech House Universal Personal Communication Series. Artech House, Incorporated, 1999.

[75] J. G. Proakis, *Digital communications*, 3rd ed. New York : Singapore : McGraw-Hill, 1995.

[76] C. Thein, M. Fuhrwerk, J. Peissig, and M. Schellmann, "Opportunistic spectrum access in TVWS : A comparative coexistence study for LTE," *Dynamic Spectrum Access Networks (DYSPAN), 2012 IEEE International Symposium*, pp. 289–298, 16-19 Oct. 2012.

[77] R. Zhang, "Analysis of energy-delay performance in multi-hop wireless sensor networks," Ph.D. dissertation, Institut National des sciences appliqu ???es de Lyon, 2009.

[78] "Backhauling X2." [Online]. Available : http://cbnl.com/sites/all/files/userfiles/files/Backhauling-X2.pdf

[79] "LTE quick guide." [Online]. Available : http://www.tutorialspoint.com/lte/pdf/lte_quick_guide.pdf

[80] "M3 project, anr-10-vers-0010." [Online]. Available : http://www.agence-nationale-recherche.fr/projet-anr/?tx_lwmsuivibilan_pi2%5BCODE%5D=ANR-10-VERS-0010

Résumé

L'avènement de terminaux avancés permet l'accès à des services toujours plus gourmands en bande passante, avec notamment le déploiement de services de vidéo mobile sans couture offert par le mode diffusion mobile intégré standardisé par le 3GPP. Dans le même temps, la communauté « broadcast » s'est adaptée aux nouveaux usages de télévision mobile avec la norme DVB-NGH (Digital Video Broadcasting - Next Generation Handheld).

Dans ce contexte, l'objectif de cette thèse est d'étudier la convergence spectrale entre les deux réseaux DVB et LTE en déployant une petite cellule LTE au sein d'une grande cellule DVB. Les deux technologies utilisent une forme d'onde OFDM (Orthogonal Frequency Division Multiplexing), en liaison descendante pour le LTE, et possèdent donc quelques similarités tout en étant assez différentes par leurs caractéristiques. Dans ces travaux, nous nous intéressons aux performances atteignables lorsque les deux systèmes se recouvrent spectralement sans coopération. Le problème considéré étant analogue à un problème d'utilisateur secondaire opérant en mode recouvrement avec un utilisateur primaire, on commence par étudier le problème de la capacité ergodique du système secondaire, i.e. utilisateur LTE, sous contraintes de puissance moyenne générée par le secondaire sur le primaire, i.e LTE sur DVB**,** et de puissance crête au secondaire lorsque l'utilisateur primaire interfère sur le secondaire. Le problème est résolu analytiquement dans le cas général du canal croisé avec évanouissements de Rayleigh.

Dans un deuxième temps nous étendons cette étude préliminaire au cas où la forme d'onde des deux systèmes primaire et secondaire est effectivement de type OFDM. En considérant d'abord un modèle simple de recouvrement total des sous-porteuses, nous dérivons la capacité ergodique globale ce qui nous permet d'évaluer l'influence des paramètres des systèmes, comme le nombre de sous-porteuses de chaque système ou les puissances interférentes, sur les capacités globales et individuelles. Nous nous intéressons ensuite à l'optimisation de la capacité globale où deux stratégies sont étudiées. D'une part, la capacité globale étant la somme de deux fonctions convexe et concave respectivement, la solution obtenue conduit au minimum de capacité globale mais mène à une situation d'équilibre entre les systèmes DVB et LTE. D'autre part, la maximisation de la capacité globale sous contrainte conduit à favoriser largement un système sur l'autre.
Enfin, une étude fine de l'interférence causée par un système sur l'autre par recouvrement partiel est menée. L'effet de la variation du taux de recouvrement spectral entre les bandes du DVB et du LTE sur l'efficacité spectrale globale est étudié. On suppose ensuite que le récepteur possède une capacité de réjection de l'interférence permettant de déterminer le recouvrement optimal maximisant la capacité globale.

Les différentes contributions de ces travaux ont permis d'avoir une approche théorique sur la modalité d'allocation de puissance des deux systèmes DVB et LTE co-existants et sur le taux de recouvrement approprié entre leurs spectres respectifs**.** Cette étude pourrait être utile pour les opérateurs intéressés par un scénario de déploiement dense afin de choisir les configurations optimales des ressources dans une perspective de réutilisation agressive des fréquences.

Abstract

Since the launch of the first numerical mobile telecommunications networks in the nineties, the quantity of the transmitted data over these networks is increasing year by year. Advanced user equipments enable to implement more and more bandwidth consuming services such as mobile TV and multimedia internet, available in the integrated mobile broadcast mode recently standardized by the 3GPP group. In the meanwhile, the digital video broadcasting – next generation handled (DVB-NGH) has been released in order to satisfy the increasing demand for mobile TV. These technologies compete for a more and more constrained spectral resource leading to question the possibility to deploy DVB and Long Term Evolution (LTE) services in a spectral overlay mode as it has been investigated by the M^3 project funded by the National Research Agency.

In this context, this thesis aims at studying the spectral convergence between DVB and LTE networks by deploying a small LTE cell in a large DVB cell. Both technologies present some similarities, i.e. both use orthogonal frequency division multiplexing (OFDM) waveform (in downlink for LTE), but technical characteristics remain rather different between those. In this work, we deal with achievable performance when DVB and LTE spectrally overlap without cooperation.

The considered problem being analog to the Secondary User (SU) – Primary User (PU) coexistence in overlay scenario, the SU ergodic capacity under average power generated on PU and peak power at SU constraints is investigated. An analytic solution is propose in X-Channel with Rayleigh fading.

In a second time, SU and PU are considered to be LTE and DVB respectively with their particular OFDM signal characteristics. With a first model of overlapping subcarriers, LTE and DVB ergodic capacities and global capacity as well are derived in closed form allowing to study the influence of several system parameters on ergodic capacities. The global capacity is then optimized using a convex-concave procedure leading to the minimum on the global capacity but to balanced capacity on individual links. On a second hand, global capacity maximization leads to favor one system over the other.

Last but not least, a careful study of the interference caused by one system over the other by partial overlay is led. The effect of spectral overlap ratio between DVB and LTE systems over the global spectral efficiency is investigated. Advanced interference rejection ability is then assumed at receivers and the optimal spectral overlap, i.e. maximizing the global capacity, is then derived in that case.
The different contributions in this work give a theoretical approach on the power allocation modality of two coexisting DVB and LTE systems and on the appropriate spectral overlap ratio between their respective spectrum. This study can be useful for operators interested in dense network deployment scenarios to decide the operating point of allocated resources in a very aggressive frequency reuse pattern.

Utiliser la police Arial Taille 9 en bleu dans les champs texte « résumé » et « abstract » - Texte justifié -
Ne pas dépasser le nombre de caractères des cadres de texte ci-dessus.
Ne pas modifier la taille des cadres de texte

N° d'ordre : XXXXXXX
Institut National des Sciences Appliquées de Rennes
20, Avenue des Buttes de Coëmes • CS 70839 • F-35708 Rennes Cedex
Tel : 02 23 23 82 00 - Fax : 02 23 23 83 96